Fall 12-2014

Utilization of Aqueous RAFT Prepared Copolymers to Improve Anticancer Drug Efficacy

Andrew Christopher Holley
University of Southern Mississippi

The University of Southern Mississippi

UTILIZATION OF AQUEOUS RAFT SYNTHESIZED COPOLYMERS TO IMPROVE ANTICANCER DRUG EFFICACY

by

Andrew Christopher Holley

Abstract of a Dissertation
Submitted to the Graduate School
of The University of Southern Mississippi
in Partial Fulfillment of the Requirements
for the Degree of Doctor of Philosophy

December 2014

ABSTRACT

UTILIZATION OF AQUEOUS RAFT SYNTHESIZED COPOLYMERS TO IMPROVE ANTICANCER DRUG EFFICACY

by Andrew Christopher Holley

December 2014

The advent of controlled radical polymerization (CRP) techniques, along with advancements in facile conjugation chemistry, now allow synthetic tailoring of precise, polymeric architectures necessary for drug/gene delivery. Reversible addition-fragmentation chain transfer (RAFT) polymerization and its aqueous counterpart (*a*RAFT) afford quantitative control over key synthetic parameters including block length, microstructure, and placement of structo-pendent and structo-terminal functionality for conjugation of active agents and targeting moieties. The relevance of water-soluble and amphiphilic (co)polymers synthesized by RAFT for *in vitro* delivery of therapeutics in biological fluids is an especially attractive feature. In many cases, polymerization, binding, conjugation, and stimulus-induced release can be accomplished directly in aqueous media. However, specific problems, barriers, and challenges regarding rational design of polymeric delivery systems for therapeutic siRNA still exist.

This dissertation focuses on RAFT synthesized (co)polymers as vectors and functional constructs to overcome delivery challenges. In section I, a modular copolymer consisting of HPMA and glutamic acid was synthesized to overcome hurdles of endosomal escape. Glutamic acid undergoes a coil-to-helix transition at endosomal pH-values, and these helices were stabilized with HPMA. As a proof-of-concept, the pH-responsive constructs demonstrated membrane disruption *via* red blood cell hemolysis and dye release from fluorescein-loaded POPC vesicles. In section II, hydrophilic-*block*-

cationic copolymers were complexed with siRNA to ascertain the structure-property relationships governing siRNA release from block ionomer complexes (BICs). It was determined that the stability of the complexes, which increases with increasing cationic block length, delayed the time required to achieve gene suppression. These results indicated that decomplexation was facilitated *via* an ion exchange/substitution mechanism. In section III, AS1411, an anticancer biologic, was delivered utilizing hydrophilic-*block*-cationic copolymers. The prepared BICs were found to be monodisperse (PDIs < 0.1) and charge neutral (i.e., N:P = 1). The anti-proliferative ability of AS1411 was then assessed utilizing hydrophilic-*block*-cationic copolymers as delivery vehicles. After 72 h, AS1411 demonstrated successful cellular inhibition; however, negligible anti-proliferative activity was witnessed when AS1411 was delivered utilizing hydrophilic-*block*-cationic copolymers. This reduction in drug activity was attributed to reduction of available drug caused by increased BIC stability as was determined in Section II.

The University of Southern Mississippi

UTILIZATION OF AQUEOUS RAFT PREPARED COPOLYMERS TO IMPROVE ANTICANCER DRUG EFFICACY

by

Andrew Christopher Holley

A Dissertation
Submitted to the Graduate School
of The University of Southern Mississippi
in Partial Fulfillment of the Requirements
for the Degree of Doctor of Philosophy

Approved:

Dr. Charles L. McCormick
Committee Chair

Dr. Sergei I. Nazarenko

Dr. Derek L. Patton

Dr. Daniel A. Savin

Dr. Faqing Huang

Dr. Karen S. Coats
Dean of the Graduate School

December 2014

ACKNOWLEDGMENTS

My sincerest gratitude goes to my research advisor Dr. Charles L. McCormick, for giving me the opportunity to perform research under his guidance. I specifically thank him for providing an environment which supports and fosters independence, problem solving, and creativity. These features allowed for me to develop into a more well-rounded scientist than I could have possibly dreamed, and no amount of words can adequately convey my appreciation. I also thank Dr. Faqing Huang for allowing me to work in his laboratories, his thoughtful discussions, and most importantly, his time. Additionally, I thank the rest of my committee Dr. Derek Patton, Dr. Daniel A. Savin, and Dr. Sergei Nazarenko for their support and guidance. I could not have chosen a better committee group, and they have been a blessing.

I cherish the interactions that I have had with both past and present McCormick group members. I specifically thank Dr. Deedee Smith, Dr. Wenming Wan, Dr. Adam W. York, Dr. Matthew G. Kellum, Dr. Joel D. Flores, Dr. Anthony Convertine, Brooks A. Abel, and Keith H. Parsons. I also give appreciation to Sarah Exley for reading my documents for “clarity” and for numerous discussions/arguments about our favorite books. From her efforts, she has helped me become a much better writer.

I am forever indebted to Dr. Austin Baranek and Dr. Joshua Hanna. Without their friendship, life during graduate school would have been meaningless and monotonous. They will remain life-long friends, and I thank them from the bottom of my heart.

I also thank my collaborators Dr. G. Reid Bishop, Dr. Jacob G. Ray, Dr. John J. Correia, Dr. Randy Wadkins, and Dr. Daniel F. Lyons. Without these individual's energy and knowledge, I would not have succeeded in my research efforts. More specifically, without Dr. Bishop's guidance, support, and friendship, I would not be where I am today.

Furthermore, I thank Dr. Vijay Rangachari and Dr. William J. Jarret for the use of the circular dichroism spectropolarimeter and NMR assistance, respectively.

I gratefully acknowledge research funding from the MRSEC and EPSCoR programs of the National Science Foundation.

Most importantly, I am very thankful to my family and friends. Without their love and encouragement, I would have failed many years ago, and I also thank them for the man that I have become.

Last but certainly not least, I thank Dana Froelich for her support both in an academic setting and as a dear friend. Without her diligence, this research would not have been possible, and without her shoulder, I would still be at rock bottom.

TABLE OF CONTENTS

LIST OF TABLES

Table

LIST OF ILLUSTRATIONS

Figure

LIST OF SCHEMES

Scheme

LIST OF EQUATIONS

Equation

LIST OF ABBREVIATIONS

AIBN	2,2-Azobis(2-methylpropionitrile)
Abs	absorbance
APMA	N-(3-aminopropyl) methacrylamide hydrochloride
*a*RAFT	aqueous reversible addition fragmentation chain transfer
ASEC	aqueous size exclusion chromatography
ATRP	atom transfer radical polymerization
AUC	analytical ultracentrifugation
AuNP	gold nanoparticle
BICs	block ionomer complexes
BLGA	γ-benzyl-L-glutamate
BMA	butyl methacrylate
CD	circular dichroism
Comp	composition
C_p	heat capacity
CPADN	cyanopentanoic acid dithionaphthalenoate
CRP	controlled radical polymerization
CTA	chain transfer agent
CTP	4-cyanopentanoic acid dithiobenzoate
Cy3	cyanine-3
DAPI	4’,6-diamidino-2-phenylindole
diNHS-FA	di-N-hydroxysuccinimide-folate
DCC	N,N’-dicyclohexylcarbodiimide
DCT	dodecyl cyanovalerictrithiocarbonate

DLS	dynamic light scattering
DMA	N,N-Dimethylacrylamide
DMAEA	N,N-(2-dimethylaminoethyl) acrylate
DMAEMA	N,N-(2-dimethylaminoethyl) methacrylate
DMAPMA	N,N-(3-dimethylaminopropyl) methacrylamide
DMF	dimethylformamide
DMSO	dimethyl sulfoxide
DNA	deoxyribonucleic acid
DP	degree of polymerization
DSC	differential scanning calorimetry
dsDNA	double stranded deoxyribonucleic acid
dsRNA	double stranded ribonucleic acid
DTT	dithiothreitol
ε	molar extinction coefficient
EDTA	ethylenediaminetetraacetic acid
EPR	enhnaced permeation and retention effect
FA	folic acid or folate
FAM	6-carboxyfluorescein
FBS	fetal bovine serum
FCS	fetal calf serum
fPOPC	fluorescein POPC
ΔG	gibb's free energy
GAPDH	glyceraldehyde 3-phosphate dehydrogenase
GFP	green fluorescence protein

GLuc	gaussia luciferase
GNPs	gold nanoparticles
H*b*C	hydrophilic-*block*-cationic
ΔH_{Cal}	calorimetric enthalpy
HPLC	high pressure (performance) liquid chromatography
HPMA	N-(2-hydroxypropyl)methacrylamide
ΔH_{VH}	van't Hoff enthalpy
IONPs	iron oxide nanoparticles
IPECs	interpolyelectrolyte complex
KB	human epidermal cancer cells (nasopharynx)
macroCTA	macro chain transfer agent
MALLS	multi-angle laser light scattering
M_n	number-average molecular weight
mRNA	messenger ribonucleic acid
MTT	3-(4,5-dimethylthiazol-2-yl)-2,5-diphenyltetrazolium bromide
MW	molecular weight
M_w	weight-average molecular weight
MWCO	molecular weight cut-off
NCA	N-carboxyanhydride
NHS	N-hydroxysuccinimde
N:P	nitrogen to phosphate ratio
nt	nucleotide
NIPAM	N-isopropylacrylamide
NMR	nuclear magnetic resonance

OEGA	oligo(ethylene glycol) acrylate
PAA	poly(acrylic acid)
PBS	phosphate buffered saline
PC	polycarbonate
pDbB	P(DMAEMA-*b*-BMA)
PDI	polydispersity index
PEG	poly(ethylene glycol)
PEGA	poly(ethylene glycol) acrylate
PEI	poly(ethylene imine)
POPC	1-plamitoyl-2-oleoyl-sn-glycero-3-phosphocholine
pSMA	poly(styrene-alt-maleic anhydride)
RAFT	reversible addition fragmentation chain transfer
RBC	red blood cell
RISC	RNA-induced silencing complex
ROP	ring-opening polymerization
RNA	ribonucleic acid
RNAi	ribonucleic acid interference
ΔS	entropy
SFRP	stable free radical polymerization
siRNA	small interfering ribonucleic acid
SLS	static light scattering
SPDP	N-succinimidyl 3-(2-pyridyldithio) propionate
ssDNA	single stranded DNA
TBE	trisborate EDTA

TEA	triethylamine
TFA	trifluoroacetic acid
T_m	melting temperature
Uv/Vis	ultraviolet/visible
V-501	4,4’-azobis(4-cyanovaleric acid)
VEGF	vascular endothelial growth factor

CHAPTER I

INTRODUCTION

The targeted delivery of nucleic acid-based therapeutics has recently become one of the most active areas of research in the rapidly developing field of nanomedicine. Unprecedented advances in synthetic polymer chemistry over the last decade now allow for precise control of macromolecular structure and thus rational design of biologically-relevant carriers with functional components engineered to aid in stabilization, trafficking and stimulus-induced release of "packaged" therapeutic agents. This chapter will focus exclusively on synthetic (co)polymers and their conjugates prepared *via* controlled radical polymerization (CRP) that have potential for therapeutic delivery of small interfering RNA (siRNA). Criteria for efficient delivery and efficient gene "knockdown" through the RNA interference (RNAi) are presented based on current understanding of cellular delivery pathways. Emphasis is placed on synthetic carrier structures and features of controllable segments which lend themselves to polyplex formation, siRNA packaging, targeting, uptake, endosomal escape, and delivery to messenger RNA (mRNA) targets.

Although research with siRNA/CRP polymers is in its infancy relative to more mature areas of DNA therapy, rapid growth is forecasted due to fewer intra-cellular barriers to delivery and to the structural control afforded by new synthetic techniques, often accomplished directly in aqueous media. It is interesting to note from a historical perspective that discoveries of the RNA interference (RNAi) pathway[1] and reversible addition-fragmentation chain transfer (RAFT) polymerization[2] were both reported in 1998.

Rational Design of Polymer-Based Delivery Vehicles

The concept of tailoring synthetic polymer vehicles (vectors) for site-selected delivery and release of therapeutic agents was pioneered by Ringsdorf over 35 years ago.[6] He and his colleagues suggested a simple "depot" model (Figure 1) in which the therapeutic agent could be attached in a facile manner *via* a hydrolytically- or enzymatically-degradable spacer to a water-soluble, non-immunogenic (co)polymer backbone having requisite components for complex protection, solubility and circulation under physiological conditions. Therapeutic cargo could be trafficked either passively or actively (the latter by including targeting moieties) to specific "depot" sites for stimulus-induced release as directed by endogenous cell components. The model was later extended for attachment of a diagnostic component to track location of the carrier, thus setting the stage for dual purpose theranostic (therapeutic/diagnostic) vehicles. The concepts of this seminal model remain at the forefront of rational design strategies for polymeric vehicles utilized for pharmaceutical delivery, including siRNA therapeutics. However, only recently have facile polymerization and orthogonal chemistries been developed that yield precise architectures, segment lengths, selected sizes, functionality, and narrow molecular weight distributions required. For example, the CRP syntheses of well-defined (co)polymers with pH-responsive, tertiary and secondary amine segments necessary for reversible polyplex formation with polynucleotides have recently been reported.[7] More specifically, rationally-designed siRNA polyplexes with targeting moieties have shown therapeutic potential *in vitro* as demonstrated by cell-specific delivery and gene silencing *via* the RNAi pathway. It should be noted that despite fundamental distinctions of nucleotide structure and trafficking,[8] many of the recent approaches to siRNA delivery have precedence in DNA delivery utilizing a variety of

polymer types including classical, or controlled chain growth polymers, dendrimers, polymers from ring-opening polymerization, and those prepared from synthetic-bioconjugate techniques. Nano- and micro-structured particles, micelles, polymersomes, microemulsions, hydrogels, transition metal complexes, carbon nanotubes, and inorganic complexes have been reported. The reader is directed to a number of comprehensive reviews of these DNA delivery vectors.[9–20]

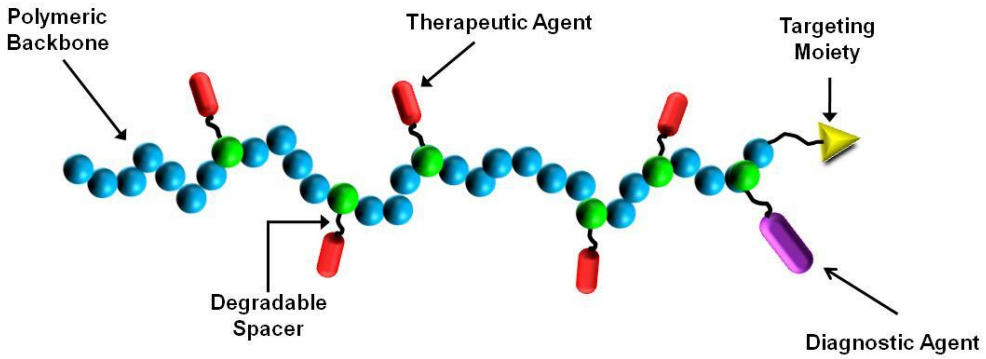

Figure 1. Components of the Ringsdorf "depot" model.

RNA Interference (RNAi)

RNA interference (RNAi) is a gene silencing effect induced by RNA duplexes that ultimately results in messenger RNA (mRNA) cleavage, thus inhibiting expression of target proteins. Importantly, RNAi potentially offers a pathway for therapeutic treatment of a variety of diseases including genetic, degenerative, and viral diseases as well as cancer.[21] In a recent Chemical Society Review,[22] Gaynor et al. present the mechanism of RNAi as currently understood. A simplified seven step pathway (Figure 2) is detailed that starts with the formation of siRNA duplexes generally 21–23 nucleotides in length and having a two-nucleotide overhang at the 3' end. The duplexes, which can be prepared synthetically or by endogenous processing of longer hairpin or double-stranded RNA (dsRNA), have precise sequences such that the antisense or "guide" strand is

complimentary to the target messenger RNA (mRNA) transcribed from the gene to be "silenced." The siRNA duplex associates with cytoplasm proteins and is trafficked to the RNA-induced silencing complex (RISC) for removal of the sense or "passenger" strand, thus activating the complex for target mRNA recognition and complementary binding. RISC contains a protein with endoribonuclease activity that cleaves the mRNA backbone specifically between nucleotides 10 and 11 relative to the 5' end of the guide strand. Ideally, after dissociation from the cleaved mRNA, recycled RISC can then target other mRNA strands. For further discussion of kinetics, biodistribution, stabilization, cellular uptake, chemical modification, possible interferon response, and off-target effects operative in RNAi, the reader is referred to several recent reviews.[21–29]

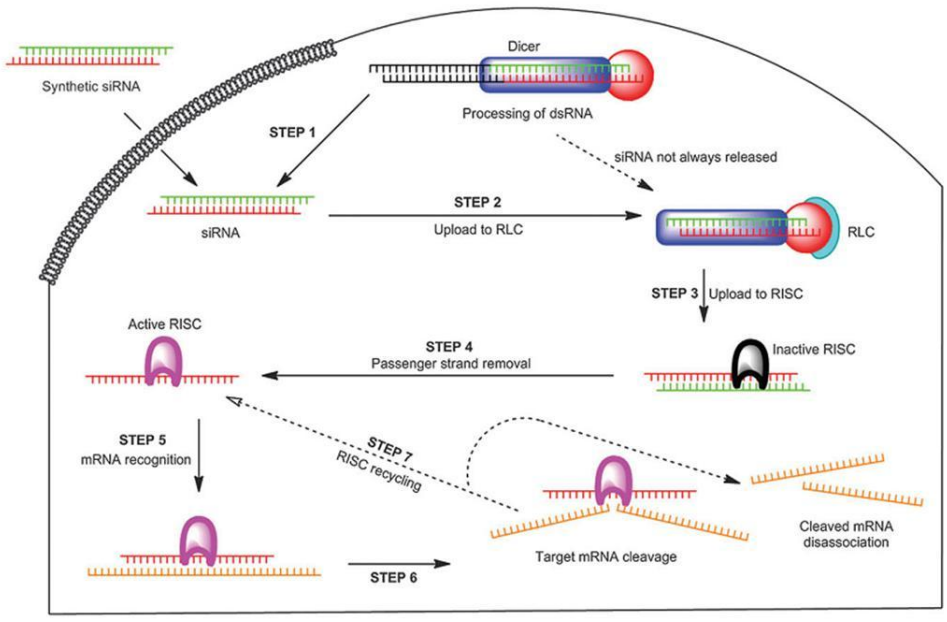

Figure 2. The RNA interference (RNAi) pathway.[22]

Barriers to siRNA and General Approaches to Therapeutic Delivery

RNAi therapy has been highly touted due to its simplicity (relative to other forms of oligonucleotide intervention) and applicability to a large number of diseases. Advantages are that interference occurs at the translational rather than the transcriptional level, relatively small doses of siRNA are required, and lower toxicity is generally observed. However, efficient delivery necessitates overcoming significant barriers (Figure 3) that stem from the physicochemical properties of siRNA and systemic interactions during trafficking to cytoplasm targets.[23–29]

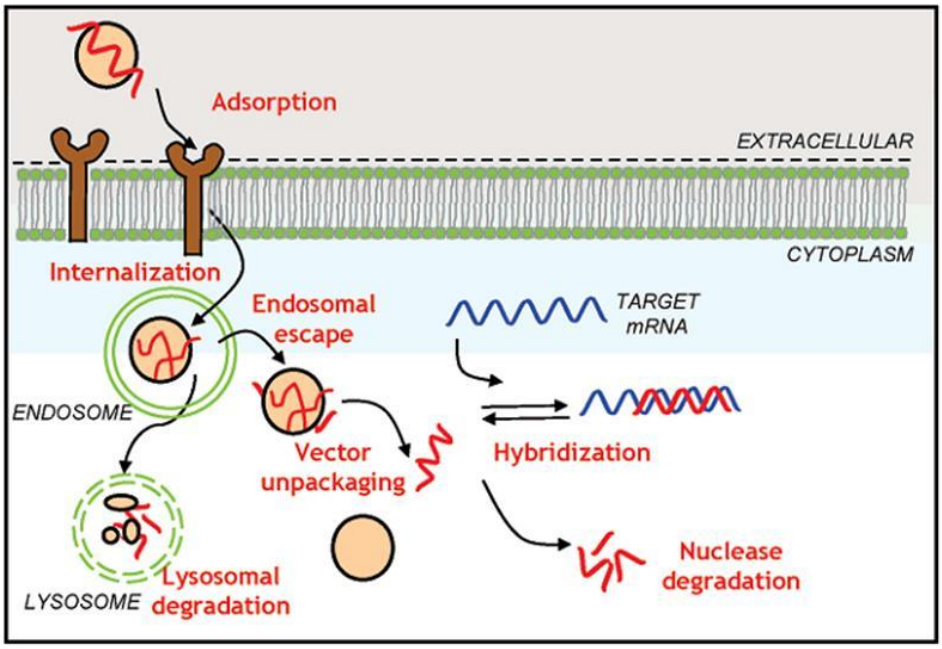

Figure 3. Cellular barriers to oligonucleotide delivery.[21]

Cellular delivery of siRNA and other polynucleotide therapeutics has been accomplished utilizing a number of viral and non-viral vectors.[10,12,19,20] Controlled polymer-based carriers, the focus of this review, are designed to eliminate or suppress repulsive electrostatic interactions between double stranded siRNA and the cellular

surface.[8,26,28] The formation of interpolyelectrolyte complexes (IPECs or polyplexes) between therapeutic RNA and cationic polymer segments, not only accomplishes this, but also may induce compaction of longer dsRNA while conferring protection from endonucleases encountered in RNAi. Cellular entry can occur by non-specific or targeted polyplex uptake. Wong et al. recently reviewed several pathways for endocytic uptake in polymer-mediated gene delivery: phagocytosis, macropinocytosis, clathrin-mediated endocytosis, caveolae-mediated endocytosis, and clathrin- and caveolae-independent endocytosis.[19] Although all of the above result in enclosure of the polyplexes within transport vesicles formed from the plasma membrane, subsequent trafficking and processing modes are different and the factors determining the specific pathway are not well elucidated at this point. Most studies so far have dealt with DNA, and there are likely to be differences between DNA and siRNA polyplex internalization based on size and interpolyelectrolyte registry. However, there are some structural similarities that may be identified. In general, non-specific endocytosis can be triggered by (a) charge-mediated interactions of cationic polyplexes with sulfated or carboxylated glucosamine residues on membrane-bound proteoglycans and/or (b) hydrophobic associations of lipophilic residues on the complex with the phospholipid layers of the cell membrane.[19,28] Recently, cell penetrating peptides, 5 to 40 amino acids in length with amphipathic and cationic segments have shown potential for binding polynucleotides and facilitating membrane translocation.[30] These peptides may enter non-specifically into the phospholipid membrane by several postulated mechanisms including: formation of peptide-lined pores, direct penetration, transient uptake, and induced endocytosis.[30]

Targeted delivery is accomplished by incorporating ligands that bind to receptors on the cell surfaces. Receptor-mediated targeting and delivery of therapeutics to specific

cell lines has been widely studied utilizing a plethora of targeting ligands including endogenous folate and transferrin and exogenous peptides, glycoproteins, and antibodies.[21,28,29] To date, however, only a few of these have been reported for targeted delivery of siRNA utilizing CRP carriers.[22,23,25]

Once cellular uptake has occurred, the resulting polyplex-bearing vesicle may be recycled to the surface, routed to cellular organelles, or participate in the endo-lysosomal pathway.[28] As illustrated in Figure 3, the polyplex must escape the endosome vesicles before the latter mature to lysosomes in order to avoid enzymatic degradation. The maturation of the early endosomes to lysosomes is accompanied by a pH reduction from ~6 to ~5.[22] As such, polymers with pH responsive amine segments (pKa values from 5 to 7) have been utilized in the polyplex to act as a "proton sponge." Protonation results in osmotic swelling and disruption of the endosome and release or "escape" of the polyplex to the cytoplasm.[22,28] Peptides that undergo coil-to-helix transformations as pH is lowered have also been conjugated to polymeric carriers to induce disruption of the endosomes.[21,23,25] After endosomal escape, polyplex dissociation must occur in order to enter the RNAi pathway.[28] Reduction of strength of interpolyelectrolyte complexes has been the most common method of choice to date. Polymer architecture (linear, star, dendrimer, branched, etc.), registry and spacing of charges, molecular weight, amphiphilicity, reversible cross-linking and other structural characteristics can, in principle, be altered to effect facile dissociation.[21–23,28]

While many laboratory and clinical studies have reported remarkable advances in nucleic acid delivery using both classical polymers and those with designed, precise architectures, there is a clear need for tailored siRNA delivery vehicles that are dynamic, responding to *in situ* stimuli encountered in delivery to specific cell types. Given the

large number of structural variables and possible cellular interactions identified in the literature to date, Roth[28] has proposed an "integrated mathematical modeling" approach to rational design of delivery vehicles. His approach involves development of kinetic models of antisense and siRNA silencing by first describing oligonucleotides and their targets in discrete locations or "compartments" within the cells. Differential equations based on conservation of mass are then derived for each of the relevant species, for example polymer-bound, free, and mRNA-hybridized siRNA in either endosome or cytoplasmic environments. Roth has typically employed 10 species and 20 parameters, the latter measure or derived from literature reports, to develop his models. Some knockdown experiments in specific cell lines appear to validate these models.[30] Successful implementation of such approaches can be anticipated in the future and will be aided by rapidly evolving analytical methods capable of elucidating cellular entry and trafficking mechanisms.

Controlled Radical Polymerization (CRP) and Therapeutic Vehicle Design

Carrier vehicles designed with criteria consistent with the Ringsdorf "depot" model, previously introduced and shown in Figure1, possess essential modular components: a water-soluble or amphiphilic polymer backbone, therapeutic agent binding sites, and pendent targeting and/or diagnostic moieties. Initial progress toward optimal design based on such models was restricted by the absence of sufficiently facile polymerization techniques affording control over molecular weight, molecular weight distribution, placement of structo-pendent or structo-terminal reactive functional groups, polymer architecture (blocks, stars, etc.), and solubility. As controlled radical polymerization (CRP) techniques, including stable free radical polymerization (SFRP),[30] atom transfer radical polymerization (ATRP),[31] and RAFT[32–34] have evolved during the

last few years, additional tools for rational design of delivery vectors with the above requisite parameters have become available. RAFT and more specifically its aqueous counterpart aqueous reversible addition-fragmentation chain transfer (*a*RAFT)[4,5,35] are arguably the most relevant of the known CRP techniques for preparing delivery vehicles for use in biological fluids. Not only are these particularly versatile for polymerizing a wide range of charged and reactive monomers, in many cases polymerization, conjugation, therapeutic loading, targeted delivery, and stimuli-responsive release can all be accomplished directly in aqueous media.[35]

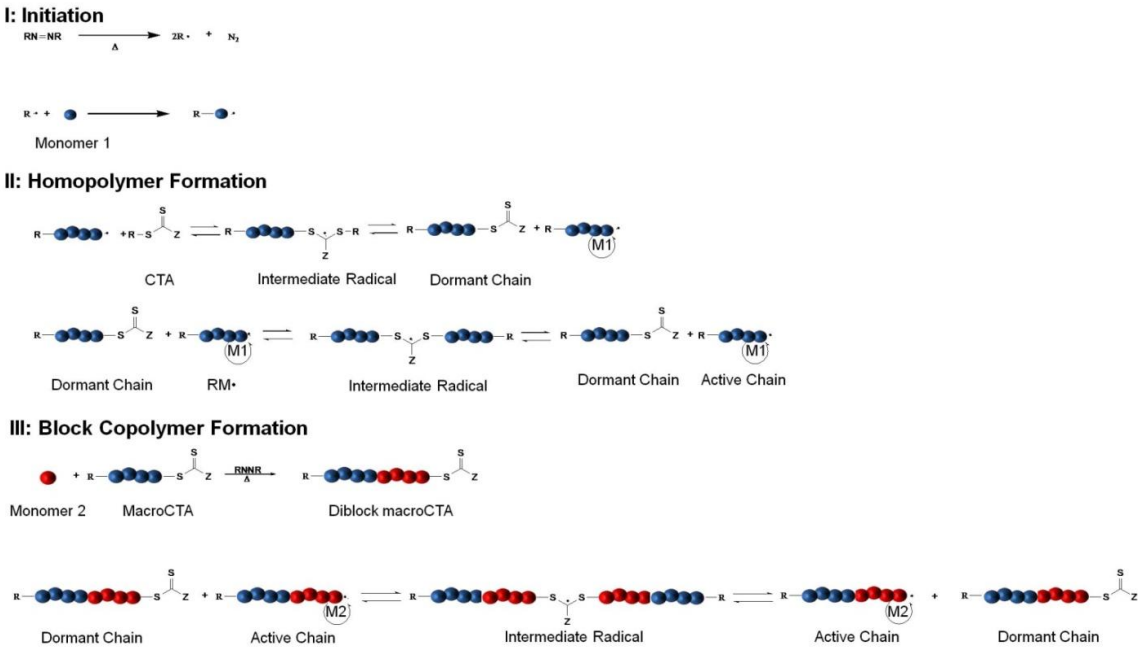

Figure 4. Key steps in formation of homo- and block copolymers via RAFT polymerization.

Key steps in the RAFT polymerization process, first proposed by the CSIRO group[2] and later adapted specifically for water,[4,5] are shown in Figure 4 in order to illustrate the method's utility for synthesizing modular, water-soluble therapeutic delivery vehicles discussed in this review. RAFT polymerization is a degenerative chain transfer

process that begins in step I, Figure 4 when an initiator, for example a water-soluble diazo initiator, decomposes to yield a primary radical, R•, which then adds to a water-soluble monomer 1. In step II, a chain transfer agent (CTA), a thiocarbonylthio compound, reacts with the primary oligomeric radical to produce an intermediate radical that subsequently eliminates R• which in turn adds to monomer 1. The CTA is key to control of molecular weight and ”livingness“ of the RAFT process and various thiocarbonylthio species including dithioesters, xanthates, dithiocarbamates, and trithiocarbonates have been utilized.[32–34] The degree of stabilization of the intermediate radicals in steps II and III of Figure 4 depends on the nature of Z as does the rate of R• or kinetic chain scission from the intermediate for subsequent addition to monomer 1. Active (propagating) radicals eventually reach equilibrium with dormant chains, termed macroCTAs. The reversible nature of the degenerative process, the equilibrium favoring the dormant chains, and the apparent inability of the intermediate radical to add to monomer result in the polymerization having a “living” nature with degree of polymerization increasing linearly with conversion. MacoCTAs can be extended, for example, by the sequential addition of a second water-soluble monomer as shown in step III of Figure 4, resulting in the formation of stimuli-responsive block copolymers.[7,35]

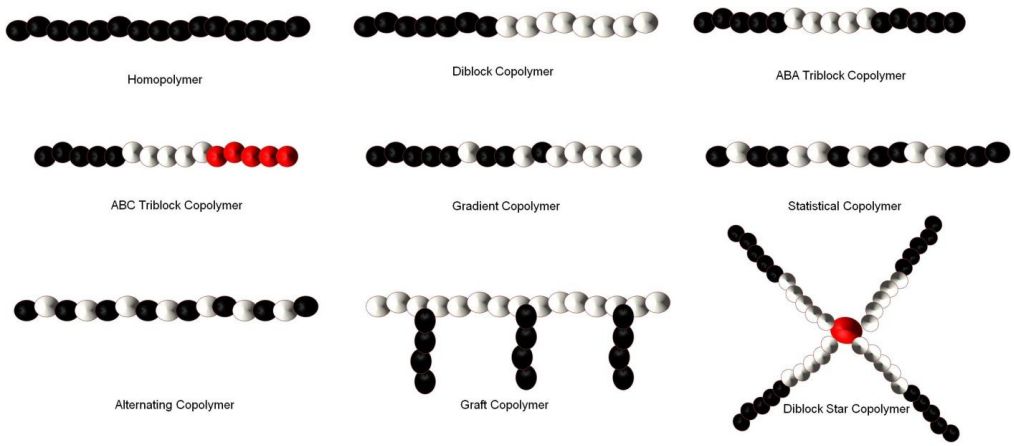

Figure 5. Varying architectures from CRP techniques amenable to siRNA binding.

An important advantage of RAFT and other CRP polymerization techniques is the ability to prepare well-defined polymers with specified architectures (Figure 5). Of interest to siRNA therapeutics are diblock, triblock, brush, and star architectures prepared from amine-functional monomers that can be synthesized *via a*RAFT directly in water without the need for protecting groups.[7] R and Z functionality can be altered to allow structural variation as well as facile post-polymerization reactions.[35] The nature of the segments and the molecular weight-dependent hydrodynamic volume under aqueous conditions, in principle, can be critically controlled by selecting from a wide variety of water-soluble monomers,[7,35] designing CTAs and their conjugates,[36] and specifying the monomer/CTA ratios.[7,33–36] As detailed later, packaging and protection from enzymatic degradation have recently been accomplished by direct, molecular level complexation of siRNA with specified segments (for example those with cationic charges) or those presented on nano size, self-assembled complexes (e.g., micelles, vesicles, polymersomes and their conjugates and crosslinked versions). As mentioned previously, secondary and tertiary amine-containing segments are thought to elicit endosomal disruption and polyplex release by taking advantage of the "proton sponge" or buffering effect. For

example, interpolyelectrolyte complexes between siRNA and PDMAPMA (poly(3-(N,N-dimethylamino)-propyl methacrylamide)) (or other protonated tertiary amine segments of block copolymers)[37–44] can be prepared with varied nitrogen-to-phosphate (N/P) ratios, affecting not only solubility but also cell entry by non-specific endocytosis and eventual release from the endosome. Neutral, water-soluble monomers such as N,N-dimethylacrylamide (DMA)[45–48] or N-(2-hydroxypropyl)-methacrylamide (HPMA)[14,49–62] can be copolymerized statistically or as blocks in order to maintain water solubility and prevent rapid clearance from the blood stream. Amphiphilicity can be adjusted by adding hydrophobic monomers (e.g., butyl acrylate[38,39,63]) or those responsive to temperature (N-isopropylacrylamide (NIPAM))[64] or pH (secondary and tertiary amine-containing monomers).[37–44] AB diblock or ABA triblock systems of the type, shown in Figure 5, can be prepared utilizing dithioester or trithiocarbonate CTAs that have near-perfect end group functionality since the R group of the initiator and that of the CTA are identical. Such telechelic end groups can play important roles in attaching moieties for targeted delivery or for attaching diagnostic agents. Reactive functionalities, such as active esters, exchangeable disulfides, and primary amines, can also be readily accommodated by copolymerizing functional monomers *via* RAFT.[7,35] A number of recent papers and reviews discuss facile chemical or bioconjugation methods utilizing reactive monomers or CTAs with appropriate functionality (Figure 6).[13,42,65–71] Notable milestones allowing the construction of delivery vehicles were the first controlled polymer syntheses by Scales, Convertine, York et al. of the hydrophilic monomers DMA, HPMA, NIPAM and the protonated (cationic) DMAEMA, DMAPMA, and APMA monomers (Figure 6) *via* *a*RAFT polymerization.[45,52,72,73] Though beyond the scope of this chapter, the reader is referred to recent reviews of post-polymerization modification methods including

orthogonal “click” chemistries which have been or can potentially be utilized in delivery.[66,74–89]

Linear Polymer Vehicles

Literature reports of linear homopolymers with controlled structures utilized for gene delivery are almost exclusively on P(DMAEMA) synthesized *via* RAFT or ATRP.[90–97] However, as previously mentioned, complexes must be cationically-charged overall to maintain particle dispersion. Although this and favorable interactions at the cell surface promote uptake, problems of nucleotide release from the interpolyelectrolyte complex later in the process affect efficiency of delivery.[98,99]

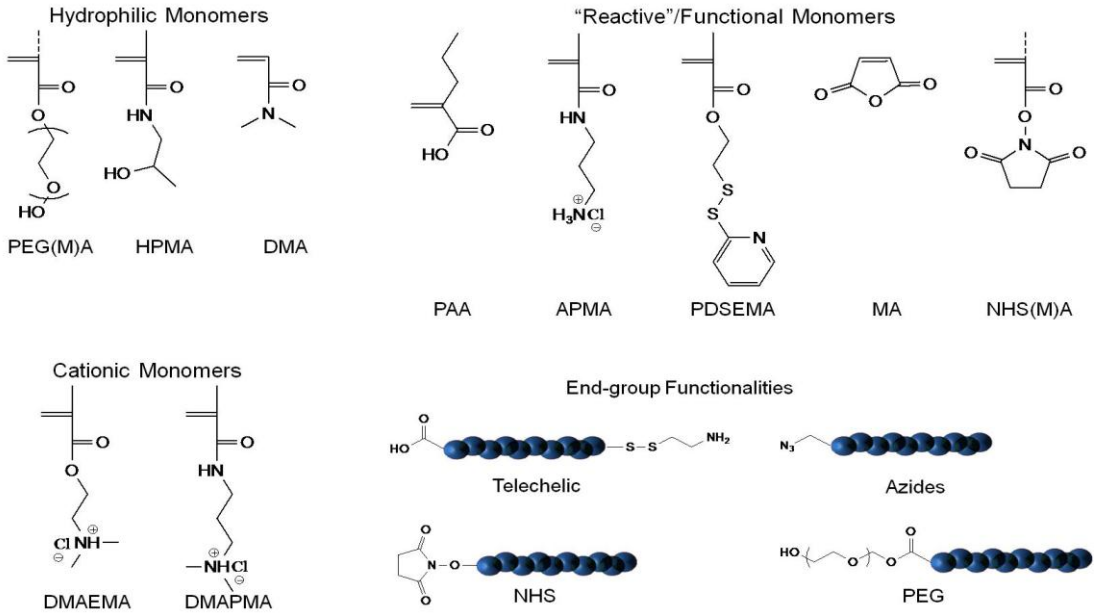

Figure 6. Reactive monomers and functional groups utilized for delivery vehicles prepared *via* RAFT Polymerization.

Perhaps the most widely studied systems for the delivery of siRNA have been block copolymers comprised of hydrophilic and cationic segments.[98,100–102] These copolymers can form near-neutral interpolyelectrolyte complexes with negatively charged

siRNA and have the added benefit of remaining soluble and stable in solution. However, while the hydrophilic block can increase stability/shielding and circulation time, it has also been shown to decrease uptake as compared to its positively charged counterparts.[98,103] To combat this problem, York et al. utilized targeting entities for receptor-mediated endocytosis.[42] Copolymers containing a cationic block of DMAPMA and a hydrophilic block of HPMA-*s*-APMA were synthesized for siRNA delivery (Figure 7). The APMA (N-(3-aminopropyl)methacrylamide hydrochloride) monomer has primary amine functionality for attaching a targeting group. These monomers were polymerized under buffered, aqueous RAFT conditions yielding copolymers of ~ 50 kDa with narrow polydispersity index (PDI) values of ~1.1. Folic acid, a well-known and extensively studied targeting group moiety,[104–108] was conjugated to the polymers *via* post-polymerization modification of the primary amines of APMA with efficiencies of > 80 %. The resulting targeted copolymer was then complexed with siRNA to yield near-neutral sterically protected complexes ~ 15 nm in diameter. These complexes were incubated with cell lines that expressed both high levels (KB cells) and low levels (A549 cells) of folic acid receptors. The targeted complexes showed high selectivity for KB cells and 60% knockdown of the gene coding for human *Survivin*.

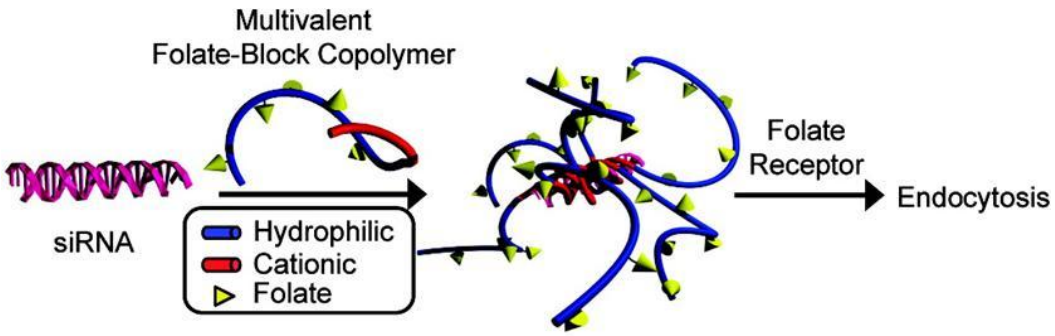

Figure 7.Poly[(HPMA-*statistical*-APMA)-*block*-DMAPMA] copolymers complexed with siRNA for targeted gene delivery.[43]

Folic acid serves as an excellent moiety to serve as a cellular targeting group, but there have been a few methods which utilize an alternative approach to promote cellular recognition. Utilizing a PEG macroCTA, Schultz and coworkers prepared poly(GPMA) which incorporated FAB antibody fragments at the α-terminus. These fragments targeted the HER2 receptor, a member of the epidermal growth factor family that is overexpressed in one-third of breast cancers, and cellular recognition was increased by 10-fold. As a consequence, a major reduction in mRNA and protein levels (> 90%) was achieved. Alternatively, mannose and cholesterol have been conjugated to RAFT synthesized block copolymers, and while these targeting ligands promoted efficacious delivery, these systems warrant further insight as the design of these systems provides methods to overcome additional barriers (*vide infra*).

One of the most significant bottlenecks in the delivery of siRNA to cells is release from endosomal compartments after uptake.[16,109–111] One strategy has focused on the post-polymerization conjugation of endolytic agents to the hydrophilic block of these copolymers.[111] However, even with the advent of facile and quantitative chemistries in recent years,[75,78,84,88,112,113] such post-polymerization modifications involving macromolecular species can be inefficient and produce undesired by-products. Both

quantifying yields and product characterization can prove difficult.[114] Therefore, direct polymerization of CRP monomers capable of undergoing stimuli responsive transitions to "unmask" endolytic properties, such as proton sponges or hydrophobic, membrane-disrupting moieties, is an attractive approach.

Convertine et al. designed an endolytic copolymer delivery system that contained a block of 2-(N,N-dimethylamino)-ethyl methacrylate (DMAEMA) for complexation with siRNA and an ampholyte block containing butyl methacrylate (BMA), DMAEMA, and poly(propylacrylic acid) (PAA) to act as both a shielding/stabilizing and pH-responsive block.[39] The RAFT- synthesized terpolymers ranged in molecular weight from 16 kDa to 20 kDa with moderate PDIs (1.45–1.58). Despite the statistical nature of the hydrophobic block, DMAEMA and PAA were chosen to be 1:1 for neutrality, while BMA was varied to modify hydrophobic content. At physiological pH, no higher ordered structures were formed prior to the addition of siRNA. At N:P ratios of 1:1, only large aggregates were identified by dynamic light scattering (DLS), with a reduction in particle size at increasing charge ratios. Particle sizes ranged from 85–236 nm with the highest BMA content (48 mol%) giving rise to the smallest particles at N:P ratios of 4:1. Despite the higher nitrogen content, surface charge of these particles remained near neutral. The endolytic activities of these copolymers and IPECs were investigated using a red blood cell hemolysis assay at varying pH values, representing physiological conditions, early endosome, and late endosome. At physiological pH, no endolytic activity was observed due to the charge neutrality of the ampholyte block. Polymers containing the most BMA content demonstrated the greatest degree of hemoglobin release at both early and late endosomal pH. Upon acidification of the endosomal compartment, it is predicted that the carboxylic acid residues are protonated, resulting in a more hydrophobic block with an

overall net positive charge that is likely to interact with the membrane. Knockdown of GAPDH (glyceraldehyde 3-phosphate dehydrogenase – an enzyme that catalyzes glycolysis and is implicated in several non-metabolic processes, including transcription activation, initiation of apoptosis and ER to Golgi vesicle shuttling) was investigated in HeLa cells and ranged between 50–80 % depending on the polymer and formulation.

They have further modified these systems to maintain endosomolytic capability, but also, to produce polymeric carriers that offer neutral delivery of siRNA.[115] A thiolated siRNA targeting GAPDH was conjugated to poly[HPMA-*co*-PDSMA)-*block*-(PAA-*co*-DMAEMA-*co*-BMA)] (Figure 8) via a pendent disulfide exchange in the PDSMA block. The second block confers endosomolytic capability, and siRNA release occurs *via* intracellular reduction with glutathione. Under optimized conditions, a 90 % reduction in mRNA and a 60 % reduction in protein levels were achieved after 48 h. These researchers have been prolific in designing these systems, and many reports utilize the PAA/DMAEMA/BMA combination to achieve endosomal escape.

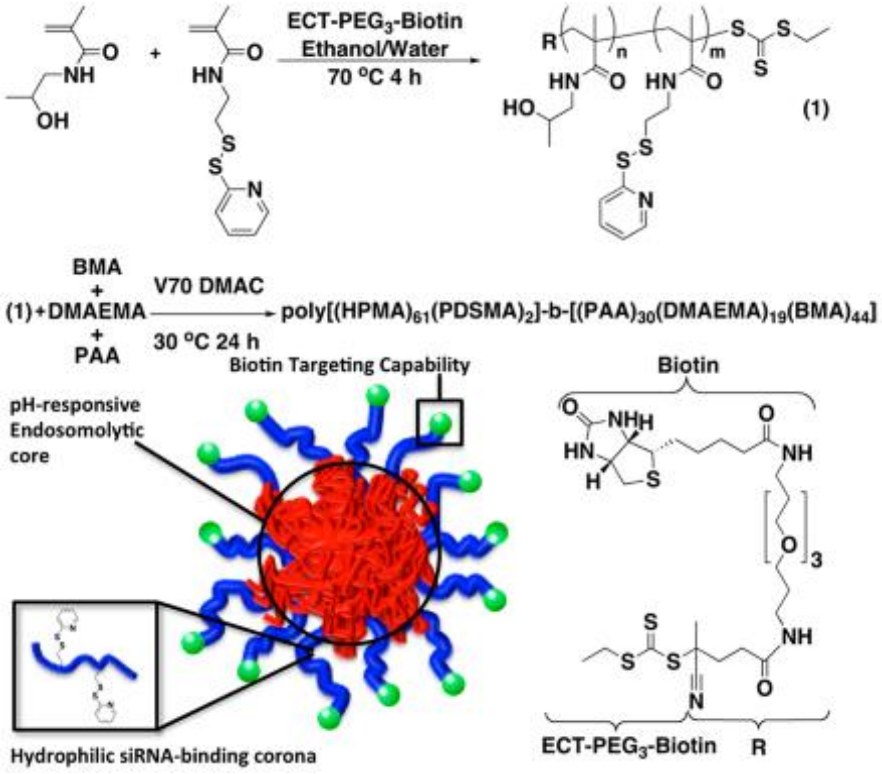

Figure 8. Preparation of poly[(HPMA-co-PDSMA)-b-(PAA-co-DMAEMA-co-BMA)] polymeric carriers for neutral delivery of siRNA.[115]

While most polymeric vehicles are designed to overcome delivery barriers, only one report focuses both on delivery challenges as well as economic viability. Reineke and coworkers[116] prepared poly(trehalose-b-AEMA) copolymers, and the rationale behind these constructs was to solve long-term storage of siRNA-polymer complexes. Trehalose, a disaccharide consisting of glucose, protects cells during oxidative stress and freezing, and it aids in cryptobiosis. The primary amine block AEMA serves to bind siRNA, while the trahalose segments confers long-term stability. Copolymer-siRNA complexes were reported to retain potency after lyophilization as demonstrated *via* luminescence assays on U-87 cells containing Gaussia Luciferase. Modest gene knockdown was observed for these systems (~ 60% reduced protein expression), but the fact that these systems remained active after long-term freezing (1 month) is remarkable.

Polymer Micelle Vehicles

The complexation of siRNA with cationic polymers results in spontaneous assembly of IPECs. It is known from the literature that the resultant size and distribution of these complexes is highly dependent upon the length of the charged segments, the total length of the polymer, and the conditions under which they are prepared.[7,117–124] Scales et al. have shown that in particular instances, a single siRNA molecule can be surrounded by multiple polymers, significantly limiting the therapeutic loading of these types of vectors.[41] Ideally, the incorporation of multiple siRNAs per polymer complex is desirable to increase the therapeutic efficiency while maintaining control over the size, shape, and distribution of the carrier.

One way to accomplish this is by the formation of the vehicle before loading the therapeutic agent. The formation of well-defined micelles and vesicles from polymers prepared *via* controlled polymerization methods is well established.[7,67,73,100,117–122,124–140] In addition to allowing for control over the size and size distribution of the vehicle, the use of micelles/vesicles as gene delivery vehicles also can mitigate toxicity. Typically cationic (co) polymers exhibit *in vitro* toxicity that increases with molecular weight and cationic charge density, both of which also increase complexation and gene knockdown ability. Utilizing lower molecular weight components, higher ordered structures can degrade/dissociate into less toxic components. Though limited by the dynamic nature of such associated entities, it has been reported that the use of nucleic acids as crosslinking polyanions can result in sufficiently stable complexes.[38,43,63,100,122,137]

In an extension of the work by Stayton and coworkers mentioned previously, micelles capable of complexing with siRNA in the corona while containing an endosomal release component in the core were prepared via RAFT polymerization.[38] The corona

consisted of DMAEMA while the core block was composed of statistically incorporated BMA, PAA, and DMAEMA (Figure 9). The hydrophobic block was synthesized to be approximately 2.5 times larger than the hydrophilic block, and the optimum incorporation of BMA was found to be approximately 50% in the hydrophobic block. Particle sizes of the resulting micelles were 45 nm at pH 7.4, and upon the addition of siRNA (N:P = 4), particle sizes remained fairly consistent at 47 nm.

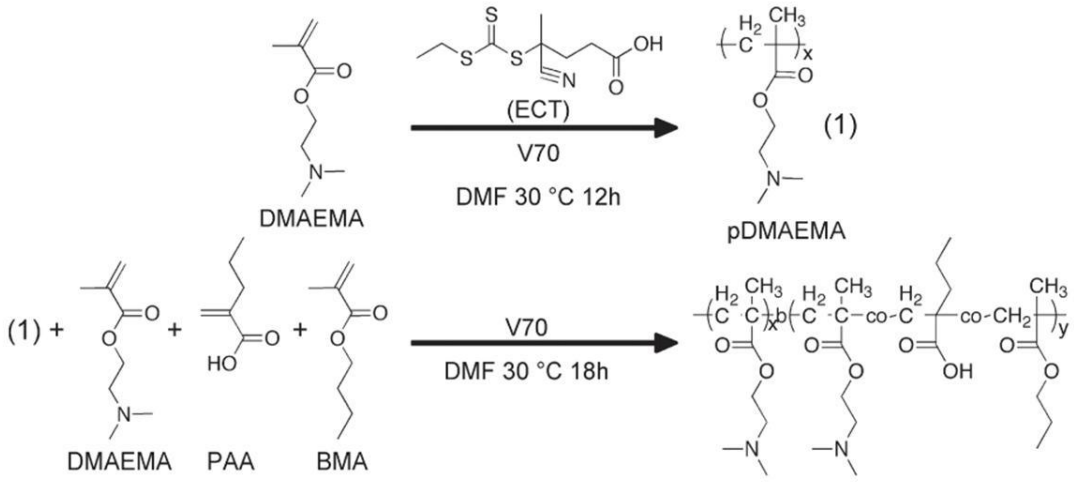

Figure 9. RAFT synthesis of hydrophilic, cationic DMAEMA macroCTA and subsequent chain extension for the preparation of an endolytic and polyampholyte block (which incorporates DMAEMA, PAA, and BMA).[39]

Membrane destabilizing ability was investigated using a red blood cell hemolysis assay. Three pH conditions were chosen to mimic cellular internalization: pH = 7.4 (extracellular), pH = 6.6 (early endosome), and pH 5.8 (late endosome). No significant hemolytic activity was observed at pH 7.4, while decreasing pH below 7.4 resulted in increasing hemolytic activity. siRNA was complexed at various N:P ratios to account for any change that might be displayed in hemolytic activity due to charge-charge interactions, and none was observed even at high N:P ratios (N:P = 8). Additionally,

differences in hemolytic activity between linear and assembled polymer solutions were negligible. Gene knockdown experiments were performed in HeLa cells with varying polymer (above and below the critical micelle concentration) and siRNA concentrations (12.5 nM–100 nM). The greatest knockdown was observed with micelles at the highest siRNA concentrations, <90%. Investigation of uptake using FAM-labeled (6-carboxyfluorescein) siRNA revealed that almost 100% of cells were transfected by micelles, compared to only 25% in the previous study with the linear polymer system.[38]

Monteiro and coworkers[141,142] prepared micellular nanocarriers which would self-catalyze their own degradation. Utilizing *a*RAFT, poly[DMAEMA$_{65}$-*block*-(ImPAA$_{45}$-*co*-BA$_{29}$)] copolymers (Figure 10) were prepared that served two functions: endosomal escape and "timed" siRNA release. The first block contains DMAEMA, which self-catalyzes hydrolysis, forming poly(acrylic acid), and this block was tuned to promote siRNA release over the course of 48 h. The release of siRNA is maximized *via* the "charge-shifting" approach; which takes advantage of charge repulsion between ionized poly(acrylic acid) and the anionic phosphodiester backbone of siRNA. The second block promotes endosomal fusion and subsequent escape. The ImPAA and BA moieties behave similarly to the influenza virus, promoting endosomal escape *via* membrane disruption. The siRNA delivered targeted *PLK1*, a kinase that maintains tumorgenic phenotypes of osteosarcoma cells, and utilizing these block copolymers, upwards of 98 % cell death was reported. Furthermore, owing to the degradability of DMAEMA, these polymeric carriers exhibited negligible toxicity, even at polymer concentrations > 300 μg/mL.

Seeking to utilize the advantageous degradability of DMAEAMA, these coworkers, prepared polymeric carriers with a star architecture.[143] These star systems were prepared *via* chain extension of a DMAEMA macroCTA with a statistical

incorporation of bis-N,N-(acryloyl) cysteine and DMAEMA. These systems were shown to be nontoxic and biodegradable under physiological conditions. siRNA was delivered to two different cell lines: pancreatic cells (MiaPaCa-2-Luc2) and lung cancer cells *H460 NSCLC). Approximately 80% reduction in mRNA and protein levels were observed in the lung cancer cell line; however, delivery to pancreatic cells was less efficient with ~50% and ~60% reduction in mRNA and protein levels, respectively. Furthermore, these star systems demonstrated mild success *in vivo* with a 60% reduction in mRNA levels in mice exhibiting lung cancer (H460).

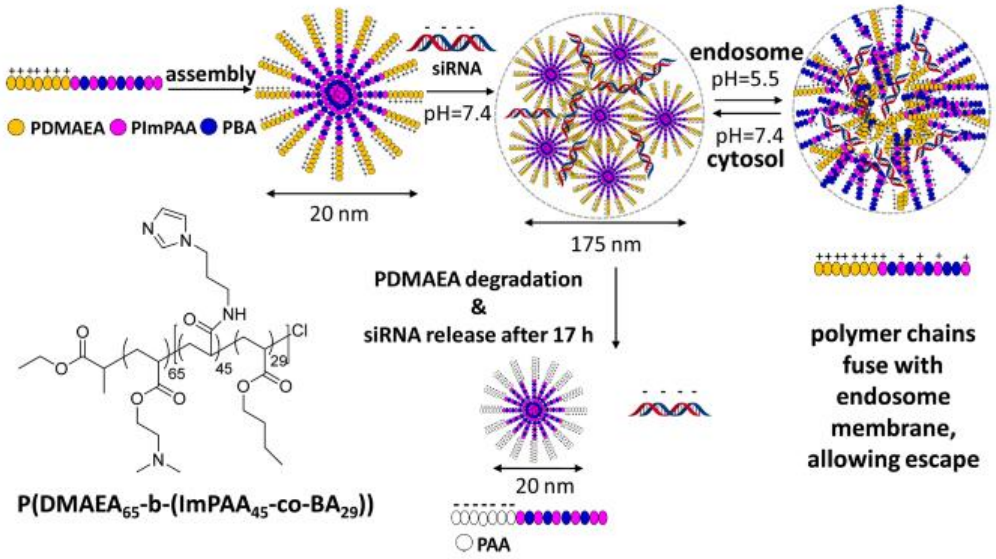

Figure 10. Preparation of poly[DMAEMA-b-(ImpAA-co-BA)] copolymers. These constructs contain a self-catalyzing mechanism that promotes siRNA release and an endosomolytic block.[143]

The use of higher ordered structures such as micelles and vesicles also present the additional option of incorporating multiple therapeutic agents. Micelles with hydrophobic cores can accommodate poorly-soluble drug payloads, while vesicles with hydrophilic cores can accommodate water-soluble drugs. Taking advantage of this option, Park and coworkers prepared biodegradable cationic micelles for co-delivery of

siRNA and paclitaxel.[44] ε-Caprolactone was polymerized (7 kDa, PDI = 1.26) and subsequently N,N'-dicyclohexylcarbodiimide (DCC)-coupled to 4-cyanopentanoic acid dithionaphthalenoate (CPADN) to prepare a macroCTA for RAFT polymerization of DMAEMA (**Figure 11**). Molecular weights ranged from 9.1 kDa to 21.1 kDa with PDIs ranging from 1.15–1.42. Micelles were prepared by direct dissolution into HAc-NaAc buffer (pH = 5.0) overnight and had CMC values of 15.8–24.0 mg/L. Particle sizes ranged from 54 nm to 132 nm, and possessed moderately positive surface charges (+29.3 mV to +35.5 mV). Complexation with siRNA was investigated using a gel retardation assay, and complete retardation was observed at N:P> 4:1. siRNA transfection was monitored in MDA-MB-435-GFP cells. The experiments were carried out utilizing N:P = 36:1 and N:P = 12:1 for the micelles, with PEI (poly(ethylene imine)) (25 kDa) and DMAEMA homopolymers utilized as positive controls. The micelles had much higher transfection ability as compared to the positive controls. Cytotoxicity of the micelles was investigated in PC3 cells. The micelles were loaded with paclitaxel (6.8 wt%), and possessed a higher drug efficacy than free paclitaxel which the author attributed to enhanced endocytosis of the micelles. Cells incubated with the free drug had viabilities of around 70%, whereas cells incubated with drug-loaded micelles had viabilities of approximately 50%, independent of the micelle concentration used. Co-delivery was investigated in PC3 cells with paclitaxel-loaded micelles complexed with siRNA at N:P = 24. Co-delivery resulted in 90% down-regulation of VEGF (vascular endothelial growth factor) expression whereas branched PEI exhibited 75% down-regulation. Interestingly, co-delivery of the therapeutic agents was slightly more efficient (90% vs. 80%) than micelle delivery of siRNA alone.

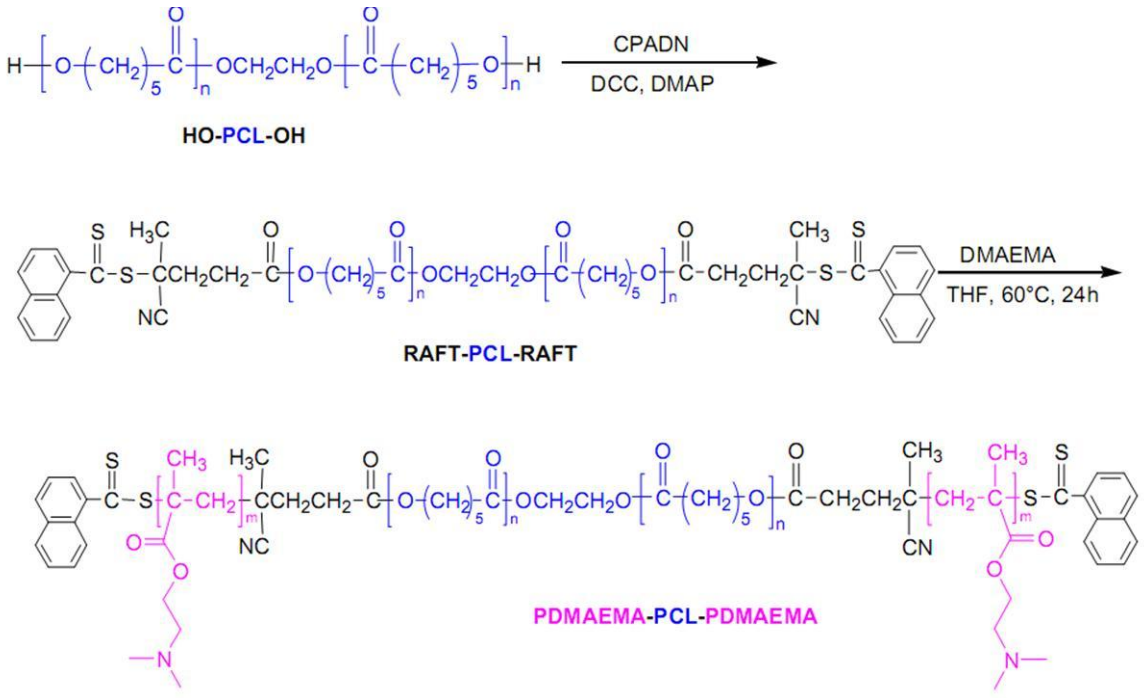

Figure 11. Synthetic pathway for the preparation of Poly(DMAEMA-block-CL-block-DMAEMA) degradable copolymers.[44]

Stayton and coworkers have also developed a multitherapeutic micellar system consisting of doxorubicin, an anthracycline utilized in many cancers, and siRNA against plk1, which has been shown to cause cell-cycle arrest and apoptosis in cancer cell lines as well as increased sensitivity to chemotherapeutics.[63] The complexes they report consist of three basic components: (1) cationic micelles composed of P(DMAEMA-*b*-BMA) diblock copolymers (pDbB), (2) siRNA, and (3) anionic, pH-sensitive poly(styrene-alt-maleic anhydride) (pSMA) polymers that mediate endosomal escape (Figure 12). pDbB was synthesized via RAFT using dodecyl cyanovalerictrithiocarbonate (DCT) CTA and 2,2'-azobis(2-methylpropionitrile) (AIBN) radical source. The overall Mw of the copolymer was 9.4 kDa with a PDI of 1.2. The pSMA was also synthesized *via* RAFT using 4-cyanopentanoic acid dithiobenzoate (CTP) and AIBN. A Mw of 48.5 kDa was targeted based on endolytic activity from previous studies.[144]

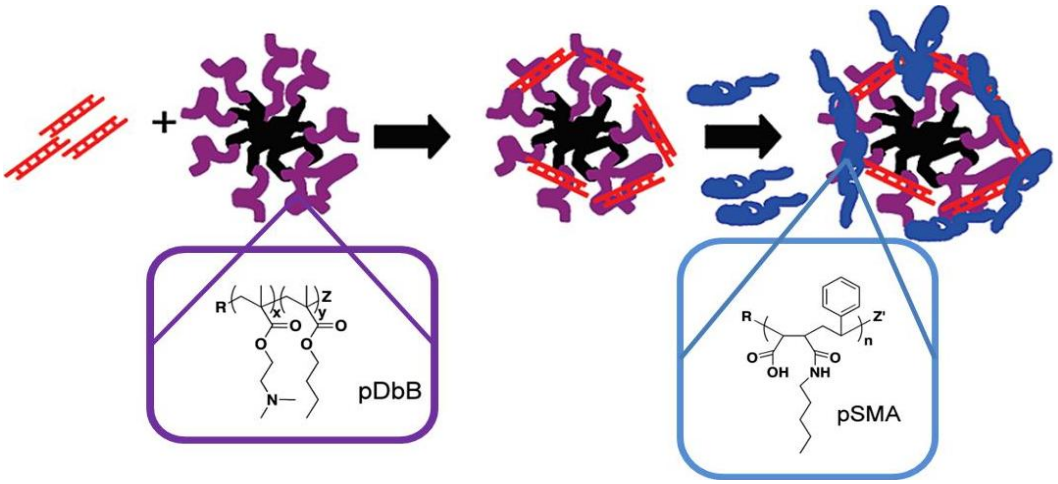

Figure 12. Ternary complex formation: siRNA (red), Poly(BMA) (black), Poly(D-block-B) (purple), and Poly(SMA) (blue).[63]

pDbB can form micelles at pH 7.4 such that the protonated DMAEMA block acts as the corona and the hydrophobic BMA block serves as the hydrophobic core. These micelles are positively charged with mean diameters of 37 nm. Both anionic siRNA and pSMA can be used to complex with the positively charged DMAEMA corona. Depending on the ratio of the three components, micelles with diameters varying from 30–100 nm can be obtained, all maintaining a solution- stable, slightly positively charged complex (zeta potentials ranging from 0–1.2 mV). Micelles could be co-loaded with doxorubicin up to 10 wt% with a slight increase in micelle size. The gene knockdown ability and cell viability towards doxorubicin were investigated in both drug-sensitive OVCAR8 and multidrug-resistant NCI/ADR-REDS ovarian cancer cell lines. The ternary micelle complexes were able to achieve ~50% knockdown (with or without doxorubicin) and effectively sensitized drug-resistant cells to doxorubicin resulting in a decrease in cell viability comparable to drug-sensitive cells.

Polymer-Inorganic Hybrid Carriers—Theranostics

Clearly the advent of controlled radical polymerization techniques has led to the dramatic increase in use of polymers for the construction of gene delivery vehicles. Still, many other materials have also found use in this burgeoning area. Calcium phosphate,[145] silica nanoparticles,[146–148] and carbon nanotubes[149–152] are just a small sampling of the many inorganic substrates that have been used in recent years as transfection agents.[153,154] Indeed, the use of inorganic nanoparticles has proliferated due to their ease of synthesis, wide range of sizes, and biocompatibility.[155–158] However, the application of simple inorganic nanoparticle constructs has been hindered due to their instability/aggregation, low loading efficiencies, and lack of functional "handles" for targeting group incorporation.[158]

Initially, the placement of polymers onto metal nanoparticles was attempted to address issues of stability and the incorporation of reactive functionality.[159,160] These early designs utilized ill-defined polymers, most of which were adsorbed onto the metal surface. However, developments in controlled syntheses of polymers as well as inorganic nanoparticles have led to the construction of well-defined hybrid materials. It has been through the combination of these materials that the development of "theranostics," the incorporation of therapeutic and diagnostic agents on the same platform, has occurred.[161–166] Thus, the combination of inorganic nanoparticles with organic polymers presents a class of novel delivery vehicles with enormous potential applications.

With recent advances in the synthesis of well-defined, narrowly dispersed iron oxide nanoparticles (IONPs), use of this material as both diagnostic agent[167] and a hyperthermia therapeutic has garnered increased attention.[168] IONPs have also been used in the delivery of oligonucleotides *via* interpolyelectrolyte complexation with ill-defined

cationic polymers, such as PEI, adsorbed to their surface.[29] However, their usefulness *in vitro*/*in vivo* has been limited due to instability, aggregation, and fouling of the nanoparticle surface. Boyer and Davis have been able to combat this problem by developing a "grafting to" process utilizing polymers synthesized via RAFT containing a phosphonic acid end group that has a very high affinity for iron[169] (Figure 13). The phosphonic acid is coupled to a CTA utilized in the preparation of the polymers and ends up as a telechelic group on the terminus of the polymer chain.[170] In their most recent work, Boyer et al.[170] have shown that by "co"-grafting two homopolymers, a cationic PDMAEA (Poly(2-(N,N-dimethylamino)-ethyl acrylate)) and a hydrophilic POEGA (poly(oligo(ethylene glycol) acrylate)) onto the surface of pre-formed IONPs. The grafting density (0.12 chains/nm^2) can be greatly increased over grafting homopolymer (PDMAEA 0.07 chains/nm^2) or even a diblock copolymer (0.06 chains/nm^2) alone. This increased grafting density has direct correlation to the overall stability of the NPs, making them storable for months instead of days, and highly resistant to protein absorption. Proton transverse relaxivity rates of bare NPs were compared to polymer grafted NPs and showed no marked effect. The gene knockdown of eGFP (green fluorescent protein) in human neuroblastoma cells of these constructs was investigated using flow cytometry. Compared to the lipofectamine control (40%), the fluorescence intensity of cells incubated with the co-graft IONPs was 78%, which was attributed to decreased uptake due to pegylation of the particles. Interestingly, application of a magnetic field, which has been shown to effect the uptake of magnetic nanoparticles in cells,[171] had a dramatic effect on the transfection efficiency, decreasing the fluorescence intensity to 50%, only slightly higher than the lipofectamine control.

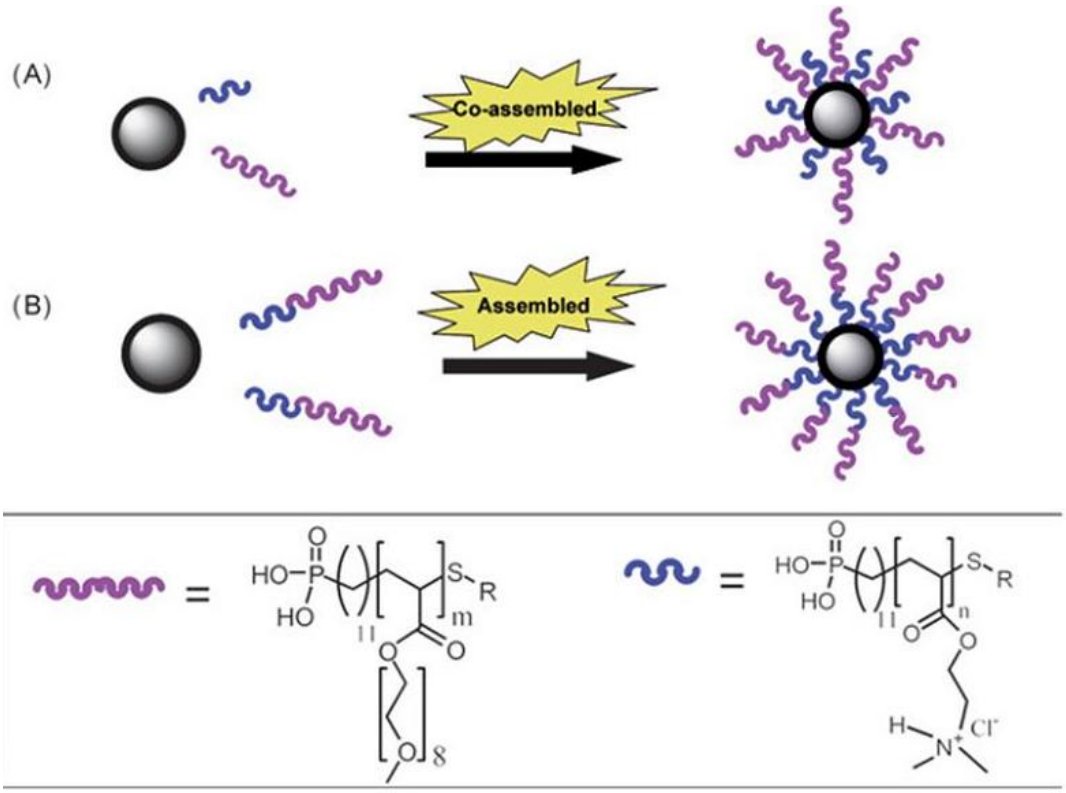

Figure 13. A graphical representation demonstrating (A) simultaneous grafting of two homopolymers, and (B) grafting of diblock copolymers.[157]

Perhaps the most successful and widely used inorganic platform is gold. Inherently non-toxic and inert, gold nanoparticles (GNPs) are easily synthesized in a range of sizes, easily functionalizable, and readily taken up by most cell lines.[172–182] Gold nanoparticles have also recently been approved by the FDA as formulated in the X-ray contrast agent, AuroVist™, and have the added benefit of functioning as a diagnostic agent.[183,184] While the functionalization of gold nanoparticles with polymers has been widely demonstrated to increase therapeutic loading,[185] incorporate targeting,[186–188] and increase circulation time and stability *in vivo*,[189] the construction of these platforms has been limited by low polymer grafting density due to inefficient ligand exchange. McCormick and coworkers have recently reported the synthesis of polymer-decorated gold nanoparticles that are formed *in situ* by the reduction of gold aurate by amine-

containing blocks on their RAFT polymers.[40,134,190,191] In particular, P(HPMA-*b*-DMAPMA) synthesized *via* aqueous RAFT was used to form and stabilize siRNA polyplexes (Figure 14).[40] The size and dispersity of these particles prior to IPEC formation with siRNA can be controlled by varying conditions including substrate concentration, amine to gold ratios, polymer block lengths, and reaction temperature. The grafting densities of the polymer-stabilized GNPs was quite high, 2.7 chains/nm^2, as compared to similar systems, likely due to the extended conformation adopted by the polymer chains on the gold surface which also leads to larger diameter particles (29 nm) than predicted for random-coils (14 nm). The sizes of the GNPs before siRNA complexation were determined by TEM to be ~ 6.5 nm. It should be noted that for the complexes shown in Figure 14, the siRNA is protected against degradation by nucleases through both steric shielding conferred by the HPMA shell and by interpolyelectrolyte complexation with the protonated segments of the polymer vector. Luciferase expression was used to determine transfection efficiency of these constructs in KB cell lines. In these studies, polymer-stabilized GNPs demonstrated identical knockdown (50%) as the commercial agent Dharmafect.

SiRNA-Polymer Conjugates

Most research on siRNA delivery has focused on the formation of interpolyelectrolyte complexes with cationic polymers. However, many questions still remain concerning the binding strength of these complexes, the mechanism of siRNA release, and how these parameters affect gene knockdown efficiency.[8,10,16,19,21,23,25,26,28,29,122] A number of barriers to delivery might be overcome by designing better therapeutic carriers utilizing modular concepts introduced by the original Ringsdorf model, for example utilizing cleavable functionality to release siRNA.

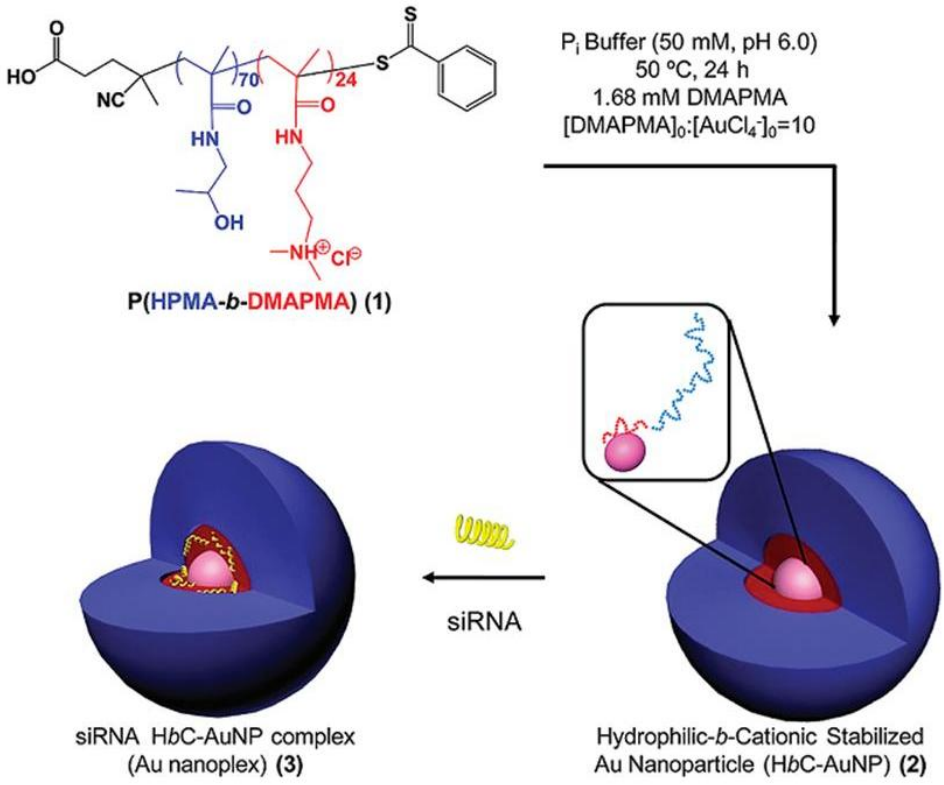

Figure 14. Reduction of $AuCl_4^-$ in the presence of Poly(HPMA-*block*-DMAPMA) copolymers to form hydrophilic-*block*-cationic AuNPs and subsequent complexation of siRNA.[40]

Much effort in the conjugation of biomolecules to RAFT polymers has focused on modification of the chain ends *via* functionality incorporated from the R or Z groups of the CTA agent (Figure 6).[53,66,71,192–200] However, to be applicable to the delivery of siRNA,the conjugation used must be reversible/cleavable. Bulmus and Maynard have several examples of reversible conjugation to the terminus of polymers *via* a disulfide linkage.[44,192,193,196,200,201] Perhaps the most promising for delivery was conjugation of siRNA to a water-soluble poly(ethylene glycol)-containing acrylate utilizing elegant RAFT chemistry. [196] Simple conjugation of poly(ethylene glycol) (PEG) to siRNA via a disulfide bond has been shown to both increase the circulation time and protect against premature degradation.[202–204] Pyridyl disulfide propanol was coupled to the CTA 2-(ethyl

trithiocarbonate)propionic acid and used to polymerize poly(ethylene glycol) acrylate (PEGA) (Figure 15). Linear kinetic plots were obtained in DMF at 60 ^{o}C with AIBN as an initiator after a 20 m inhibition period. Conversions up to 80% with PDIs approaching 1.2 were obtained. Retention of the end group was confirmed by ^{1}H NMR. Thiol exchange between the 5'-end of the siRNA and the pyridyl disulfide was accomplished with 88% yield. Complete cleavage of siRNA could be achieved under reductive conditions with dithiothreitol (DTT).

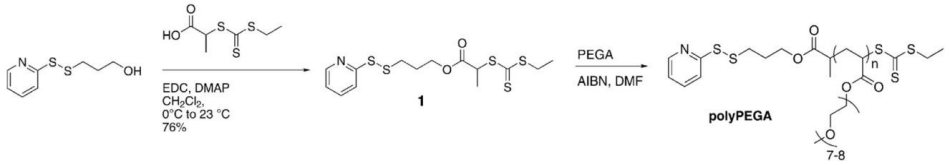

Figure 15. Synthesis of a pyridyl disulfide functionalized CTA and subsequent RAFT polymerization of PEGA.[179]

This thiol exchange strategy, developed by Bulmus and coworkers initially for protein conjugation to RAFT polymers,[193] was also utilized by York et al. for conjugation of siRNA to RAFT polymers at multiple sites along the backbone.[70] Instead of conjugating one siRNA per polymer, they were able to incorporate multiple siRNAs to increase the therapeutic payload and potentially increase the efficiency (Figure 16). HPMA was copolymerized with APMA using V-501 (4,4'-azobis(4-cyanovaleric acid)) as the initiator and CTP as the CTA. The final polymer was end-capped with AIBN due to the potential toxicity of the CTA end group.[205] N-succinimidyl 3-(2-pyridyldithio) propionate (SPDP) was used to functionalize the free amines of the APMA. Thiol exchange with the sense strand of the siRNA was accomplished with 89% efficiency. Folic acid was then conjugated to the remaining free amines for targeting. The anti-sense strand was subsequently complexed to the polymer conjugate. Release of siRNA from

the polymer was demonstrated under intercellular conditions with 5 mM glutathione. About 60% of the siRNA was released in a 4 h period.

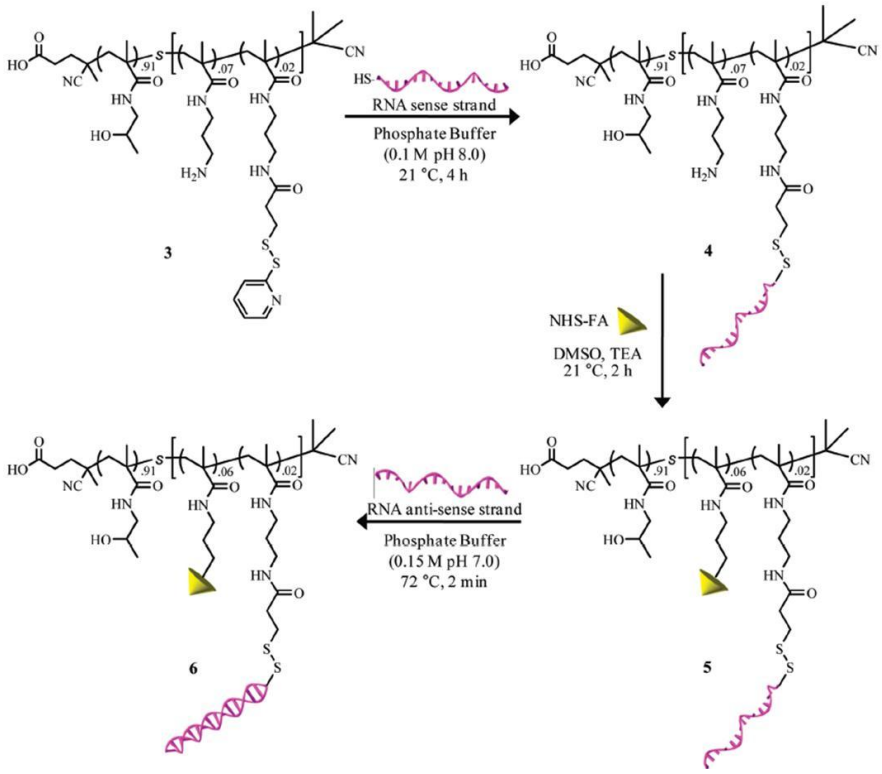

Figure 16. Reaction pathway for the synthesis of both RNA and folate conjugated copolymers and subsequent hybridization with RNA antisense strands.[70]

This chapter has focused on utilizing RAFT polymerization to prepare constructs for drug/gene delivery applications. In principle, these carriers were rationally designed to overcome hurdles in achieving efficient delivery of siRNA. While these systems succeeded in their stated objectives, the focus was on developing "novel" polymeric carriers and not elucidating underlying structure-behavioral relationships governing efficient and efficacious delivery. This dissertation seeks to elucidate such underlying structure-property relationships, providing further insight in the rational design of polymeric drug/gene delivery carriers.

CHAPTER II

OBJECTIVES OF RESEARCH

While ideas for efficacious drug/gene delivery have been in circulation for many years, techniques for achieving successful delivery have only recently emerged. Specifically, reversible addition-fragmentation chain transfer (RAFT) and its aqueous counterpart *a*RAFT. This polymerization method allows for facile preparation of (co)polymers with tailorable architectures, pre-determined molecular weights, directly in water. Serendipitously, small interfering RNA (siRNA), an anticancer biologic, was discovered the same year as RAFT. With siRNA, virtually any gene of interest may be removed post-transcriptionally. However, delivery of siRNA possesses several barriers: reduced cellular uptake due to charge repulsion, lack of cellular specificity, and reduced circulation due to rapid clearance. With these challenges in mind, several researchers (see Chapter I) as well as the McCormick group, have developed polymeric delivery vehicles utilizing the RAFT process which significantly enhance siRNA efficacy *in vitro*. Specifically, polymeric carriers which possess endosomal escape abilities, cell targeting functionality, and self-degradative mechanisms have been prepared. Despite these advancements, the precise mechanisms of siRNA release and delivery to targeted cells have yet to be elucidated. Fundamental insights into the barriers which limit drug efficacy must be achieved before true potential can be achieved.

This dissertation seeks to ascertain structure-property relationships affecting endosomal escape and drug release. Furthermore, this dissertation is divided into three sections. The first section describes the synthesis of pH-responsive poly[HPMA-*block*-(L-Glu)] copolymers as well as their ability to prompt membrane disruption; these novel, endolytic copolymers were specifically designed to address endosomal escape. The

second section describes the structure-property relationships involved in complex dissociation. A series of hydrophilic-*block*-cationic copolymers consisting of poly[(HPMA-*stat*-APMA)-*block*-DMAPMA) were prepared *via a*RAFT to elucidate a pathway for siRNA release, and how this release profile affects gene suppression *in vitro*. The last section investigates the effects on drug efficacy *via* modifications to oligonucleotide secondary structure. A novel therapeutic, AS1411, a G-quadruplex forming single-stranded DNA, was utilized since defects in secondary structure are less tolerable for this anticancer biologic. Again, hydrophilic-*block*-cationic copolymers were utilized as polymeric carriers to ascertain drug efficacy *in vitro*.

The specific objectives of this research are the following:

1. Prepare well-defined macroCTAs comprised of HPMA and APMA.
2. Prepare well-defined hydrophilic-*block*-cationic copolymers *via* chain extensions of macroCTA with DMAPMA.
3. Modify HPMA macroCTA *via* thiol-ene Michael addition for the conversion into a macroinitiator.
4. Prepare pH-responsive, endolytic block copolymers consisting of HPMA and γ-benzyl glutamic acid utilizing HPMA macroinitiator.
5. Characterize all (co)polymers, macroCTAs, and macroinitiators with respect to Mw, Mn, PDI, and molar composition utilizing ASEC-MALLS and 1H NMR.
6. Determine coil-to-helix transitions of poly[HPMA-*block*-(L-Glu)] copolymers utilizing a pH-stimulus *via* circular dichroism.

7. Determine structure-property relationships of poly[HPMA-*block*-(L-Glu)] copolymers which promote hemolysis and dye leakage from artificial membranes under conditions mimicking the endosome.
8. Prepare charge neutral block ionomer complexes comprised of an oligonucleotide and poly[(HPMA-*stat*-APMA)-*block*-DMAPM hydrophilic-*block*-cationic copolymers.
9. Characterize block ionomer complexes with respect to size, charge, and structure utilizing dynamic light scattering, ζ-potential, gel electrophoresis, and circular dichroism.
10. Determine structure-property relationships governing binding strength, stoichiometry, electrostatic complex dissociation, and gene suppression utilizing solution differential scanning calorimetry, analytical ultracentrifugation, and relative luminescence.
11. Ascertain the effects of secondary structure modification of G-quadruplexes on drug efficacy delivered by poly[(HPMA-*stat*-APMA)-*block*-DMAPMA copolymers utilizing circular dichroism, dynamic light scattering, ζ-potential, gel electrophoresis, and cell viability.

CHAPTER III

EXPERIMENTAL

Materials

All reagents were purchased from Sigma and used without further purification unless otherwise noted. N-(3-aminopropyl)methacrylamide (APMA) was purchased from Polysciences. 4,4'-Azobiscyanovaleric acid (V-501) (Wako) and azobisisobutryonitrile (AIBN) were recrystallized twice from methanol. 4-cyano-4-[(ethylsulfanylthiocarbonyl)sulfanyl]pentanoic acid (CEP),[39] 4-cyano pentanoic acid dithiobenzoate (CTP),[206] di-N-hydroxy succinimide activated folic acid (diNHS-FA),[42] and N-(2-hydroxypropyl)methacrylamide (HPMA)[207] were prepared as previously reported. N,N-(3-dimethylamiopropyl)methacrylamide (DMAPMA) and triethylamine (TEA) were distilled prior to use. HPLC purified oligonucleotides (siRNA against Gaussia Luciferase and the dsDNA analogue of siRNA) were purchased from Integrated DNA Technologies, Inc. The siRNA sequences targeting Guassia Luciferase are as follows: Sense strand 5'-AGAUGUGCAACUUUUGCUACCGCAUCU-3' and the antisense strand 5'-AGGAGAUGCGGUAGCAAAAGUUGCACAUCUUU-3'. The DNA analogue sequences of siRNA are as follows: Sense strand 5'-AGATGTGCAATTTTGCTACCGCATCT-3' and the antisense strand 5'-AGGAGATGCGGTAGCAAAAGTTGCACATCTTT-3'. Oligonucelotides (siRNA and dsDNA) were heated at 95 °C for 10 min and were allowed to slowly cool to room temperature prior to use. Concentrations of oligonucleotide (siRNA and dsDNA) are reported as duplex concentrations unless otherwise noted. The Biolux® Gaussia Luciferase assay kit used for the determination of gene suppression was purchased from New England Biolabs, Inc. Gibco® RPMI 1640 cell culture media (with and without folic

acid) were purchased from Life Technologies Corporation. KB cells (human epidermal cancer cells) expressing the Gaussia Luciferase gene (KB-GLuc) were prepared as previously reported. For reactions requiring nitrogen, ultrahigh purity nitrogen (purity ≥ 99.998%) was used. Spectra/Por® regenerated cellulose dialysis membranes (Spectrum Laboratories, Inc) with a molecular weight cut-off of 12–14 kDa were used for dialysis.

Polymer Synthesis

Synthesis of γ-Benzyl-L-Glutamate-NCA

γ-Benzyl-L-glutamate (10 g, 42.1 mmol) was added to a flame-dried reaction flask equipped with a stir bar and placed onto a Schlenk line; the flask was evacuated under reduced pressure followed by the introduction of nitrogen. Approximately 100 mL of THF was added to yield a final concentration of ~0.1 g/mL, and the slurry was stirred under nitrogen for 20 min at 75 ^{o}C. Triphosgene (6 g, 20.2 mmol) dissolved in 10 mL of THF was added to the mixture under a nitrogen atmosphere, and a drying tube was attached to the reaction flask. The reaction was allowed to proceed for ~ 1 h, as THF slowly evaporated to give a final volume of ~ 20–30 mL. After cooling, the mixture was precipitated into hexanes. The recovered precipitate was then re-dissolved in THF; 2–3 g of decolorizing charcoal was then added and the mixture was allowed to stir overnight to remove residual hydrochloric acid. The mixture was then passed through a Celite column to remove charcoal and re-precipitated into hexanes and cooled overnight. The resulting white powder was collected and dried under vacuum overnight to produce γ-Benzyl-L-glutamate-NCA, with standard yields between 75 and 85 %: ^{1}H NMR (DMSO-d_6) δ 9.15–9.05 (Ring, COOH-N**H,** s), 7.40–7.25 (Ar, s), 5.15–5.05 (Ring, COOH-C**H**-CH_2, t) 2.60–2.40 (COOH-C**H**$_2$, d) 2.2–1.80 (COOH-CH_2-C**H**$_2$, m).

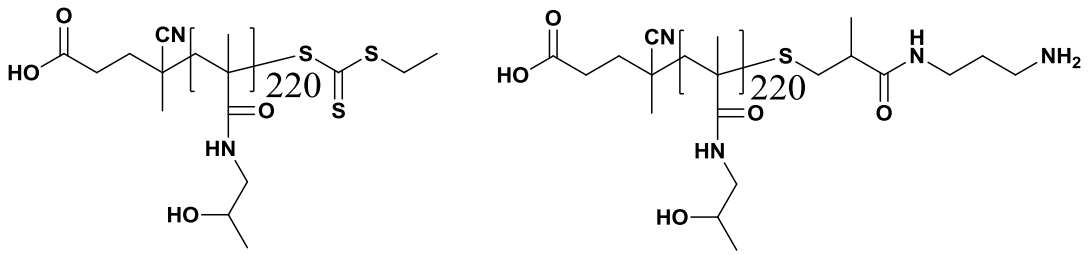

(**P1**) (**P2**)

Figure 17. Structures of poly(HPMA) (**P1**) and poly(HPMA)-NH_2 macroinitiator (**P2**).

*MacroCTA of poly(HPMA) (**P1**)*

A poly(HPMA) macroCTA (**P1**) was prepared employing V-501 as the primary radical source and CEP as the chain transfer agent at 70 °C. To a 50 mL round-bottomed flask HPMA (2.86 g, 0.02 mol) dissolved in acetate buffer (pH 5.2, 0.27 M acetic acid and 0.73 M sodium acetate) was added and diluted to a final volume of 20 mL ($[M]_o$ = 1 M). The round-bottomed flask was septum-sealed and purged with nitrogen for 1 h prior to polymerization. The macroCTA was reacted at a $[M]_o$/[CTA] ratio = 400/1, while the [CTA]/[I] ratio was kept at 5/1, and the polymerization was allowed to proceed for 3.5 h before being quenched with liquid nitrogen followed by exposure to air. **P1** was isolated by dialysis (pH 3–4) at 4 °C and recovered by lyophilization yielding 1.6 g (93%).

*Poly(HPMA) End-Capping with APMA (**P2**)*

P1 was converted into a macroinitiator (**P2**) *via* simultaneous aminolysis and thiol-ene Michael addition with APMA. The reaction is as follows. **P1** (305 mg, 9.5 μmol) was combined with APMA (170 mg, 0.95 mmol) in a septum sealed scintillation vial equipped with a stir bar, then dissolved in 5 mL of DI H_2O, and the pH elevated to 10 with 0.1 M NaOH. The reaction temperature was maintained at 70 °C for 48 h. **P2** was isolated by dialysis in DI H_2O for 48 h and recovered by lyophilization yielding 300 mg (98%).

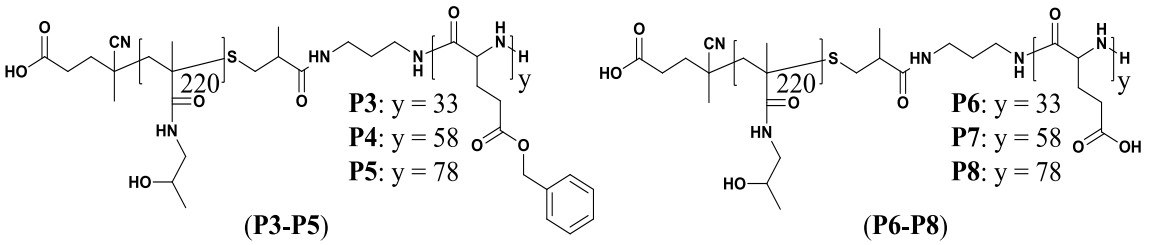

Figure 18. Structures of poly[HPMA-*block*-(γ-benzyl-L-glutamate)] (**P3**–**P5**) and poly[HPMA-*block*-(L-Glu)] (**P6**–**P8**) block copolymers.

*Poly(HPMA) Chain-Extension with γ-Benzyl-L-Glutamate-NCA (**P3**–**P5**)*

Poly(HPMA)-NH_2 (**P2**) was used to initiate ring opening polymerization (ROP) of the γ-Benzyl-L-glutamate-NCA, thereby yielding polypHPMA-*block*-(benzyl-L-glutamate)] block copolymers. A typical reaction is as follows. In a 25 mL round-bottomed flask, **P2** (50 mg, 1.56 μmol) was dissolved in 5 mL of dry DMF. γ-Benzyl-L-glutamate-NCA (10.3 mg, 38.9 μmol) was also dissolved in 5 mL of dry DMF and was immediately added *via* a glass, gas-tight syringe to the macroinitiator solution. Reactions were carried out for 5 days at 0 °C under a nitrogen atmosphere.[208] The polymer was precipitated into ether, re-dissolved in chloroform, and re-precipitated into ether to eliminate unreacted NCA.

*Deprotection of Poly[HPMA-block-(γ -Benzyl-L-Glutamate)]Block Copolymers (**P6**–**P8**)*

Benzyl protecting groups were removed by hydrolysis in a 50:50 mixture of trifluoroacetic acid (TFA) and hydrobromic acid (HBr)[208] at room temperature, followed by dialysis and lyophilizaton to yield pH-responsive **P6**–**P8** block copolymers. Recovered yields were ~ 95 %.

*Synthesis of poly(HPMA-stat-APMA) macroCTA (**P9**)*

A poly(HPMA-*stat*-APMA) macroCTA (**P9**) (CTA) was prepared employing V-501 as the primary radical source and CTP as the chain transfer agent at 70 °C. HPMA (6.80 g, 47.5 mmol) and APMA (405 mg, 2.28 mmol) were added to a 100 mL round-bottomed flask, dissolved in 1 M acetate buffer (pH 5.2, 0.27 M acetic acid and 0.73 M sodium acetate), and diluted to a final volume of 50 mL ($[M]_o$ = 1M). The initial feed composition was 95 mol % HPMA and 5 mol % APMA. The round-bottomed flask was septum-sealed and purged with nitrogen for 1 h prior to polymerization. The HPMA-stat-APMA macroCTA was prepared with a $[M]_o$/[CTA] ratio = 800/1, while the [CTA]/[I] ratio was kept at 5/1; the reaction was allowed to proceed for 3.5 h. The polymerization was quenched by rapid cooling in liquid nitrogen followed by exposure to air. **P9** was isolated by dialysis (pH 3–4) at 4 °C and recovered by lyophilization with a yield of 93%.

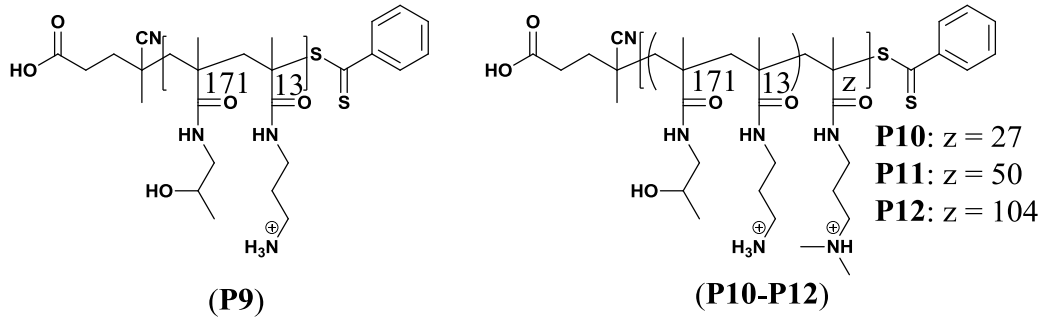

Figure 19. Structures of poly(HPMA-*stat*-APMA) macroCTA (**P9**) and poly[(HPMA-*stat*-APMA)-*block*-DMAPMA] (**P10**–**P12**) block copolymers.

*Synthesis of poly[(HPMA-stat-APMA)-block-DMAPMA] copolymers (**P10**–**P12**)*

P9 was chain extended with DMAPMA also using V-501 as the radical source at 70 °C. DMAPMA and **P9** were added to a round-bottomed flask, dissolved in acetate buffer to give [M]o = 1M. The round-bottomed flask was septum-sealed and

subsequently purged with nitrogen for 1 h. Block copolymers were prepared with a $[M]_o/[CTA] = 200$, while the [CTA]/[I] was kept at 5/1. Each polymerization was terminated at predetermined time intervals by rapid cooling in liquid nitrogen and subsequent exposure to air. The poly[(HPMA-stat-APMA)-block-DMAPMA] copolymers were purified by dialysis (pH 3–4, 4°C) and recovered by lyophilization with yields of 92–97%.

Thiocarbonylthio moieties from poly[(HPMA-stat-APMA)-block-DMAPMA] copolymers were removed following a standard literature procedure.[209] A typical reaction is as follows: P10 (500 mg,11.8 μmol) was added to a 25 mL round-bottomed flask and dissolved with 6.0 mL of DMF. Azobisisobutyronitrile (AIBN; 49.1 mg, 0.300 mmol) was then added to the flask giving an AIBN/copolymer ratio of 25:1. The following solution was then septum-sealed and purged with nitrogen for 1 h and allowed to react at 70 °C for 4 h. The resulting copolymer was precipitated from DMF in cold, anhydrous diethyl ether and washed repeatedly. This step was repeated three times, and the copolymer was dried *in vacuo* overnight. The recovered yields were 85–89%.

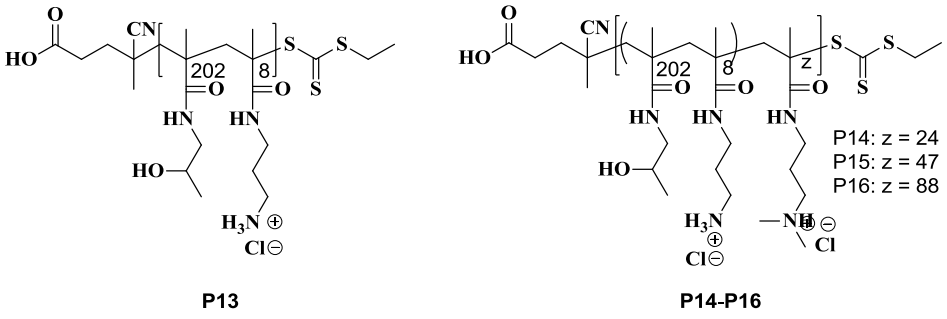

Figure 20. Structures of poly(HPMA-*stat*-APMA) macroCTA (**P13**) and poly[(HPMA-*stat*-APMA)-*block*-DMAPMA] (**P14**–**P16**) block copolymers.

Copolymer functionalization with folic acid

DiNHS-FA was prepared following a standard literature procedure.[42] Following isolation of the chain terminated block copolymer, the pendent, functional, primary amine groups from the incorporated APMA were labeled with NHS-activated folic acid. A typical reaction is as follows: 50 mg (1.18 μmol) of **P10** copolymer was dissolved in 390 μL of DMSO to give a final concentration of 3.00 mM. A total of 150 times excess of diNHS-FA (116 mg) was then dissolved in 350 μL of DMSO, and the **P10** copolymer solution was added to the diNHS-FA solution at a rate of 20 μL every 20 min. Triethylamine (TEA) was added to a final concentration of 39 mM to serve as a catalyst. The resulting solution was shielded from light and allowed to react for 48 h at room temperature. Following reaction, excess ammonium hydroxide (100% by volume) was added to quench the remaining activated esters from activated folic acid. Quenching was carried out for 24 h. The resulting reaction mixture was then directly placed in dialysis tubing and was first dialyzed against 0.6 M NaCl solution for 24 h followed by dialysis against DI water for 3 days. The folate-conjugated **P10**–**P12** copolymers were recovered by lyophilization with yields of 96–98%.

Formation of Hydrophilic-block-Cationic/Oligonucleotide Complexes

Preparation of copolymer/GLuc DNA complexes for solution differential scanning calorimetry

Folic acid labeled hydrophilic-*block*-cationic copolymers (**P10**–**P12**)/GLuc DNA complexes were prepared with a N:P ratio = 1 (i.e., neutral complexes). The GLuc DNA duplex concentration was maintained at 75 μM for all complexes. A typical preparation is as follows: 128 μL of a 600 μM GLuc DNA stock solution was combined with 417.7 μL of sodium cacadylate buffer (10 mM NaAs). Next, 454.3 μL of a 370.4 μM **P10** stock

solution was added. The GLuc DNA/copolymer complex solution was vortexed and equilibrated for 30 min. After equilibration, the solution was degassed for 30 min prior to DSC measurements. The DNA and polymer stock solutions were prepared in 10 mM sodium cacadylate buffer at pH 7.2.

Preparation of copolymer/siRNA complexes for gene suppression

Folic acid labeled hydrophilic-*block*-cationic copolymers (**P10**–**P12**) /siRNA complexes were prepared with a N:P ratio = 1; the siRNA concentration was maintained at 100 nM. A typical preparation is as follows: 1.298 μL of a 185.2 μM **P10** solution was combined with 3.3 μL of a 20 μM siRNA stock solution. This copolymer/siRNA complex solution was then diluted with 127.4 μL of RPMI 1640 medium containing no FBS. The solution was mixed by vortexing and equilibrated for 30 min. After equilibrating, the solution was further diluted with 528 μL of RPMI 1640 medium (supplemented with FBS) and vortexed to ensure a homogenous solution. The RNA and polymer stock solutions were prepared in 10 mM phosphate buffer at pH 7.4.

Fluorescein-POPC (fPOPC) Liposome Preparation and Dye Release Studies

The preparation of dye loaded POPC liposomes followed a standard literature procedure.[210] In a 25 mL round-bottomed flask, 5 mg of POPC was dissolved in 10 mL of chloroform. Then the chloroform was removed by rotary evaporation, and subsequently, the flask was placed under a high vac for 8 h. The resulting film was hydrated with PBS at the appropriate pH containing fluorescein (40 mM). The film was subjected to five freeze-pump-thaw cycles, and subsequently extruded (20 passes) through two stacked 200 nm pore PC membranes at 40 °C. Finally, free fluorescein was removed *via* a Sephadex-25 column eluted with PBS (20 mM Pi, 150 mM NaCl) at the appropriate pH. The resulting fPOPC liposomes possessed hydrodynamic radii of 90 nm with PDIs < 0.2.

P6–**P8** Block copolymers (200 μg/mL) were incubated with fPOPC at the appropriate pH for 1 h at room temperature. The mixture was then vortexed, and the fluorescence intensities measured using a PTI spectrofluorometer. Measurements were acquired with a 460 nm excitation (isobestic point) and 520 nm emission. The slit widths were adjusted for each pH and ranged from 0.5 mm–0.3 mm (pHs 4.0–7.4). All fluorescein dye release experiments were performed in triplicate with Triton-X100 (0.1 wt%) utilized as the positive control, and the percent release was determined using equation 1, in which F(T) is the fluorescence observed when incubated with Triton-X100, F(P) is the fluorescence observed when incubated with **P6**–**P8** copolymers, and F(C) is the fluorescence observed with nothing added to the prepared POPC lipids.

$$\% \text{ Release} = [F(T) - F(P)]/[F(T)-F(C)] * 100 \quad (eq\ 1)$$

Red Blood Cell Hemolysis Assay

Bovine Blood was drawn into vacutainers containing EDTA. The blood was centrifuged, plasma decanted, and washed with 150 mM NaCl (three times). Finally, the red blood cells (RBC) were resuspended in PBS (10 mM Pi, 150 mM NaCl) at either pH 7.4 or pH 5.5 to mimic physiological and endosomal pHs, respectively. Varying concentrations (10 μg/mL–400 μg/mL) of **P6**–**P8** copolymers (100 μL) were incubated with 100 μL of RBC for 1 h at 37 °C. After incubation, the solution was centrifuged, and the supernatant was monitored at 541 nm for the presence of hemoglobin. All hemolysis experiments were performed in triplicate. Triton-X100 (0.1 wt%) was utilized as the positive control, and the percent release was determined using equation 2, in which A(T) is the absorbance observed when the liposomes are incubated with Triton-X100, A(P) is the absorbance observed when incubated with **P6**–**P8** copolymers, and A(C) is the absorbance observed with nothing added to the red blood cells.

$$\%\ Release = \left[\frac{A(T)-A(P)}{A(T)-A(C)}\right] * 100 \quad (eq\ 2)$$

Gene Suppression of Gaussia Luciferase in KB Cells

Cell culture

KB-GLuc cells were maintained and proliferated in RPMI 1640 (with folic acid) medium supplemented with 10% fetal bovine serum (FBS), 100 units/mL penicillin, and 100 µg/mL streptomycin at 37 °C in 95% air humidified atmosphere and 5% CO2.

Gene suppression

Twenty four hours prior to treatment, the KB-GLuc cell medium was replaced with RPMI 1640 medium containing no folic acid and was supplemented with 10% FBS. Then the cells (12,000 cells per well) were seeded in a 48 well plate (Corning Inc.). Cells were treated with 200 µL of a hydrophilic-*block*-cationic copolymer (**P10**–P**12**)/siRNA complex solution. Dharmafect was utilized as the positive control, and the preparation of Dharmafect/siRNA complexes followed the manufacturer protocols. The delivered siRNA concentration was maintained at 100 nM for all complexes, and the KB-GLuc cells were treated for 24–48 h prior to measurement. The extent of *Gaussia* Luciferase suppression was determined using a Biolux® Gaussia Luciferase assay kit (New England Biolabs, Inc.). After incubation, 10 µL of medium was transferred to a 96 well plate and combined with 10 µL of assay buffer. The luminescence was immediately determined utilizing a Biotek Synergy2 MultiMode Microplate Reader. All gene suppression studies were performed in triplicate. The passage number for KB-GLuc cells was 11.

Characterization

Determination of (Co)Polymer Molecular Weight via Aqueous Size Exclusion Chromatography

Poly(HPMA) (**P1**), Poly(HPMA)-NH_2 (**P2**), and Poly[HPMA-*block*-(L-Glu)]s (**P6**–**P8**) were characterized by aqueous size exclusion chromatography (ASEC) using an eluent of 20 wt% acetonitrile/0.05 M Na_2SO_4 (aq) at a flow rate of 0.300 mL/min at 25 °C, TOSOH Bioscience, LLC TSKgel columns (4 and 6 μm), a Polymer Laboratories LC1200 UV/Vis detector, a Wyatt Optilab DSP interferometric refractometer (λ = 690 nm), and a Wyatt DAWN-DSP multi-angle laser light scattering (MALLS) detector (λ = 633 nm). Absolute molecular weights and polydispersities were calculated using the Wyatt Astra (version 4) software. The d*n*/d*c* measurements were performed with a Wyatt Optilab DSP interferometric refractometer (λ = 690 nm) at 35 °C and determined using Wyatt DNDC (version 5.90.03). Conversions for the **P1** and the chain extension with γ-Benzyl-L-glutamate-NCA were determined by comparing the area of the monomeric UV signal detected at 274 nm at t_0 to the area at t_x using a Polymer Laboratories LC1200 UV/vis detector.

Poly(HPMA-*stat*-APMA) (**P9**) and Poly[(HPMA-*stat*-APMA)-*block*-DMAPMA] (**P10**–**P12**) copolymers were characterized by aqueous size exclusion chromatography (ASEC) using an eluent of 1 wt% acetic acid/0.1 M Na_2SO_4 (aq) at a flow rate of 0.250 mL/min at 25 °C, Eprogen, Inc. CATSEC columns (100, 300, and 1000 Å), a Polymer Laboratories LC1200 UV/Vis detector, a Wyatt Optilab DSP interferometric refractometer (λ = 690 nm), and a Wyatt DAWN-DSP multi-angle laser light scattering (MALLS) detector (λ = 633 nm). Absolute molecular weights and polydispersities were calculated using the Wyatt Astra (version 4) software. The d*n*/d*c* measurements for **P9**

and **P10**–**P12** (co)polymers were performed with a Wyatt Optilab DSP interferometric refractometer (λ = 690 nm) at 35 °C and determined using Wyatt DNDC (version 5.90.03). Conversions for **P9** and the chain extension with DMAPMA were determined by comparing the area of the monomeric UV signal detected at 274 nm at t_0 to the area at t_x using a Polymer Laboratories LC1200 UV/vis detector.

Determination of (Co)Polymer Compositions via ^{1}H NMR

P3–**P8** block copolymer compositions before deprotection were determined with a Varian Mercury^{PLUS} 300 MHz spectrometer in DMSO-d_6 supplemented with 15 wt % TFA, and spectra were recorded with a delay time of 2 s. ^{1}H NMR was used to determine the copolymer composition of **P3**–**P5** copolymers by integration of the relative intensities of the methyne-proton resonances of HPMA at 3.75 ppm and the aromatic-proton resonances of γ-benzyl L-glutamate at 7.2 ppm.

Hydrophilic-*block*-cationic copolymer (**P10**–**P12**) compositions were determined with a Varian Mercury^{PLUS} 300 MHz spectrometer in D_2O, and spectra were recorded with a delay time of 2 s. ^{1}H NMR was used to determine the copolymer composition of **P9** and **P10**–**P12** (co)polymers by integration of the relative intensities of the methyne-proton resonances of HPMA at 3.75 ppm and the dimethyl-proton resonances of DMAPMA at 2.75 ppm.

Conjugation of folic acid to **P10**–**P12** copolymers was verified by ^{1}H NMR and UV/vis spectroscopy. ^{1}H NMR was performed on a Varian Mercury^{PLUS} 300 MHz spectrometer in DMSO-d_6 with delay times of 2s. The amount of conjugated folic acid was estimated by integration of the methyne-proton resonance of HPMA at 3.75 ppm and the proton resonance of folic acid at 8.64 ppm (s, PtC7H, 1H). These values were estimated by employing a Lorentzian/Guassian line fit using MestReNova (version 6.0.2-

5475). UV/vis spectroscopy was carried out using a PerkinElmer Lambda 35 spectrophotometer for folic acid conjugated **P10**–**P12** copolymers. An average extinction coefficient of 8000 $M^{-1}cm^{-1}$ for free folic acid in phosphate buffer (10 mM Pi, 100mM NaCl, pH 7.4) was used to determine the number of folic acid units.

Determination of Hydrodynamic Radius for (Co)Polymers and (Co)Polymer-Oligonucleotide complexes

Variable-angle dynamic light scattering (DLS) measurements of hydrophilic-*block*-cationic copolymer/siRNA complexes under aqueous conditions were performed using incident light of 633 nm from a Spectra Physics Model 127 He-Ne laser operating at 40 mW. The angular dependence (60°–120° in 10° increments) of the autocorrelator functions was determined with a Brookhaven Instruments BI-200SM goniometer with an avalanche photodiode detector and TurboCorr correlator. DLS measurements were carried out at a complex concentration (siRNA + FA-block copolymer) of 1.0 mg/mL in phosphate buffer (10 mM Pi, pH 7.4) at 25 °C. The mutual diffusion coefficients (D_m) were determined from the relation

$$\Gamma = D_m q^2$$

in which Γ and q^2 represent the decay rate of the autocorrelation function and the square of the scalar magnitude of the scattering vector, respectively. The hydrodynamic radius (R_h) was then calculated from the Stokes-Einstein equation

$$D_m \approx D_0 = k_b T / 6\pi R_h$$

in which η is the solution viscosity, k_b is Boltzman's constant, and T is the temperature in Kelvin. Zeta-potential measurements were carried out at a complex concentration of 0.5 mg/mL in 20 mM NaCl solution at pH 7.4 using a Malvern Zetasizer Nano Series

Instrument. Samples were vortexed to ensure a homogeneous solution and equilibrated for 30 min at 25 °C prior to measurement. To remove dust, samples were centrifuged at 14,000 RPM for 10 min. Both DLS and zeta-potential measurements were performed in triplicate.

*Circular Dichroism of poly[HPMA-b-(L-Glu)]s (**P6**–**P8**)*

The ellipticity of **P6**–**P8** copolymers was determined utilizing a Jasco J-815 circular dichroism spectropolarimeter. Samples were dissolved in DI H_2O, and the pH was adjusted with 0.1 M HCl. Final sample concentrations ranged from 0.3–0.5 mg/mL, and solutions were allowed to equilibrate for 1 day prior to measurement. The spectra were obtained with a scan rate of 10 nm/min, a 0.5 nm bandwidth, and a time constant of 2 s. The signal-to-noise for all spectra was doubled by averaging four scans. The formation of α-helices was determined by monitoring the presence of the characteristic double minima at 220 and 208 nm.[211]

The ellipticity of the oligonucleotides (siRNA and GLuc DNA) as well as the **P10**–**P12**/oligonucleotide complexes was determined utilizing a Jasco J-815 circular dichroism spectropolarimeter. Oligonucleotides were prepared in phosphate buffer (10 mM Pi, pH 7.4) at a concentration of 1.0 μM. Oligonucleotide/**P10**–**P12** copolymer complexes were also prepared in phosphate buffer but at a concentration of 0.5 μM. Spectra were recorded with a scan rate of 10 nm/min, a 0.5 nm bandwidth, and a time constant of 2 s. The signal-to-noise was doubled for all spectra by averaging four scans. To determine defects of the secondary structure, the characteristic peaks of B-form oligonucleotide (right-handed helices) at 280 nm (maximum), 250 nm (minimum), and 260 nm crossover (from positive to negative) were monitored for discrepancies before and after complexation.[212]

Differential Scanning Calorimetry of Hydrophilic-block-Cationic Polymers and Hydrophilic-block-Cationic-Oligonucleotide Complexes

All calorimetric experiments were carried out using a Calorimetric Sciences Corporation Nano DSC-II solution differential scanning calorimeter (DSC). Sodium cacadylate buffer (10 mM, pH 7.2) was used for the running buffer. The GLuc DNA (analogue of Gaussia Luciferase siRNA) concentration was maintained at 75 μM while the concentrations of hydrophilic-*block*-cationic (**P10**–**P12**) copolymers were adjusted to maintain a nitrogen-to-phosphate (N:P) ratio equal to 1 (i.e., neutral complexes). CpCalc (Version 2.1, Calorimetric Sciences Corp.) was used to subtract buffer-buffer scans from buffer-sample scans. Linear-polynomial baselines were applied to each scan for the determination of the molar heat capacity.

Determination of Copolymer-Oligonucleotide Complex Binding Strength Utilizing Analytical Ultracentrifugation

Sedimentation-velocity experiments were performed in a Beckman XLA Analytical Ultracentrifuge at 20 °C at 50K rpm. Data were collected at 260 nm and processed in DCDT+ to produce g(s) sedimentation coefficient distributions.[213] A fixed concentration of ssDNA was titrated with increasing concentrations of **P10** or **P11**. Data were converted to S_w and analyzed to a 1:1 binding model in Scientist 3.[214]

CHAPTER IV

RESULTS AND DISCUSSION

Section I. Endolytic, pH-Responsive HPMA-b-(L-Glu) Copolymers Synthesized via Sequential Aqueous RAFT and Ring Opening Polymerizations

Overview

Remarkable progress has been made over the last decade in the design of polymeric vehicles in order to achieve cellular targeting,[215] increased blood circulation,[216–218] drug/gene protection,[219–221] reduced cytotoxicity,[222–225] etc.[20] Despite these advances, a number of challenges remain for efficacious gene/drug delivery.[226,227] An ideal carrier should provide protection and solubility during circulation as well as a mechanism for targeting and entry into specified cells. Once delivered the drug/gene/carrier complex must overcome other critical barriers including trafficking to the lysosome, where the cargo can be degraded, or transport outside the cell into the extracellular milieu. A promising approach for an ideal polymeric drug vehicle is inclusion of a modular segment promoting disruption of the endosomal membrane at an appropriate time, allowing drug/gene release into the cytoplasm.

Some polymeric carriers rely on an osmotic swelling mechanism ("proton-sponge effect") to escape the endosome. Alternatively, poly(amido amines), prepared by Duncan[228–230] and Wagner,[231] and poly(aspartamides), prepared by Kataoka and coworkers,[232–234] exploit the enhanced buffering capacity of pendant and backbone amines to facilitate endosomal swelling and rupture. While these systems demonstrate improved efficacy both *in vitro* and *in vivo*, the toxicity of amines is still a concern as is the necessity of a "charge-shielding" block such as PEG or HPMA. In order to alleviate unwanted electrostatic effects and undesirable toxicity, Convertine et al.[38,39,235] prepared

endosomolytic block copolymers containing N,N-(2-dimethylaminoethyl)methacrylate (DMAEMA), propylacrylic acid, and butyl methacrylate (BMA). DMAEMA served to bind siRNA, while propylacrylic acid masked the hydrophobic BMA. At endosomal pH, propylacrylic acid segments are protonated, thus increasing the hydrophobicity of the block copolymer and destabilizing the endosomal membrane.

Naturally-occurring peptides and proteins provide several pathways for endosomal disruption *via* hydrophobic alignment between the α-helix and bilayer surface, usually resulting in electrostatic interactions of the membrane that promote permeability.[236] Such pH-responsive coil-to-helix transitions are attractive features of these biopolymers that offer opportunities for synthetic mimicry. Peptides based on melittin,[237] a component of bee venoms, as well as the lytic amino-terminus of the influenza virus HA-2[238] have been conjugated to polymeric vehicles increasing pDNA and siRNA efficacy both *in vitro* and *in vivo*. To realize a nature-inspired mimic, N-carboxyanhydride (NCA) polymerization[239–241] has been used to prepare synthetic peptides that undergo stimuli-responsive conformational changes into α-helices, β-sheets, and other ordered structures.[242] These conformational changes are facile and reversible, and they have been capitalized on for triggered drug release *in vitro*.[243]

In recent years our research has centered on the development of a modular drug/siRNA delivery platform, capitalizing on the attributes afforded by aqueous RAFT polymerization[7] for synthesis of biologically relevant systems.[40,41] (For example, homo- and block copolymers of (3-guanidinopropyl)methacrylamide (GPMA) were shown to serve efficiently as cell-penetrating mimics of natural peptides.[244] Folate targeting groups for receptor-mediated endocytosis have also been attached to both interpolyelectrolyte siRNA complexes[42] and amphiphilic diblock copolymers with disulfide-bound, pendant

siRNA.[245] While siRNA uptake and trafficking to the endosome occurred with both of these charge-neutral delivery vectors, only the former showed significant gene knockdown. We attribute negligible gene suppression to inability of the latter construct as designed to escape the endosome. Herein, we report the controlled synthesis, characterization, and endolytic activity of a series of HPMA-*block*-(L-Glu) copolymers specifically designed to elicit membrane disruption. To our knowledge, this facile synthetic approach using sequential RAFT polymerization and aminolysis to produce a telechelic, amine-functional macroinitiator followed by NCA polymerization and hydrolysis has not been previously reported. The pH-dependent coil-to-helix transitions of the L-glutamic acid (L-Glu) block were followed by circular dichroism. Membrane disruption was demonstrated by red blood cell hemolysis and fluorescein release from POPC vesicles.

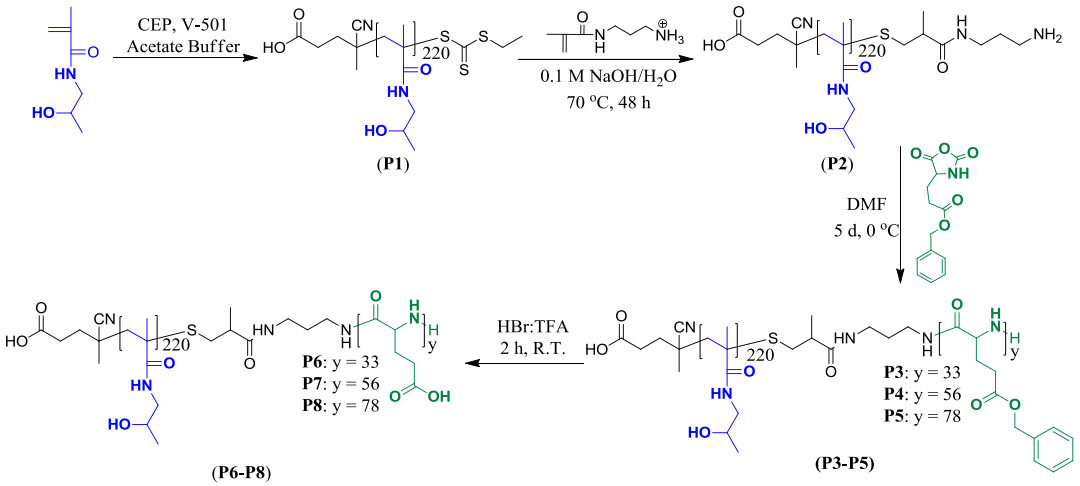

Scheme 1. Synthetic pathway for the preparation of **P6**–**P8** copolymers.

Synthesis of HPMA Homopolymer and Chain-end Functionalization

P1 was prepared *via* aqueous RAFT polymerization (Scheme 1) in order to yield a water-soluble, biocompatible segment with telechelic[246,247] functionality appropriate for further modification to a macroinitiator for block copolymerization. The polymerization was carried out in acetate buffer (pH 5.2) at 70 °C using 4-cyano-4-[(ethylsulfanylthiocarbonyl)sulfanyl]pentanoic acid (CEP) and 4,4'-azobis(4-cyanopentanoic acid) (V-501) as the CTA and initiator, respectively. **P1** was end-capped with a primary amine containing monomer N-(3-aminopropyl)methacrylamide (APMA) *via* simultaneous aminolysis and thiol-ene Michael addition. To ensure quantitative thiol-ene coupling, the pH was elevated (>10) to deprotonate the amine, and the reaction was allowed to proceed at elevated temperature (70 °C) for an extended period of time (48 h). End-capping efficiency was determined *via* a Ninhydrin assay[248] (See Appendix), and primary amine incorporation exceeded 96%. Aqueous size exclusion chromatography (ASEC) was used to determine PDIs, molecular weights, and macro disulfide coupling; the ASEC chromatograms (Figure 20) are shown prior to and after chain-end functionalization with APMA, indicating narrow distributions (PDIs <1.1).

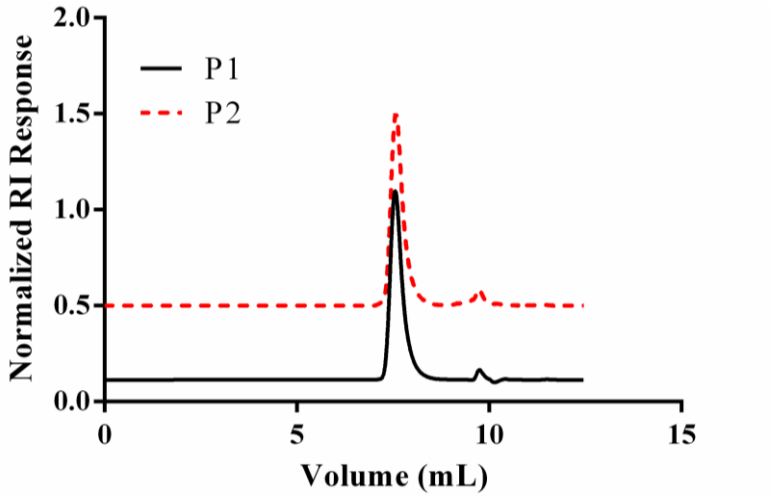

Figure 21. ASEC-MALLS of **P1** (black) and **P2** (red). **P2** is offset for clarity.

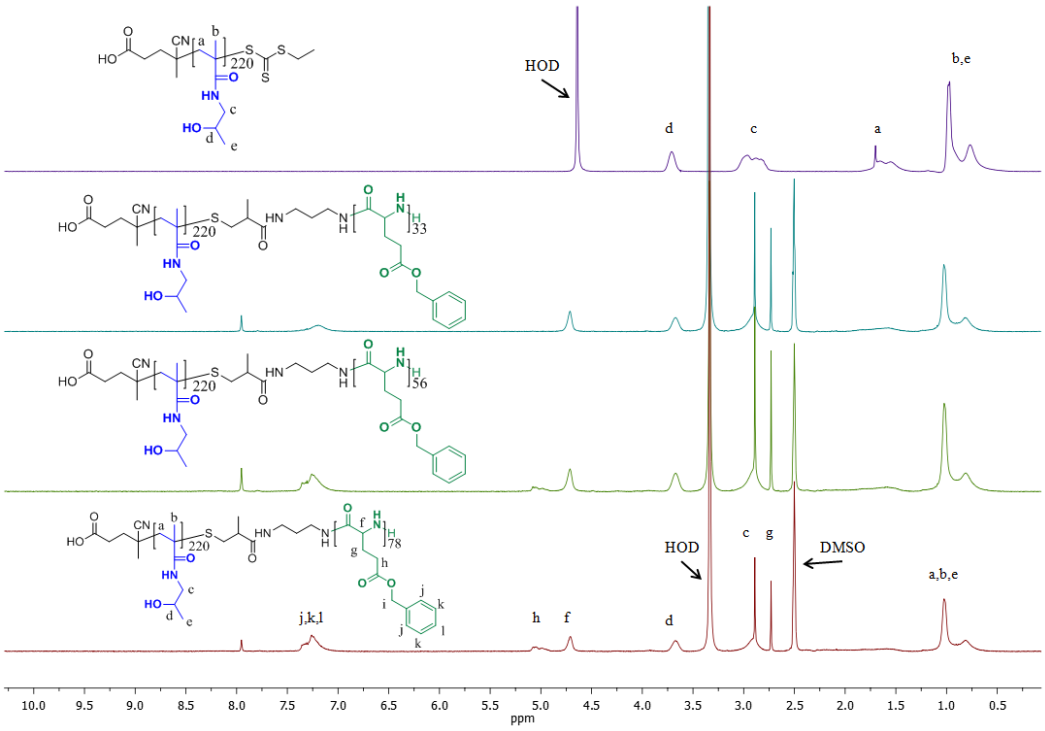

Figure 22. ^{1}H NMR of **P2** and **P3**–**P5**. **P2** was recorded in D_2O while **P3**–**P5** were recorded in DMSO-d_6 supplemented with TFA (15 wt%).

Synthesis of (HPMA-b-Glu) Block Copolymers

Utilizing **P2** as a macroinitiator, a series of chain extensions was accomplished *via* ring opening polymerization of N-carboxyanhydride, γ-Benzyl-L-glutamte-NCA, in DMF. By altering the [M]/[I] ratio, where [M] = γ-Benzyl-L-glutamte-NCA (benzyl protected glutamic acid) and [I] = P(HPMA)-NH_2, a range of block lengths was targeted. In order to prevent anticipated side reactions,[239,249–252] the polymerizations were conducted at 0 °C under an atmosphere of nitrogen. Copolymer compositions for the block copolymers were determined using ^{1}H NMR by comparing the relative intensities of the aromatic-protons resonances of benzyl L-glutamate units at 7.2 ppm to the methyne-proton resonances of the HPMA repeats at 3.75 ppm. Spectra of the poly($HPMA_{220}$)-NH_2 macroinitiator (**P2**) and three copolymers with benzyl-L-glutamate blocks of DP 33, 58, and 78 are shown in Figure 21. Deprotection of benzyl-L-glutamate units was accomplished under acidic conditions at room temperature using a 50:50 mixture of TFA and HBr.[208,253] Copolymer molecular weights, PDIs, compositions, and d*n*/d*c* values are presented in Table 1. Size exclusion chromatograms (Figure 22) indicate successful chain extension with shifts to lower elution volume as the polymerization progressed. The copolymer molecular weights determined directly by ASEC-MALLS correlate well with those calculated from NMR compositional data; PDI values are narrow, ranging from 1.08–1.20. The deviations in experimental and theoretical M_n values are relatively small and may be attributed to incomplete conversion of the HPMA macroCTA to the amine-terminated macroinitiator upon addition of APMA.

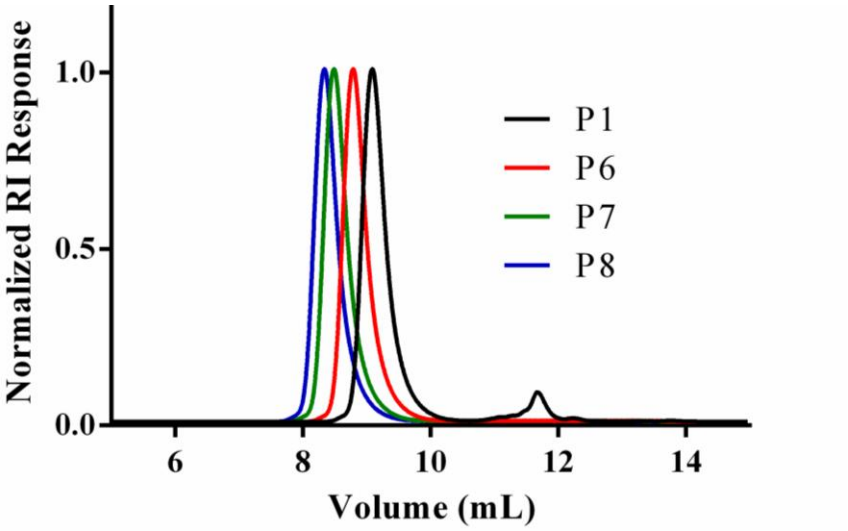

Figure 23. ASEC-MALLS of **P1** (black), **P6**(red), **P7** (blue), and **P8** (cyan).

α-Helix Formation

Circular dichroism[211] is an exceptionally valuable technique for ascertaining structural information of proteins,[254] nucleic acids,[255] and chiral self-assemblies.[256] By measuring the differences between left-handed and right-handed absorbances of chiral or asymmetric species, insight into the secondary structure can be gained. The utility of the **P6**–**P8** copolymers according to our synthetic design lies in the pH-responsive L-glutamic acid block which upon protonation is expected to self-assemble into an α-helix. Ultimately, these α-helices should mimic those discussed in the introduction and disrupt the integrity of lipid membranes. Figure 23 illustrates the pH-dependence of the coil-to-helix transition for each block copolymer as well as for **P1**. Not surprisingly, **P1** alone shows no evidence of α-helix structure. However, as the pH is reduced, the CD spectra indicate pronounced development of α-helices for both **P7** (Figure 23-C) and **P8** (Figure 23-D); however, **P6** with the lowest glutamic acid block length (Figure 23-B) exhibits a spectrum lacking discernible evidence of helix formation. As the pH is further lowered, the characteristic signal of the copolymers with longer helical L-Glu blocks becomes

even more pronounced; eventually, the signal is lost at pH values below 4.5 due to precipitation and/or onset of flocculation.

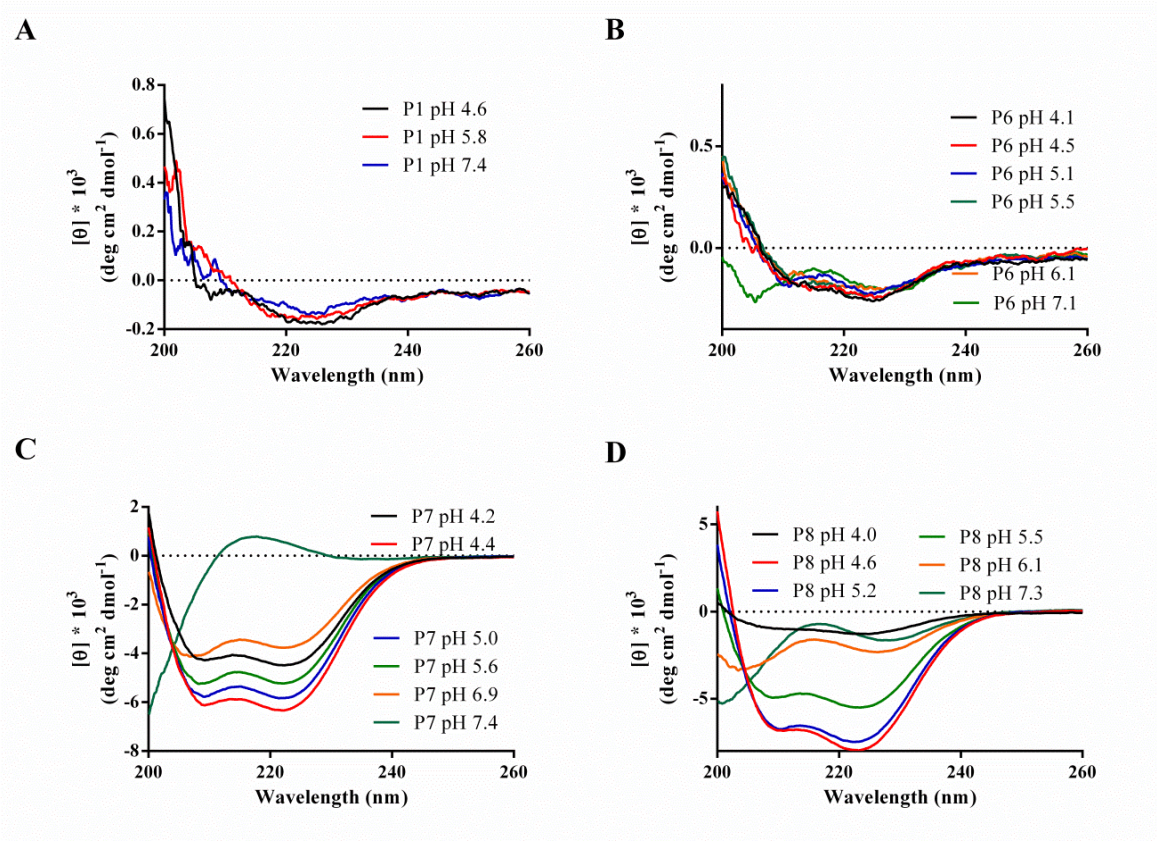

Figure 24. MRE as a function of pH for (A) **P1**, (B) **P6**, (C) **P7**, and (D) **P8**.

Fluorescein Release from POPC Lipid Membranes and Red Blood Cell Hemolysis

Leakage of fluorescent dyes from artificially prepared liposomes is a commonly used assay to elucidate membrane-particle interactions, and it is widely employed in the study of antimicrobial peptides/polymers.[257–260] This technique is well suited for studying membrane disruption at endosomal conditions. By varying the pH, the endolytic activity with respect to α-helical content was investigated using fluorescein loaded 2-oleoyl-1-palmitoyl-*sn*-glycero-3-phosphocholine (POPC) lipids (fPOPC). **P6**–**P8** (200 μg/mL) copolymers were incubated with fPOPC liposomes for 1 h prior to measurement. Figure

24 shows the extent of fluorescein release from liposomes as a function of pH **P6**–**P8** copolymer as well as for the HPMA macroinitiator normalized to L-Glu content. No fluorescein release is observed until pH values are progressively lowered below 6. For **P7** and **P8**, maxima representing 80 % and 70 % release, respectively, occur at pH 5.0; Only ~ 30 % release was observed for **P6**. These values are consistent with CD data. As the pH drops, L-glutamate units are converted to α-helix forming L-glutamic acid, and the extent of fPOPC membrane leakage is related to helical block content.

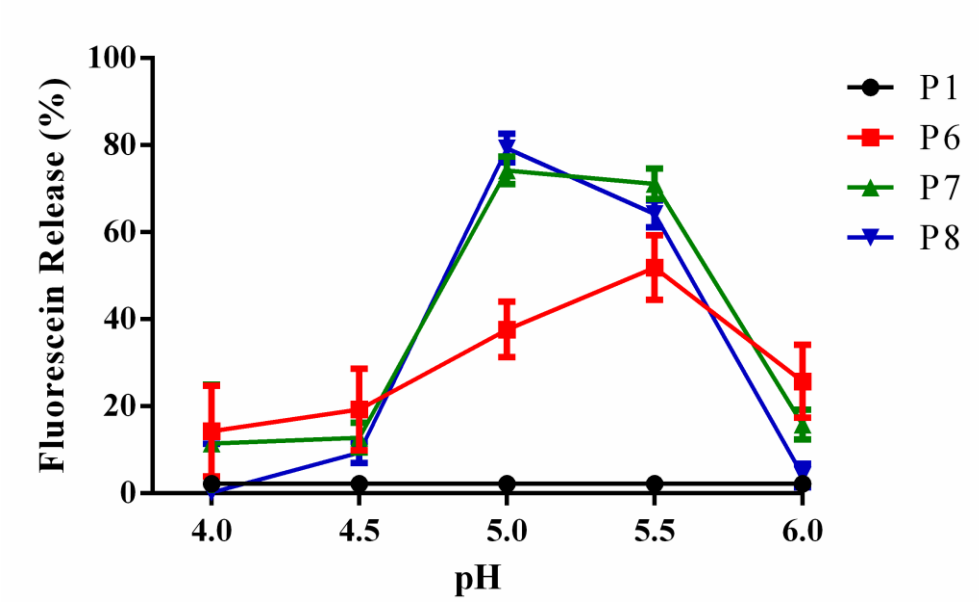

Figure 25. Fluorescein release from POPC liposomes as a function of pH. fPOPC liposomes were incubated 1 h with **P6** (black), **P7** (red), and **P8** (cyan). Triton-X100 was utilized as the positive control. Error bars represent the standard deviation.

The endolytic characteristics of these stimuli-responsive copolymers were also investigated utilizing a red blood cell hemolysis assay at pH 5.5. Figure 25 shows % hemolysis as a function of block copolymer concentration, normalized for L-Glu units. As expected **P1** shows no hemolytic activity, while **P7** and **P8** show notable concentration-dependent release profiles, reaching values of nearly 90 % after 1 h of

incubation. On the other hand, **P6** which has a much shorter block length displays substantially lower hemolysis across the concentration range. These results seem to be in agreement with previous studies indicating a helical block length dependence on membrane destabilization.[236]

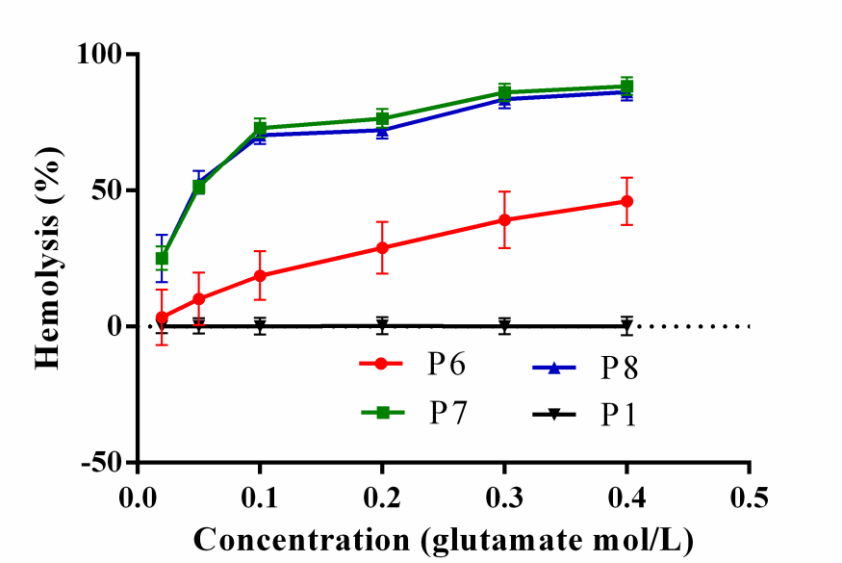

Figure 26. Percent hemolysis as a function of copolymer concentration at pH 5.5. Triton-X100 was utilized as the positive control, and the error bars represent the standard deviation of triplicate experiments.

Table 1

Molecular weight (M_n, M_w), polydispersity (PDI), composition, conversion, and dn/dc values for P6–P8 copolymers.

Sample	$M_{n,Th}$[a] (kDa)	$M_{n,exp}$[b] (kDa)	M_w[b] (kDa)	PDI[b]	Comp (%)[c]	% conv.[d]	d*n*/d*c*[e]
P2	30.6	32.1	34.5	1.08	100:0	53	0.170
P6	34.8	37.8	44.6	1.18	87:13	96	0.145
P7	39.1	42.1	50.5	1.20	79:21	98	0.145
P8	42.8	45.6	53.4	1.17	65:25	94	0.144

[a]Theoretical M_n, ($M_{n,Th}$), calculated from conversion (ρ) using $M_{n,Th} = ([M]_o/[CTA]) \times M_{w,monomer} \times \rho + M_{w,CTA}$. [b]As determined by aqueous SEC-MALLS. [c]As determined by ^{1}H NMR. [d]Conversions were determined by comparison of the UV signal at 274 nm of the monomer at t_0 to that at t_x. [e]Determined by Wyatt Optilab DSP interferometric refractometer (λ = 690 nm).

Section II. Block Ionomer Complexes Consisting of siRNA and Aqueous RAFT Synthesized Hydrophilic-block-Cationic Copolymers: Monitoring Complex Dissociation and the Effects on Gene Suppression

Overview

The discovery of siRNA,[1] the effector molecule in the RNA interference (RNAi) pathway in 1998, has resulted in extensive interventive therapy research giving the potential to regulate nearly any gene of interest.[261–263] However, in vitro delivery of siRNA alone is limited because of enzymatic degradation and lack of cell specificity. As a result, numerous approaches to more efficient delivery have been investigated.[20,264,265] One promising approach capitalizes on the formation of interpolyelectrolyte complexes (IPECs) between the anionic groups along the phosphodiester backbone and a hydrophilic cationic polymer.[266,267] These IPECs stabilize the RNA from nucleases;[41] however, the molar ratio of cationic to phosphodiester repeating units should be ≈ 1. Nitrogen-to-phosphate (N:P) values greater than one lead to non-specific transfection and those less than one to reduced cellular uptake. Recent advances in controlled polymerization techniques including RAFT,[2,33,268] *a*RAFT,[35,48] ATRP,[269] and ROMP[270] now allow the formation of well-defined cationic block copolymers in which block length and stoichiometry along the IPEC can be "tuned." These complexes are often referred to as block ionomer complexes (BICs) and possess a balance of non-complexing hydrophilic segment(s) and binding segments. A potential advantage of BICs is the reduction of off-target effects and toxicity.[271]

The formation of IPECs has been extensively studied and in general, three parameters constitute complex formation;[272,273] hydrogen bonding, hydrophobic effects, and charge. Poly(ethylene glycol) (PEG) has been shown to form stable complexes with

proteins at low pH and up to pH 8, and such complexes are formed strictly through hydrogen bonding.[274,275] Hydrophobic interactions are more difficult to ascertain, and the effects of hydrophobicity are generally manifested in a cooperative fashion.[276,277] Xia et al. demonstrated enhanced binding to lysozyme by introducing a pyrene label to poly(2-acrylamido methylpropylsulfate).[278] The enhanced biding resulted from interactions between the probe and lysozyme's hydrophobic cleft. Interestingly, molecular dynamics simulations have demonstrated oligonucleotide strand separation when complexed with weakly interacting charge associations in conjunction with hydrophobic moieties such as gold nanoparticles.[279] IPECs based on charge are most common and are routinely employed for nucleotide delivery. IPECs prepared via electrostatic associations consistently maintain a 1:1 stoichiometry, and deviations from 1:1 binding result from drastic changes in architecture (e.g., branching). Furthermore, regardless of a strong or weak polyelectrolyte, polyion exchange and substitution readily occur when a small molecular salt is present.[280,281] Ammonium-based polymers (e.g., PEI,[19,282] DMAPMA,[40–42] DMAEMA[38,39,283]) are typically utilized for the cationic block, but polymers possessing phosphonium groups have also been reported.[284–288]

To promote efficacious delivery, polymeric vehicles incorporate multiple modes of interaction. Reineke and co-workers[289,290] investigated IPEC formation between plasmid DNA (pDNA) and poly(glycoamidoamines) (PGAAs). It was determined that while long-range charge-charge interactions drive IPEC assembly, hydrogen bonding plays a vital role in stabilizing the complexes. Furthermore, the less dense amine-containing polymers have stronger electrostatic associations with pDNA.

Our research group has focused on the development of controlled, tailored (co)polymers afforded via RAFT polymerization, and more specifically, the synthesis of

these constructs directly in aqueous media. Recent efforts have centered on a rational design for preparing polymeric drug/gene delivery systems, thus allowing construction of responsive micelles,[117,123,191] theranostics,[40] peptide mimics,[244] modular copolymers,[291,292] and vehicles for endosomal escape.[293] We have previously demonstrated targeted delivery of siRNA via BICs as well as with disulfide-bound amphiphilic copolymers.[42,70] In our experience, we have noted a block-length dependence for efficacious siRNA delivery.[41] Although mechanisms for IPEC and BIC formation have been proposed, information regarding complex dissociation and the role of block length on IPEC stability is lacking. To our knowledge, this is the first study directed toward elucidating the nature of the cationic block length with regard to gene suppression utilizing well-defined block copolymers which form stable, monodisperse BICs with oligonucleotides. Herein, we report the synthesis of hydrophilic-block-cationic copolymers prepared by *a*RAFT, and through the use of a combination of circular dichroism (CD), analytical ultracentrifugation (AUC), and solution differential scanning calorimetry (DSC), structural and binding effects on gene suppression with regard to cationic block length (DMAPMA) were ascertained. Increasing DMAPMA length promotes complex stability and increases the binding constant. Due to large binding constants, the thermodynamics of BIC dissociation could not be determined; however, the kinetics of gene suppression are indicative of an ion exchange/substitution mechanism, providing evidence for a pathway for siRNA and/or oligonucleotide release in vitro.

Synthesis of poly(HPMA-stat-APMA) macroCTA, chain extensions with DMAPMA, and Folic acid conjugation

A statistical macroCTA consisting of a theoretical feed ratio of 95 mol% HPMA and 5 mol% APMA was prepared via aqueous RAFT polymerization (Scheme 2). The polymerization was performed in 1 M acetate buffer (0.27 M acetic acid, 0.73 M sodium acetate, pH = 5.2) at 70 °C using 4-cyanopentanoic acid dithiobenzoate (CTP) and 4,4'-azobiscyanovaleric acid (V-501) as the CTA and initiator, respectively. Experimentally determined compositions for the macroCTA by 1H NMR closely resemble initial feed ratios which were calculated to be 93 mol% HPMA and 7 mol% APMA.

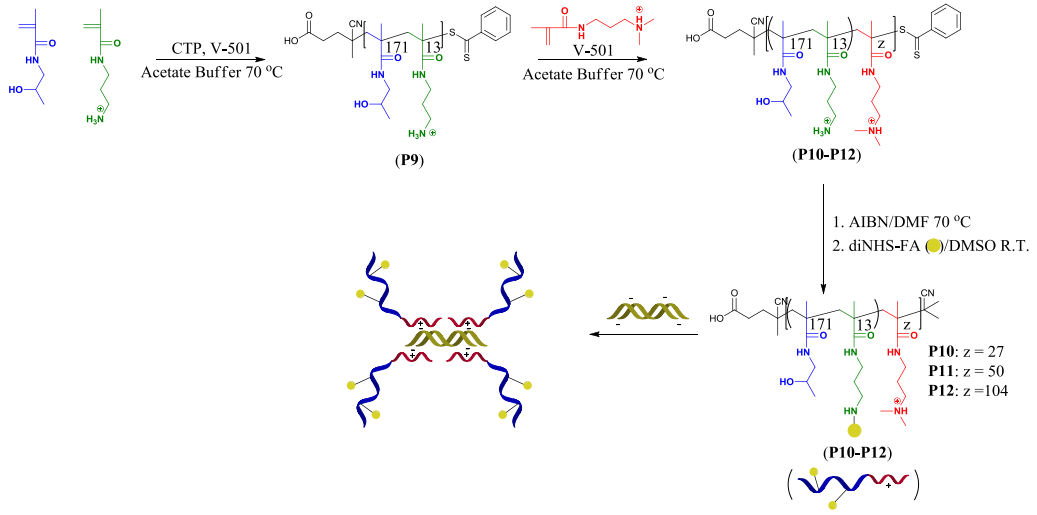

Scheme 2. Synthetic pathway for the preparation of poly[(HPMA-*stat*-APMA)-*block*-DMAPMA] copolymers and subsequent complexation with oligonucleotides.

The resulting poly($HPMA_{171}$-*stat*-$APMA_{13}$) (**P9**) macroCTA was subjected to a series of chain extensions with DMAPMA under similar conditions (Scheme 2). Figure 26 illustrates ASEC-MALLS chromatograms for the macroCTA and these subsequent chain extensions indicating shifts to lower elution volume, narrow polydispersities (PDI) (< 1.10), and unimodal peaks. Copolymer composition, copolymer molecular weights (M_n and M_w), PDI, and d*n*/d*c* values are presented in Table 2 for **P9** and poly[(HPMA-*stat*-

APMA)-block- DMAPMA] (**P10–P12**) copolymers. Copolymer compositions were determined via ^{1}H NMR by integration of the relative intensities of the methyne-proton resonance of HPMA at 3.75 ppm to that of the dimethyl proton resonances of DMAPMA at 2.75 ppm in D_2O. The compositions obtained from ^{1}H NMR correlate well with molecular weights determined via ASEC-MALLS (Figure 25).

Table 2

*Molecular weight (M_n, M_w), polydispersity (PDI), composition, conversion (ρ), and dn/dc values for **P1** macroCTA and **P2**–**P4** copolymers.*

Sample	**$M_{n,Th}$[a] (kDa)**	**$M_{n,exp}$[b] (kDa)**	**M_w[b] (kDa)**	**PDI[b]**	**Comp (%)[c]**	**% conv.[d]**	**d*n*/d*c*[e]**
P9	22.2	24.0	26.4	1.10	93:7	20	0.168
P10	27.2	29.3	31.4	1.07	80:6:14	14	0.167
P11	32.4	33.0	35.3	1.07	71:5:24	25	0.167
P12	41.4	41.5	44.4	1.07	59:5:36	47	0.165

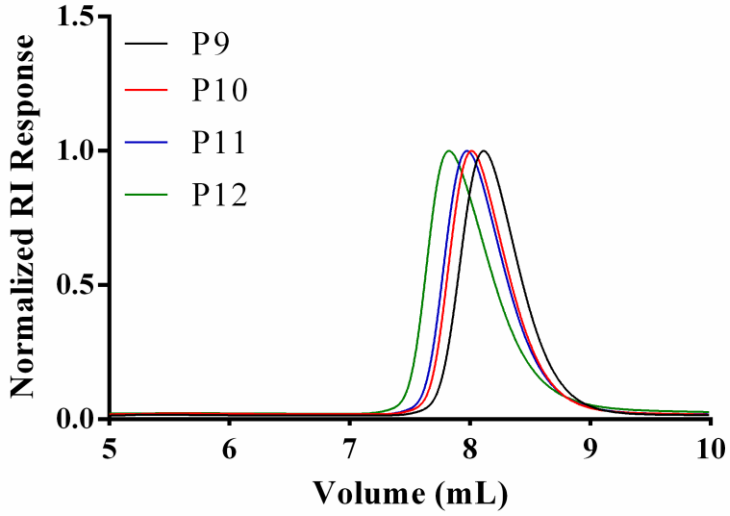

Figure 27. ASEC-MALLS of poly(HPMA-*stat*-APMA) macroCTA (**P9**) and subsequent chain extensions with DMAPMA (**P10–P12**).

The pendent, primary amine of APMA conveniently allows for facile conjugation of electrophilic compounds, and in our case, the cellular targeting moiety, folic acid (Scheme 2). Conjugation of folic acid was conducted in DMSO at room temperature for 48 h. ^{1}H NMR and UV/vis spectroscopy were used to quantify the folic acid conjugation for each hydrophilic-block-cationic copolymer (See Appendix), and the content exceeded 92% (~12 out of 13 amines). We are most concerned with the delivery of neutral complexes (i.e., nitrogen-to-phosphate (N:P) ratio = 1) as excessive cationic charges (N:P > 1) would encourage universal transfection as well as increase cytotoxicity. With folic acid pendently conjugated to APMA, allowing for targeted cellular delivery, only the tertiary amine containing block of DMAPMA will form an electrostatic association with the chosen oligonucleotide, while the HPMA segments promote water stability, biocompatibility, and non-immunogenicity. We have chosen *a*RAFT as it allows for facile synthesis of tailored architectures with predetermined molecular weights and low PDIs under mild conditions. Our narrowly dispersed, well-defined, folic acid-conjugated hydrophilic-block-cationic copolymers are especially suited for formation of homogeneous block ionomer complexes (BIC) with oligonucleotides, therefore allowing for the correlation of BIC dissociation to the extent of gene suppression in vitro.

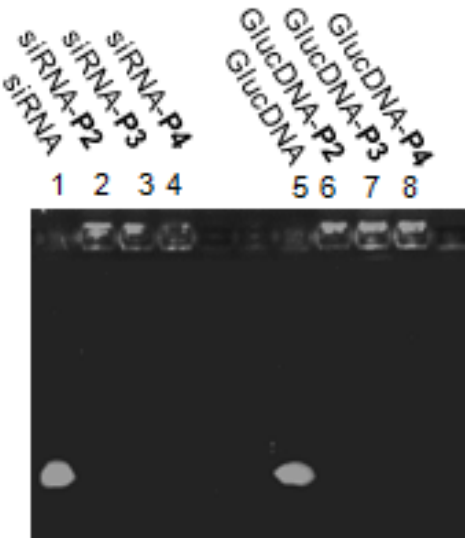

Figure 28. Gel electrophoresis of siRNA (Lane 1) and GLuc DNA (Lane 5) as well as oligonucleotide/copolymer complexes prepared with **P2** (Lanes 2 and 6), **P3** (Lanes 3 and 7), and **P4** (Lanes 4 and 8).

Table 3

The hydrodynamic radii (R_h), polydispersity (PDI), and ζ-potential for siRNA and GLuc DNA-hydrophilic-block-cationic copolymer complexes.

Sample	**R_h (nm)**	**PDI[a]**	**ζ-potential (mV)**
siRNA	N/A*	N/A*	-35.1
siRNA-**P10**	18.7	0.206	-2.16
siRNA-**P11**	26.3	0.058	1.35
siRNA-**P12**	31.7	0.046	2.38
Gluc DNA	N/A*	N/A*	-36.2
DNA-**P10**	18.9	0.214	-2.36
DNA-**P11**	26.8	0.064	-0.09
DNA-**P12**	31.8	0.042	1.87

Characterization of hydrophilic-block-cationic/oligonucleotide complexes

We chose to use a double-stranded DNA (dsDNA) which is analogous to siRNA (*vide infra*), so complexes formed with DNA should resemble those prepared with RNA for comparative purposes. Table 3 presents the hydrodynamic radius (R_h), ζ-potential, and PDI for GLuc/copolymer and siRNA/copolymer complexes. Not surprisingly, both GLuc

DNA and siRNA complexes increase in size (R_h) with increasing DMAPMA block length (18–30 nm); interestingly, these systems become more monodisperse with increasing size (PDIs < 0.2). Typically, intercomplex bridging is observed for larger cationic block lengths, and we have observed similar phenomena utilizing an analytical ultracentrifuge. Charge neutrality was confirmed by ζ- potential and gel electrophoresis (Figure 28). Lanes 2–4 and 6–8 (Figure 28) represent the BICs prepared with either siRNA or GLuc DNA, respectively; lanes 1 and 5 serve as the siRNA and GLuc DNA controls, respectively. As can be seen, both DNA and RNA condensation occur while maintaining charge neutrality, an important requirement which prevents off-target effects and cytotoxicity. The complexes prepared with GLuc DNA or siRNA are comparable, monodisperse, and charge-neutral.

Table 4

The maximum, cross-over, and minimum for oligonucleotide and oligonucleotide-hydrophilic-block-cationic copolymer complexes.

Sample	**λ_{Max} (nm)**	**$\lambda_{Cross\text{-}over}$ (nm)**	**λ_{Min} (nm)**
siRNA	262	253	235
siRNA-**P10**	263	253	234
siRNA-**P11**	263	253	234
siRNA-**P12**	266	251	233
Gluc DNA	272	260	250
DNA-**P10**	287	269	254
DNA-**P11**	293	271	253
DNA-**P12**	299	282	257

Nucleic acids possess secondary structure alterations of which can be monitored via circular dichroism (CD).[294,295] Typically, B-form (standard, right-handed helix) DNA possess three CD spectral characteristics: a 280 nm maximum, a 250 nm minimum, and a 260 nm crossover (from positive to negative).[212] However, these trends are sequence dependent. The CD spectrum for GLuc DNA is presented in Figure 29-A (black curve). Table 4 presents the minimum, maximum, and the crossover for GLuc DNA, siRNA, and oligonucleotide-hydrophilic-block-cationic copolymer complexes. The GLuc DNA possesses a 272 nm maximum, a 250 nm minimum, and a 260 nm crossover. These spectral characteristics drastically shift when complexed with hydrophilic-*block*-cationic copolymers, and when complexed with **P10**, **P11**, and **P12** to form BICs with GLuc DNA, a red shift in the maximum, crossover, and minimum is observed. Additionally, a decrease in ellipticity for the maximum and a more negative increase in the ellipticity for the minimum are observed; these trends exist for all polymers utilized. These changes in structure are similar to the melt (thermal denaturation) spectra (See Appendix) of GLuc DNA.

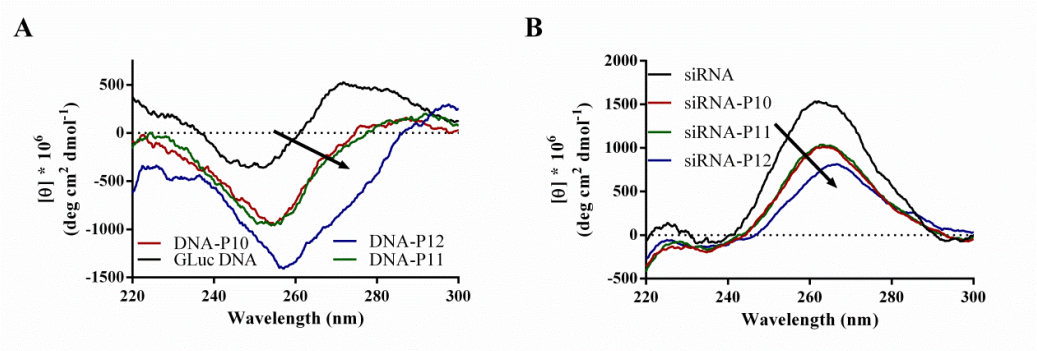

Figure 29. Molar ellipticity of (A) GLuc DNA and DNA-hydrophilic-*block*-cationic copolymer complexes, and (B) siRNA and siRNA-hydrophilic-*block*-cationic copolymer complexes.

Alternatively, RNA helices typically exist in the A-form (also right-handed helix), which possesses a 270 nm maximum, 240 nm minimum, and a 250 nm crossover. Again, these characteristics are sequence dependent. Figure 29-B depicts the molar ellipticity of siRNA (Black curve) and siRNA/hydrophilic-block-cationic copolymer complexes (Red, Blue, and Green curves). The siRNA possesses a 262 nm maximum, a 235 nm minimum, and a 253 nm crossover. These characteristics remain when siRNA is complexed with **P10**, **P11**, and **P12**, except a decrease in ellipticity for the maximum and a more negative increase in ellipticity for the minimum are observed. The changes to siRNA's spectral characteristics when bound to **P10**, **P11**, and **P12** also resemble melting spectra (See Appendix). We hypothesize that, for both siRNA and GLuc DNA, complexation slightly denatures the helix to minimize charge repulsion thus stabilizing the block ionomer complex.

Binding characteristics of Hydrophilic-block-Cationic/GLuc DNA complexes as determined via analytical ultracentrifugation and solution differential scanning calorimetry

Analytical ultracentrifugation was conducted to determine characteristics of complex formation. Utilizing double-stranded DNA (dsDNA), samples were too polydisperse to accurately determine the binding parameters, therefore the single strands (sense strand and antisense strand) were utilized for AUC. (Figure 30). **P10** (Figure 30-A) and **P11** (Figure 30-B) were titrated into a fixed amount of ssDNA. From these titrations, complexation readily occurs as evidenced by shifts to increased apparent sedimentation ($S_{Apparent}$) values. Furthermore, an association constant may be obtained via a global fit to a 1:1 stoichiometric model.[214] The binding constants related to complex formation utilizing **P10** and **P11** were in the range of 10^4 and 10^7, respectively, values

typical for electrostatic association. Although complexation was observed for **P10** and **P11**, ssDNA titrated with **P12** produced polydisperse complexes, and a binding constant was not determined.

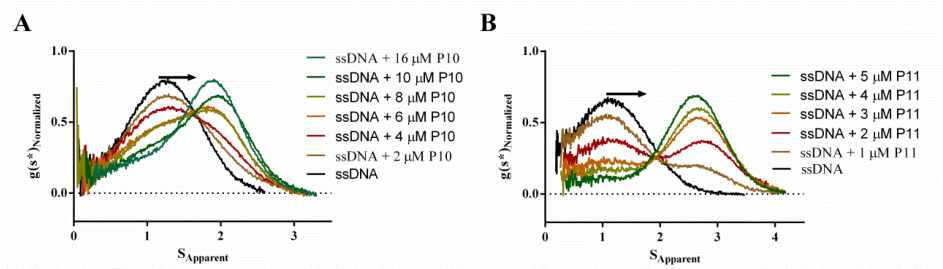

Figure 30. Monitoring the association of single-stranded DNA with hydrophilic-*block*-cationic copolymers. g(s*) sedimentation coefficient distribution of a titration of ssDNA with **P10** (A) and **P11** (B).

DSC measurements of the excess heat capacity relative to a reference cell allow thermodynamic determinations of dissociation (folded-to-unfolded).[296] From these melting profiles, complex stability can be elucidated. Due to the large amounts of material required for DSC, utilizing siRNA becomes cost prohibitive. Therefore, a dsDNA analogue of siRNA was used in all of our DSC studies.

Figure 31 depicts the molar heat capacity (MHC) thermograms, for GLuc DNA and GLuc DNA/copolymer complexes formed with **P2**, **P3**, and **P4**. The GLuc DNA duplex dissociation temperature, or melting temperature (T_m), was determined to be 54.4 °C for uncomplexed dsDNA (Figure 31-A). Furthermore, T_m values increased with DMAPMA block length (**P10**, 88.4 °C, **P11** 90.2 °C, **P12**, 91.8 °C, respectively (Figures 31 B-D). This trend of increasing T_m indicates that polymer complexation significantly stabilizes the DNA duplex, greater cationic block length conferring greater duplex stability. These findings are also corroborated by the changes in secondary structure as observed with CD (Figure 29).

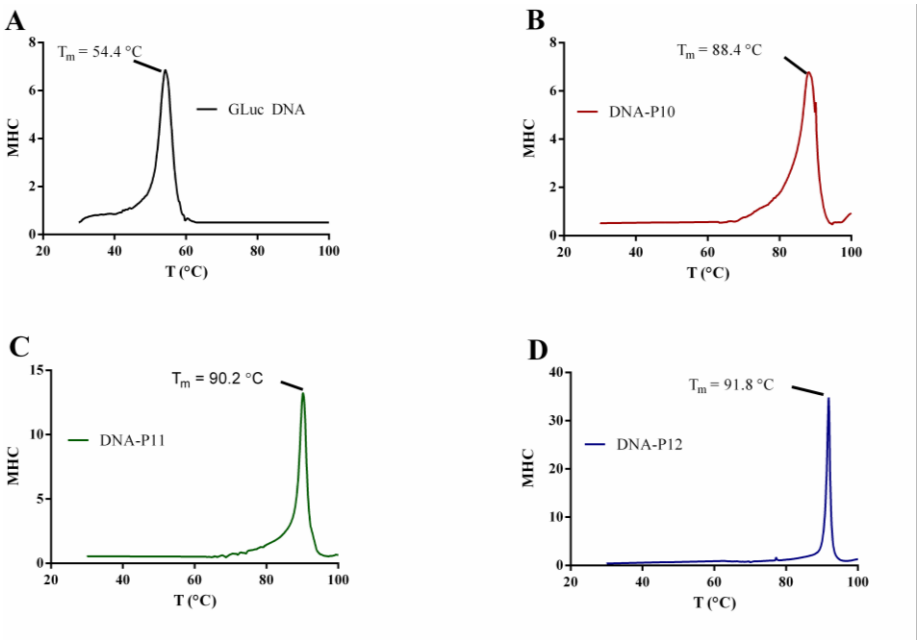

Figure 31. Molar heat capacity thermograms for (A) GLuc DNA, (B) DNA-**P10** complexes, (C) DNA-**P11** complexes, and (D) DNA-**P12** complexes.

Since the magnitude of the melting endotherm, representing the breaking of hydrogen bonds between the sense and antisense strands, may mask changes corresponding to dissociation, ssDNA was separately complexed with hydrophilic-block-cationic copolymers **P10**–**P12**. Figure 32 presents the excess heat capacity ($\Delta C_{p,XS}$) thermograms for copolymer complexes prepared with the sense and antisense strands. For the scanned temperature range (30 °C–125 °C), no dissociation is observed (i.e., no exotherm or endotherm) regardless of hydrophilic-*block*-cationic polymer utilized in complexation. The absence of dissociation is not surprising, since the binding constants are so large. A binding constant of 10^4 would indicate 1/10000 dissociated molecules. With the concentration used, the dissociated species would be at or below the detection limit for the calorimeter.

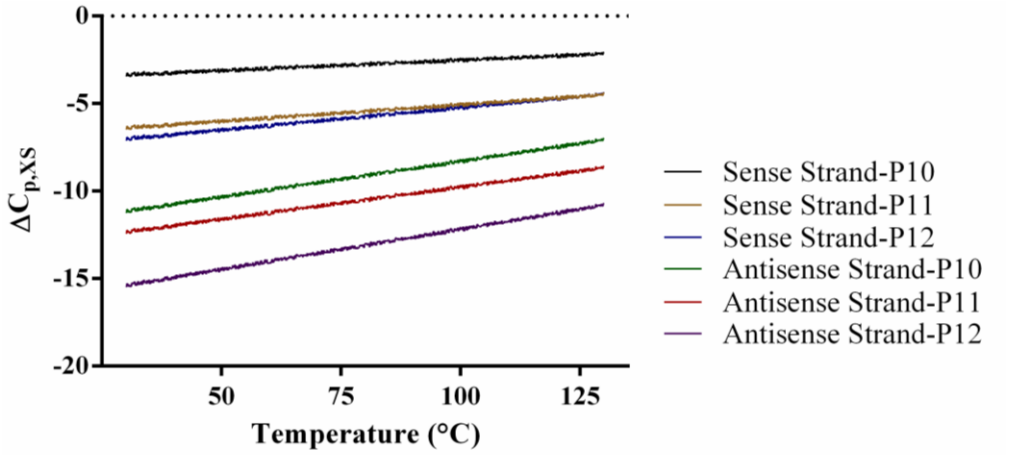

Figure 32. Excess heat capacity thermograms of hydrophilic-*block*-cationic copolymer binding to GLuc antisense and sense strands.

Gene down-regulation

To determine the role of cationic block length on gene suppression, gene down-regulation was monitored in KB cells which stably express Gaussia Luciferase. Figure 33 demonstrates the kinetics of gene knockdown as a function of DMAPMA block length. Increasing the cationic block slightly increases gene suppression as **P12** exhibits ~10 % higher suppression than **P10**; however, increasing the cationic block also increases the cytotoxicity (see Appendix). Appreciable cell death occurred with **P12** while **P10** maintained negligible cytotoxicity over a 48 h period. Interestingly, the observed gene knockdown maximum is shifted toward longer times when increasing DMAPMA block length, from 32 h for **P10** to 40 h for **P12**. These shifts in the maxima agree with literature reports for polyion exchange/substitution rates, since increasing molecular weight increases the time required for complete ion exchange.[280,281,297] Regardless of the nature of a dissociation or ion exchange/substitution mechanism, the trend is clear—an increase in binding/stability and the expected increase in time to reach maximum gene suppression.

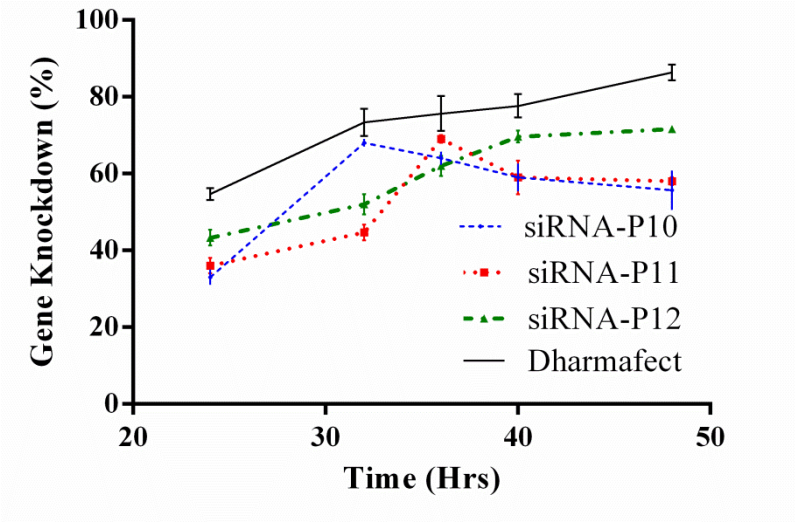

Figure 33. Gene knockdown kinetics for complexes consisting of siRNA and **P10** (blue), **P11** (red), and **P12** (green). Dharmafect was utilized as the positive control (Black). Error bars represent the standard deviation of triplicate experiments.

\

Section III. Characterization of Block Ionomer Complexes Consisting of G-Quadruplexes and *a*RAFT Synthesized Hydrophilic-*block*-Cationic Copolymers and Subsequent Polymeric Delivery of AS1411

Overview

Remarkable progress has been achieved in the development of anticancer therapeutics based on, small interfering RNA (siRNA), antisense oligonucleotides, and pDNA to name a few. The limiting factors for efficacious delivery of the aforementioned anticancer biologics are serum stability and reduced cellular internalization. A novel class of oligonucleotides incorporating G-rich sequences, which fold into G-quadruplexes, have the innate ability that appear to reduce or eliminate delivery barriers which are problematic to traditional oligonucleotide drugs. Specifically, AS1411, a 26-mer which forms a G-quadruplex, has demonstrated in vivo success in Phase I clinical trials in patients exhibiting metastatic cancer; this anticancer biologic is currently in Phase II trials. AS1411 inhibits cell proliferation *via* several possible mechanisms such as inhibition of shuttling, signal transduction, or modulating mRNA stability, although the precise mechanism has not been fully elucidated. Nonetheless, AS1411 is an aptamer for nucleolin, and binding to nucleolin is positively correlated to drug efficacy. To date, incorporation of AS1411 into polymeric vehicles has been for the purpose of cellular targeting. Herein, we report the *a*RAFT synthesis of hydrophilic-*block*-cationic copolymers which form stable, monodisperse block ionomer complexes (BICs) with AS1411. These BICs were well characterized with respect to size (R_h), polydispersity (PDI), zeta-potential, and structure. From circular dichroism spectroscopy, no alterations in secondary structure were observed. The drug efficacy of AS1411 is directly correlated to its ability to bind to nucleolin, and AS1411's potency was significantly reduced when

complexed with hydrophilic-*block*-cationic copolymers. These findings indicate complex stability plays a vital role in drug efficacy in vitro.

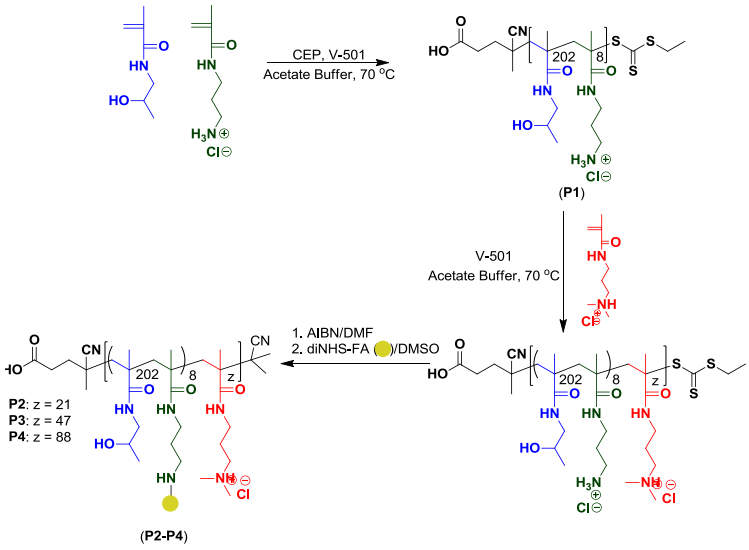

Scheme 3. Synthetic outline for the preparation of poly(HPMA$_{202}$-*stat*-APMA$_8$) macroCTA (**P12**) and hydrophilic-*block*-cationic copolymers (**P13**–**P15**).

*a*RAFT polymerization was employed to prepare a poly(HPMA-*stat*-APMA) macroCTA (Scheme 3). The polymerization was conducted in acetate buffer (1 M; 0.27 M acetic acid, 0.73 M sodium acetate) at 70 °C, utilizing 4-cyano-4-[(ethylsulfanylthiocarbonyl)sulfanyl]pentanoic acid (CEP) and 4,4'-azobiscyanovaleric acid (V-501) as the CTA and initiator, respectively. The macroCTA was prepared with a theoretical molar feed ratio of 95:5, agreeing well with measured molar compositions determined *via* ^{1}H NMR were 96 mol% HPMA and 4 mol% APMA. The macroCTA **P12** was thus determined to be poly(HPMA$_{202}$-*stat*-APMA$_8$). Utilizing **P12** a series of chain extensions was performed with DMAPMA (Scheme 3). Table 5 presents the molecular weight, polydispersity, molar composition, conversion, and d*n*/d*c* values for the macroCTA (**P12**) and hydrophilic-*block*-cationic copolymers (**P13**–**P15**). From GPC (See Appendix) successful chain extensions are evident by shifts to lower elution volume as

well as the monomodal distributions. These results are in agreement with ^{1}H NMR spectra (See Appendix).

P12 serves two purposes: HPMA confers water stability and APMA provides a functional handle to conjugate folic acid, a cellular targeting moiety. The incorporation of DMAPMA (**P13**–**P15**) provides cationic segments which electrostatically bind to the anionic phosphodiester backbone of the G-quadruplex. It is important to note that the preparation of BICs is formulated with a nitrogen-to-phosphate (N:P) ratio = 1 (i.e., neutral complexes) to ensure that off-target effects (i.e., universal transfection) and cytotoxicity ar minimized. Additionally, these well-defined, monodisperse hydrophilic-*block*-cationic copolymers allow for precise characterization of BICs prepared with these copolymers.

Table 5

Molecular weight (M_n, M_w) polydispersity (PDI), molar composition, conversion (ρ), and dn/dc values for poly(HPMA-stat-APMA) macroCTA (P1) and poly[(HPMA-stat-APMA)-block-DMAPMA] (P2–P4) copolymers.

Entry	$M_{n,Th}$[a] (kDa)	$M_{n,exp}$[b] (kDa)	M_w[b] (kDa)	PDI[b]	Comp[c] (mol%)	ρ[d] (%)	d*n*/d*c*[e]
P12	28.4	30.2	30.4	1.09	96:4	49	0.168
P13	32.4	32.5	35.1	1.06	86:4:10	11	0.167
P14	35.5	36.4	38.8	1.06	78:4:18	21	0.167
P15	42.0	43.3	46.3	1.07	68:2:30	40	0.166

[a]Theoretical M_n, ($M_{n,Th}$), calculated from conversion (ρ) using $M_{n,Th} = ([M]_o/[CTA]) \times M_{w,monomer} \times \rho + M_{w,CTA}$. [b]As determined by aqueous SEC-MALLS. [c]As determined by ^{1}H NMR. [d]Conversions were determined by comparison of the UV signal at 274 nm of the monomer at t_0 to that at t_x. [e]Determined by Wyatt Optilab DSP interferometric refractometer (λ = 690 nm).

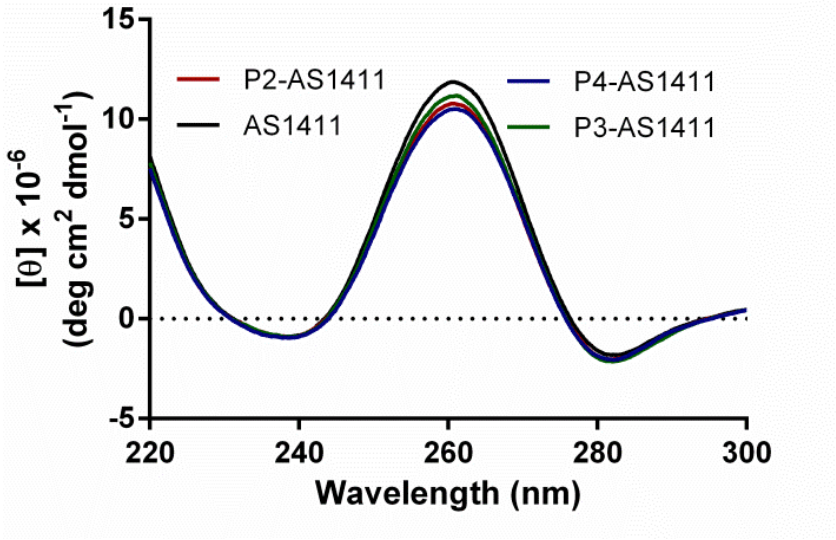

Figure 34. Circular dichroism spectra of AS1411 and AS1411/hydrophilic-*block*-cationic copolymer complexes.

Table 6

The hydrodynamic radii (R_h), polydispersity, and zeta-potential for AS1411 and AS1411-hydrophilic-block-cationic copolymer complexes.

Sample	R_h (nm)	PDI[a]	ζ-potential (mV)
AS1411	N/A*	N/A*	-11
AS1411-**P13**	19	0.047	-2.16
AS1411-**P14**	21	0.064	1.35
AS1411-**P15**	28	0.051	2.38

*The scattering intensity was too low for an accurate determination. [a]The PDI was determined at 90°.

G-quadruplex formation can be monitored via Uv-Vis spectroscopy (See Appendix). At room temperature the oligonucleotide is folded into a quadruplex, and by heating the sample above the melting temperature (T_m), the oligonucleotide unfolds. By subtraction of the absorbance scan at room temperature from the absorbance scan above theT_m, a characteristic difference spectrum can be obtained. This difference spectrum exhibits an isobestic point at 280 nm, a net hyperchromism above 285 nm, and a maximum at 295

nm; however, these characteristics are dependent upon oligonucleotide sequence, flanking sequences, and cationic counterion used. Difference spectra were recorded for AS1411. The spectral characteristics for AS1411 determined *via* Uv agree with literature reported characteristics, exhibiting a 295 maximum, 280 nm isobestic point, and a net hyperchromism. While Uv-Vis spectroscopy is a facile method for ascertaining quadruplex formation, this method proves difficult when utilizing BICs. Polymer complexation significantly increases the T_m (~40 °C), and the temperature required for denaturation of the quadruplex is above the boiling point of water. Nevertheless, circular dichroism spectroscopy (CD) can provide necessary insight into structural modifications of AS1411. Utilizing CD, parallel quadruplexes are characterized by the presence of a peak at 264 nm and a trough at 240 nm. Figure 34 presents the CD spectra for AS1411 and AS1411/hydrophilic-*block*-cationic copolymer complexes. AS1411 (Figure 34, black curve) presents a typical CD spectrum indicative of a parallel G-Quadruplex. Upon complexation no noticeable shifts in the characteristic peaks are observed (See Appendix for λ_{max}, λ_{min}, and $\lambda_{cross\text{-}over}$); In contrast, we have previously demonstrated red shifting when hydrophilic-*block*-cationic copolymers are complexed with double-stranded DNA and RNA, B-form and A-form, respectively. Two other G-quadruplex forming sequences were also utilized (See Appendix), and similar results were obtained when complexed with hydrophilic-*block*-cationic copolymers.

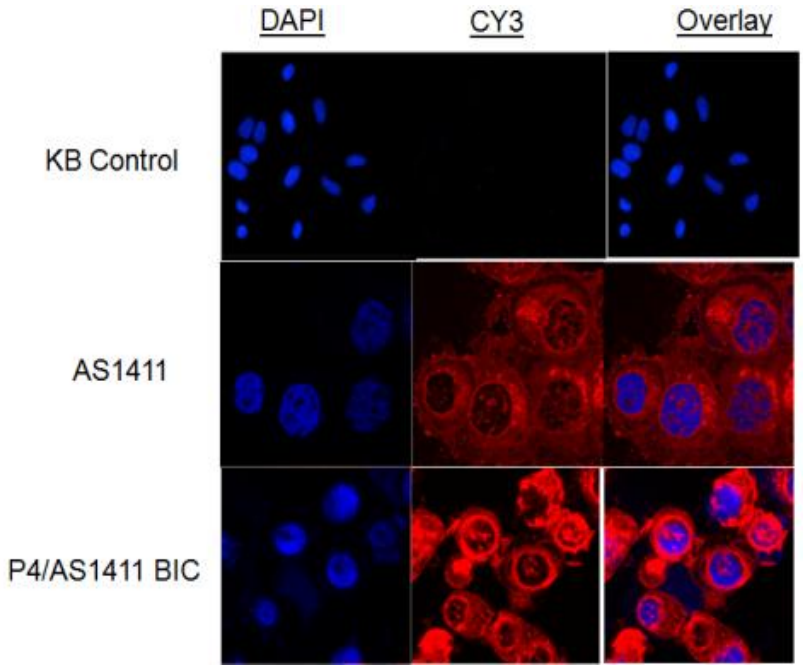

Figure 35. Confocal images of AS1411 (positive control) and **P15**/AS1411 BICs. The nucleus was stained with DAPI, and the 5'-end of AS1411 was labeled with Cy3.

To reduce universal transfection, BICs were prepared with a N:P = 1. Table 6 presents the hydrodynamic radii (R_h), polydispersity (PDI), and zeta-potential for AS1411 and AS1411/hydrophilic-*block*-cationic copolymer complexes. From zeta-potential, complexes prepared with **P13**–**P15** exhibit near-neutral values. Additionally, BICs are monodisperse, and the R_h increases with increasing DMAPMA block length; **P13** = 19 nm, **P14** = 21 nm, and **P15** = 28 nm.

Cellular entry was monitored via confocal microscopy (Figure 35). Since AS1411 enters the cells naturally, typically by macropinocytosis, it was used as the positive control; AS1411 was labeled with CY3, and the nucleus was stained with DAPI. From Figure 35-middle row, AS1411, alone, successfully enters KB cells. Utilizing **P15** as the drug carrier, cellular delivery is also achieved. Notably, signals from the CY3 fluorophore are present in both the cytoplasm and nucleus; similar results are also witnessed when utilizing **P13** and **P14** (data not shown).

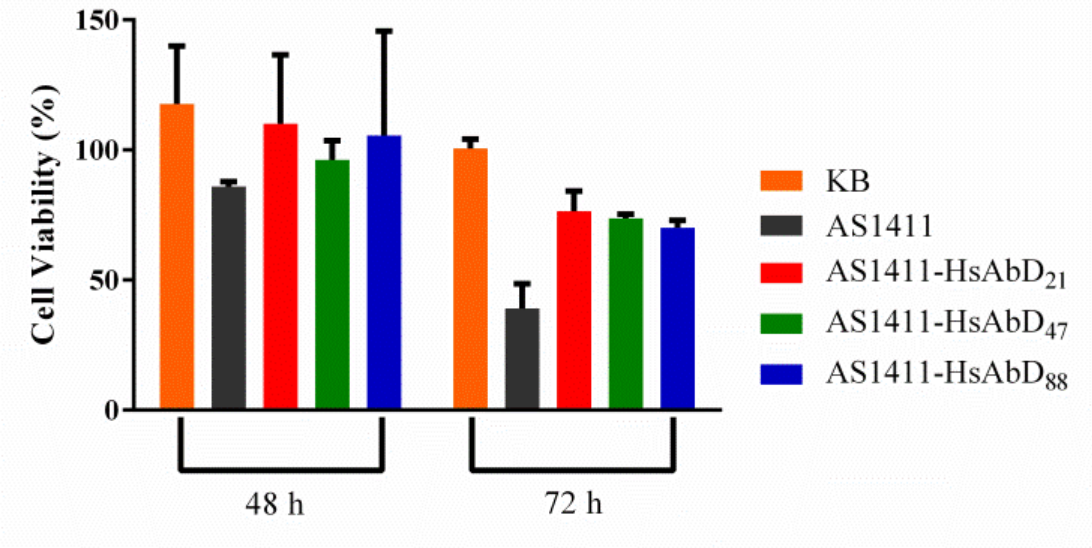

Figure 36. Cytotoxicity of AS1411 and BICs of AS1411 and **P12**, **P14**, and **P15** after 48 h and 72 h. Error bars represent the standard deviation of triplicate experiments.

Having achieved cellular delivery and entry, the anti-proliferative capability was assessed *via* cell viability assays (Figure 36). The concentration of AS1411 was maintained at 5 μM. After 48 h (Figure 36), negligible activity occurs, achieving a ~ 15% reduction in cell density. After 72 h, a ~65% reduction is observed. Interestingly, polymeric delivery of AS1411 using **P13**, **P14**, and **P15** achieve dissimilar results. After 48 h, **P13**, **P14**, and **P15** display negligible anti-proliferative activity. Additionally, after 72 h, between 20–25% in cellular reduction is observed when using **P13**, **P14**, and **P15**. We have previously reported time-delays in maximizing gene suppression utilizing siRNA. It is likely that the potency of AS1411 is reduced when delivered with hydrophilic-*block*-cationic copolymers due to the increased stability provided when the G-quad is complexed (i.e., decomplexation requires ion exchange/substitution reactions), thus delivery of this anticancer biologic would necessitate an increased amount of time before modest drug activity can be observed, since the activity of AS1411 is presumed to not be catalytic.

CHAPTER V

CONCLUSIONS

Section I. Endolytic, pH-Responsive HPMA-b-(L-Glu) Copolymers Synthesized via Sequential Aqueous RAFT and Ring Opening Polymerizations

HPMA-*block*-(L-Glu) copolymers with controlled structures, narrow PDIs, and target molecular weights were prepared by sequential aqueous RAFT and ring opening (NCA) polymerizations followed by post-reaction hydrolysis. The block copolymers with tailored L-glutamic acid sequences allow formation of membrane-disruptive helical segments at biorelevant pH values. Red blood cell hemolysis and fPOPC release studies were performed, and at moderate concentrations and sufficient block lengths (α-helical content), pH-dependent hemoglobin and fluorescein release occurred. It is anticipated that the facile synthetic approach reported here will allow further development of modular drug/gene carriers for the efficient endosomal release of anticancer drugs. While we have shown membrane disruption with these novel HPMA-*block*-(L-Glu) copolymers, future studies will be necessary to evaluate efficiency and mechanistic pathways of drug/gene delivery *in vitro*.

Section II. Block ionomer complexes consisting of siRNA and aqueous RAFT synthesized hydrophilic-*block*-cationic copolymers: Monitoring complex dissociation and the effects on gene suppression

Aqueous RAFT was utilized to prepare poly[(HPMA-*stat*-APMA)-*block*-DMAPMA copolymers with controlled lengths of DMAPMA. Well-defined BICs were prepared with siRNA and its dsDNA analogue, and the complexes formed with siRNA and GLuc DNA were comparable. AUC demonstrated increased binding constants with increasing cationic (DMAPMA) block length. Solution differential scanning calorimetry was conducted to determine BIC stability. The melting temperature of GLuc DNA, the siRNA analogue, significantly shifted to higher temperatures when complexed with hydrophilic-*block*-cationic copolymers. Furthermore, increasing DMAPMA block length increased the T_m of each block ionomer complex (**P12** > **P11** > **P10**). Since thermal denaturation of the DNA provided a large endotherm, single-stranded DNA was complexed with hydrophilic-*block*-cationic copolymers to determine thermodynamics of dissociation. Since no complex dissociation was observed under our experimental conditions, we believe that the binding constants are so high that any species dissociation would be below the instruments detection capability. While the precise nature of BIC complexation/decomplexation is not fully understood, these studies clearly demonstrate an increase in gene suppression with increasing DMAPMA block length, and more importantly, longer DMAPMA block lengths produced a time-delay in achieving a gene knockdown maximum. Additionally, the kinetics for achieving these maxima are consistent with ion exchange/substitution rates for IPECs and BICs. While we have demonstrated the effect of block length on gene suppression, the effect of the cationic-anionic registry (i.e., arrangement of cationic charges along the phosphate-helix

backbone) on binding strength, and subsequently, gene suppression is still under investigation.

Section III. Characterization of Block Ionomer Complexes Consisting of G-Quadruplexes and *a*RAFT Synthesized Hydrophilic-*block*-Cationic Copolymers and Subsequent Polymeric Delivery of AS1411

*a*RAFT was utilized to prepare poly[(HPMA-*stat*-APMA)-*block*-DMAPMA] copolymers with increasing DMAPMA block length (**P13**–**P15**). The HPMA segments confer water stability, while APMA provides a conjugation site for folic acid, a cellular targeting moiety. The cationic tertiary amines of DMAPMA serve to bind to AS1411, a G-quadruplex biologic, to form BICs. These complexes were well characterized; the hydrodynamic radii (R_h) increases with increasing DMAPMA block length (**P15** > **P14** > **P13**) and the complexes displayed near neutral zeta-potential values. Additionally, these complexes maintained narrow polydispersities (PDIs < 0.1). Circular dichroism spectroscopy (CD) was employed to ascertain structural alterations upon hydrophilic-*block*-cationic copolymer binding to AS1411. Polymer binding produces no observable shifts in the CD spectra, indicating structural modifications do not occur when AS1411 is complexed. The anti-proliferative capability of AS1411 was assessed by monitoring KB cell viability. KB cell proliferation was observed after 48 h, but ~ 65 % reduction in proliferation was achieved after 72 h when utilizing AS1411. BICs were less effective, achieving 20–25 % reduction in proliferation after 72 h. We hypothesized that complex stability for these BIC systems warrants a much longer time required for complex dissociation (e.g., ion exchange/substitution) to occur. Further studies are ongoing to probe the relationships between complex stability and AS1411's *in vitro* potency.

CHAPTER VI

FUTURE RECOMMENDATIONS

The work presented in this dissertation has provided novel insights into overcoming polymeric drug/gene delivery barriers. We have demonstrated that siRNA release is dictated *via* an ion exchange/substitution pathway, and exploiting this pathway, the time to achieve a gene suppression maximum has the potential to be tailored. We have only demonstrated this phenomenon utilizing polymeric carriers equipped with protonated tertiary amines. To explore further into these structure-property relationships, it is recommended that two systematic studies be conducted to elucidate effects imposed by the cationic structure: One study to vary the amine (cation) type, and the second study to vary the cationic charge density.

Scheme 4 presents a proposed synthetic pathway to study structure-property relationships relative to amine type. This synthetic strategy builds upon the McCormick group expertise in preparing functional, modular (co)polymers. Flores et al. demonstrated successful RAFT polymerization of unprotected isocyanates; however, these polymers could not be purified, and they required immediate functionalization. In this synthetic strategy, the isocyante is protected with an imidazole group, which can be easily displaced (i.e., quantitatively) with nucleophiles. More importantly, this pathway allows for the total block length to be equal, thus studying each amine type will relate to the ionic strength of the amine. Since the cationic block remains the same, only the binding strength between each type of amine will differ, and therefore, increased ionic strength would, hypothetically, increase the time required for complete dissociation and subsequently, gene suppression; refer to Section II of Chapter IV.

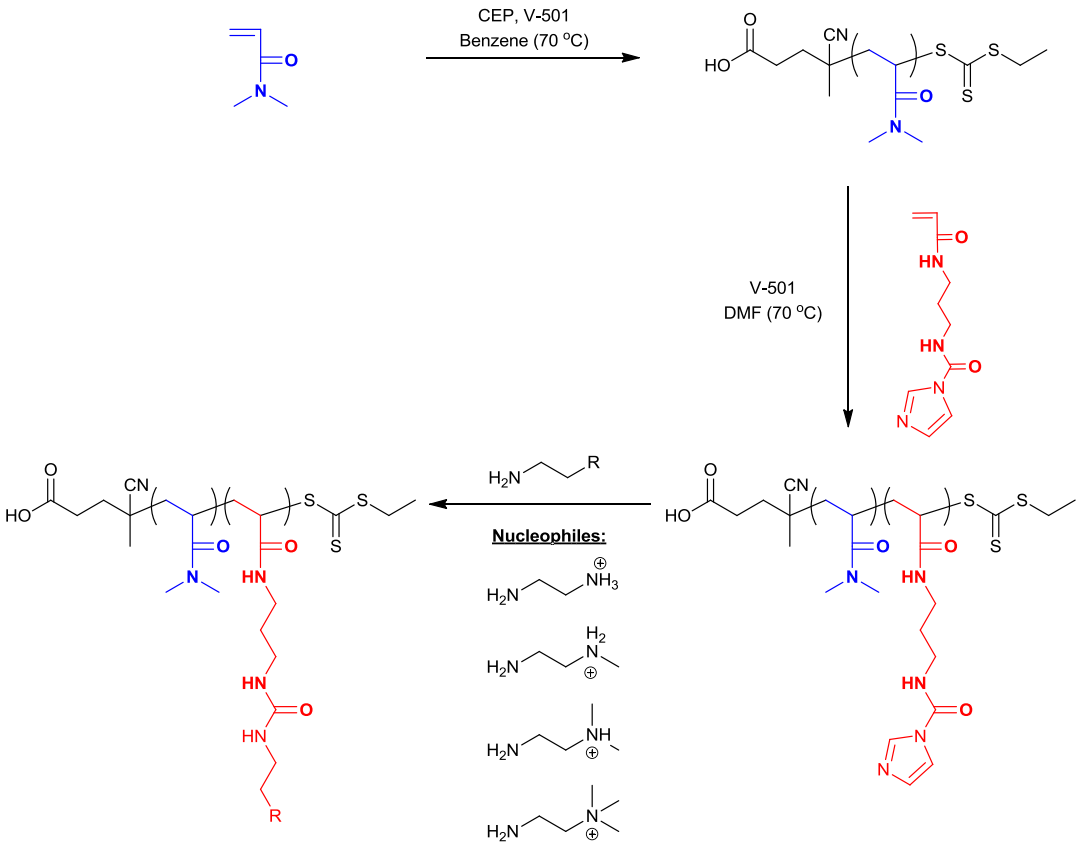

Scheme 4 Proposed synthetic pathway to synthesize block copolymers with differing amines (1°–4°).

In the second study, charge density is the focus. Scheme 5 presents a synthetic method that allows for production of polymeric carriers that vary in charge density. It is anticipated that a charge density exists such that dissociation may be monitored directly. To begin, the macroCTA remains similar to previous reports, and charge separation is achieved *via* increasing the molar composition of HPMA during chain extensions with a cationic monomer; see Table 7 for proposed molar compositions.

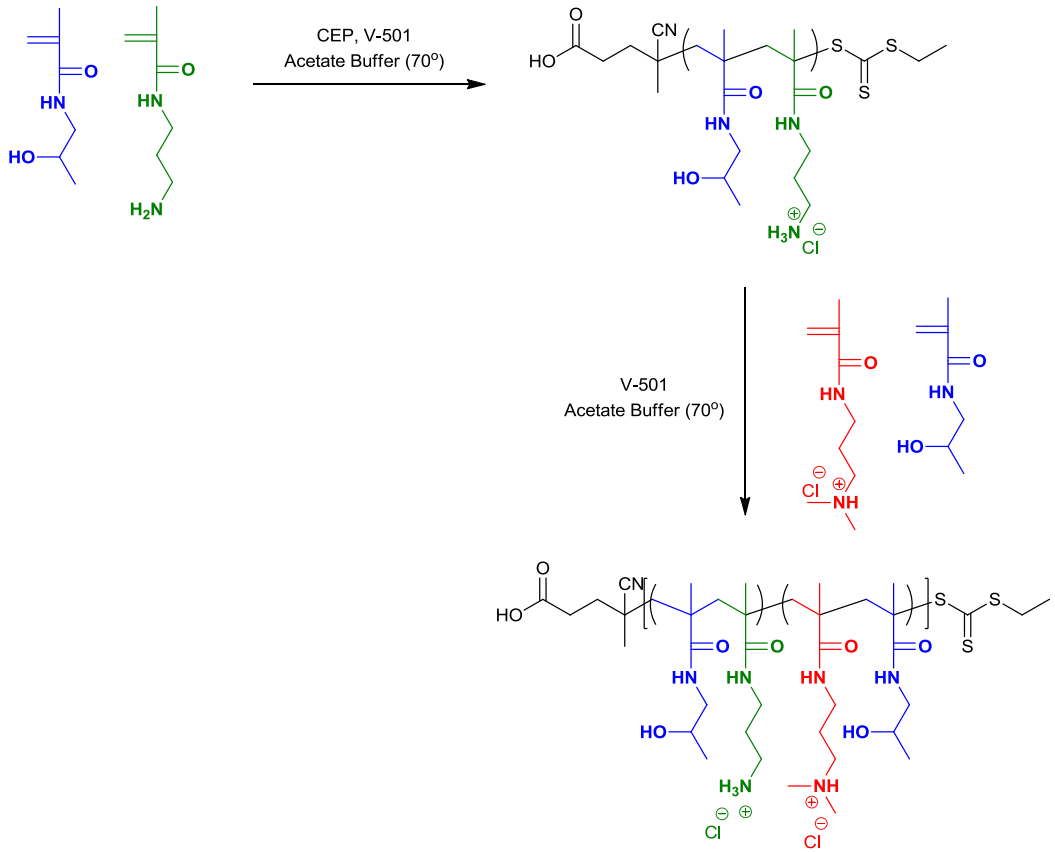

Scheme 5. Proposed synthetic pathway for the preparation of poly[(HPMA-*stat*-APMA)-*block*-(HPMA-*stat*-DMAPMA)] copolymers. In this method, The HPMA molar content in the chain extension will be varied to ensure charge separation (i.e., reduced charge density).

Table 7

Proposed hydrophilic-block-cationic copolymer compositions and degree of polymerization.

HPMA-*stat*-Folate Block (w:x)	**HPMA-*stat*-Cationic Block (y:z)**	**Total Cationic Repeats (DP)**
95:5	0:100, 10:90, 20:80, 30:70, 40:60, 50:50, 60:40, 70:30, 80:20, 90:10, 100:0	Maintained at 25

The final study aims to determine enzymatic interactions with BICs and enzymes. This study has two purposes. The first purpose is to elucidate kinetics of BIC ion exchange/substitution, and the second purpose is to ascertain the inhibition mechanisms (i.e., are hydrophilic-*block*-cationic copolymers competitive or noncompetitive inhibitors and are they reversible).

Consider the following scenario presented in Scheme 6. This scheme describes the formation of hydrophilic-*block*-cationic (H*b*C)-siRNA BICs which will undergo an irreversible exchange reaction with an analogous dsDNA. This exchange reaction is irreversible since an RNase will be present to selective cleave the siRNA into mononucleotides. It should be noted that human RNases are not capable of mononucleotide cleavage, and the RNase used should be purchased from EpiBio (Ribboshredder™-RS12100).

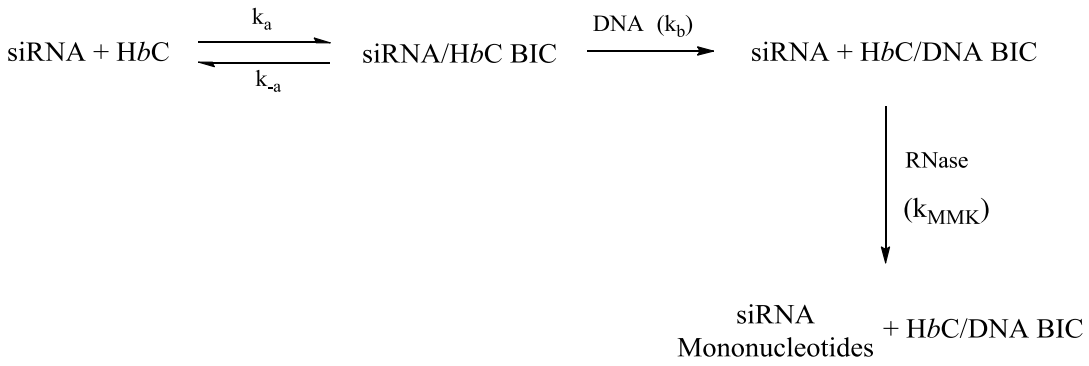

Scheme 6. Proposed reaction method for the determination of BIC ion exchange/substitution kinetics, and the inhibition mechanism.

Utilizing a photodiodearray spectrophotometer equipped with a stop-flow cuvette, the kinetics of BIC ion exchange/substitution as well as the inhibitory mechanisms may be elucidated. One will directly observe the formation of siRNA mononucleotides via an increase in absorbance at 260 nm. From this absorption increase k_b may be determined.

The challenge in this design arises from the fact that nucleases obey Michaelis-Menten kinetics, represented as k_{MMK} in the above scheme. A brief overview of enzyme kinetics is supplied, but any introductory biochemistry text will present the derivation of Michaelis-Menten equation in detail. An enzyme E combines with substrate S to form an ES complex, with a rate constant k_1. ES can dissociate to E and S, with a rate constant of k_{-1}, or ES can proceed to form product P, with a rate constant of k_2 (See Equation 3).

$$E + S \underset{k_{-1}}{\overset{k_1}{\rightleftharpoons}} ES \underset{k_{-2}}{\overset{k_2}{\rightleftharpoons}} E + P \qquad (eq\ 3)$$

The ES complex can also be reformed from E and P by the reverse reaction with a rate constant k_{-2}. However, one may simplify these reactions by considering the rate of reaction at times close to zero when there is negligible product formation, thus no reverse reaction (i.e., $k_{-2}[P] \approx 0$) (See Equation 4):

$$E + S \underset{k_{-1}}{\overset{k_1}{\rightleftharpoons}} ES \xrightarrow{k_2} E + P \qquad (eq\ 4)$$

The rate of reaction at times close to zero is determined by V_0, and it is determined for each substrate concentration by measuring the rate of product formation (siRNA mononucleotides) at early times, typically within the beginning 5 % of the reaction. V_0 can be related to the rate of catalysis to the concentrations of substrate and enzyme and the rate of the individual steps *via* the steady-state approximation to give Equation 5

$$k_1[E][S] = (k_{-1} + k_2)[ES] \quad (eq\ 5).$$

Equation 8 is simplified by defining a new constant, K_M, called the Michaelis constant:

$$K_M = \frac{k_{-1} + k_2}{k_1} \quad (eq\ 6).$$

After rearranging and solving for [ES], the equation becomes

$$[ES] = \frac{[E][S]}{K_M} \quad (eq\ 7).$$

Since the substrate concentration is usually present at a much higher concentration than the enzyme, the concentration of uncombined substrate [S] is very nearly equal to the total substrate concentration. Furthermore, the concentration of uncombined enzyme [E] is equal to the total enzyme concentration minus the concentration of the ES complex. Using this information,V_0 may be determined utilizing Equation 8:

$$V_0 = V_{max}\frac{[S]}{[S]+K_M} \quad (eq\ 8)$$

in which $V_{max} = k_2[E]_T$, and $[E]_T$ is the total enzyme concentration. Equation 10 is known as the Michaelis-Menten equation.

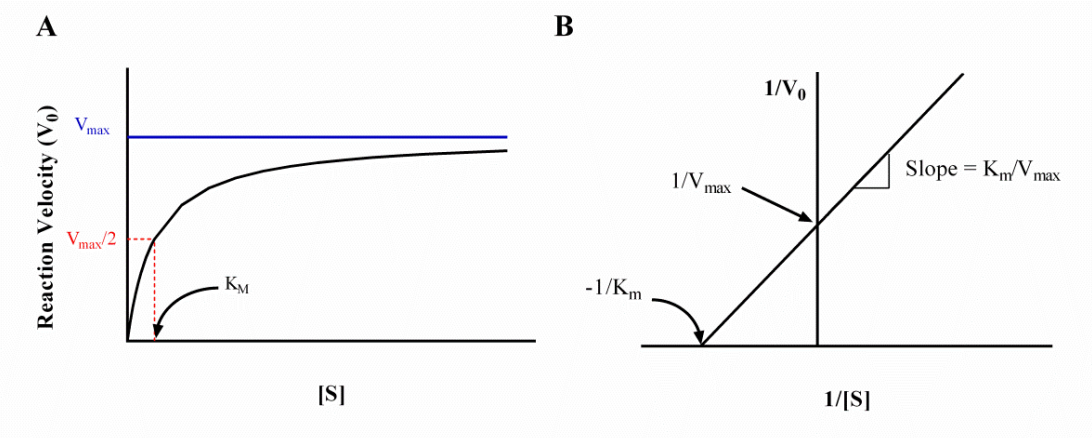

Figure 37 Enzyme kinetic plots representing typical Michaelis-Menten kinetics (A) and a Lineweaver-Burk plot (B).

This equation is important for two reasons, the equation describes the first order reaction rate (i.e., at early times [S] << K_M, $V_0 = (V_{max}/K_M)[S]$)) as well as the zero order reaction rate when [S] >> K_M ($V_0 = V_{max}$) (See Figure 37-A). Since one may determine V_{max}, and the total enzyme concentration is known, then the rate of catalysis k_2 may be

determined, and in our case, $k_2 = K_{MMK}$ (See Scheme 6). It should be noted that there are two methods for the determination of Michaelis-Menten parameters. The first method utilizes a double reciprocal plot — the Lineweaver-Burk plot (See Equation 9 and Figure 37-B).

$$\frac{1}{V_o} = \frac{K_M}{V_{max}} * \frac{1}{S} + \frac{1}{V_{max}} \quad (eq\ 9)$$

This plot yields a straight line with a y-intercept of $1/V_{max}$ and a slope of K_M/V_{max}. The x-intercept is $-1/K_M$. This method is not recommended as a means to determine the Michaelis-Menten parameters because it overestimates the x-intercept and overestimates the slope. In the second method, a double-floating parameter fit is applied to the Michaelis-Menten kinetic data. This procedure is easily accomplished utilizing Origin or GraphPad Prism graphing software, and in the case of enzyme kinetics, the equations and fitting function are built-in. This method is the most accurate means to determine the Michaelis-Menten parameters.

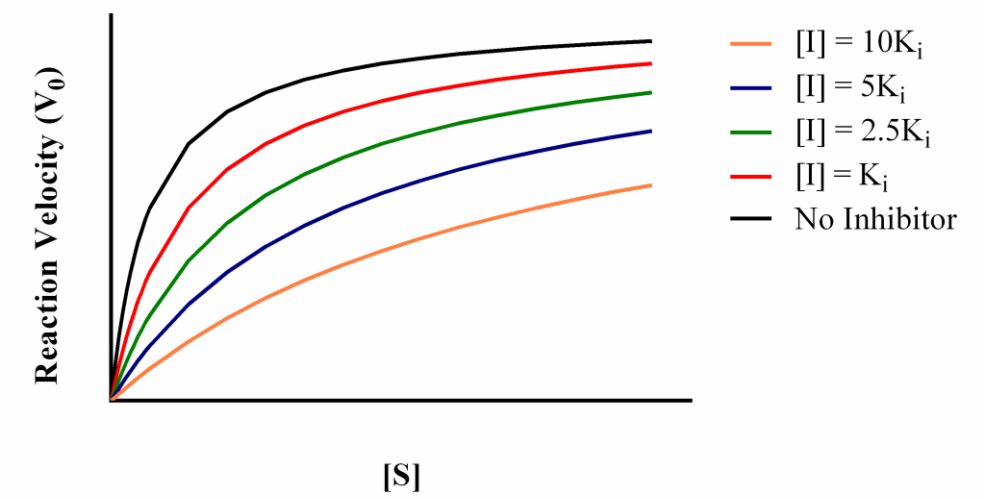

Figure 38. Data representative of competitive inhibition.

The determination of k_2 allows for the determination k_b which is the rate of BIC ion exchange/substitution. Once the rate of BIC exchange/substitution is known, the inhibitory mechanism may be ascertained. This section will provide a means to determine reversible inhibitors.

There are three types of reversible inhibitors (See Scheme 7), competitive, uncompetitive, and noncompetitive. In competitive inhibition (See Figure 38), the inhibitor competes with the substrate for the active site. The dissociation constant for the inhibitor (K_i) is given by Equation 10

$$K_i = [E][I]/[EI] \quad (eq\ 10)$$

in which [E] is the enzyme concentration, [I] is the inhibitor, and in our case, the hydrophilic-*block*-cationic copolymer utilized, and [EI] is the concentration of enzyme-inhibitor complex. The smaller the K_i, the more potent inhibition. The effect of a competitive inhibitor is to increase the apparent value of K_M. This new value of K_M, called $K_{M,\,APP}$, is determined via Equation 11.

$$K_{M,APP} = K_M\left(1 + \frac{[I]}{K_i}\right) \quad (eq\ 11)$$

In uncompetitive inhibition (See Figure 39), the inhibitor binds only to the ES complex. This enzyme-substrate-inhibitor complex ESI (i.e., BICs interacting with enzyme) does not go on to form any product thus lowering V_{max}. For uncompetitive inhibition, a lower concentration of S is required to form half the maximal concentration of ES, and the apparent value of K_M is reduced.

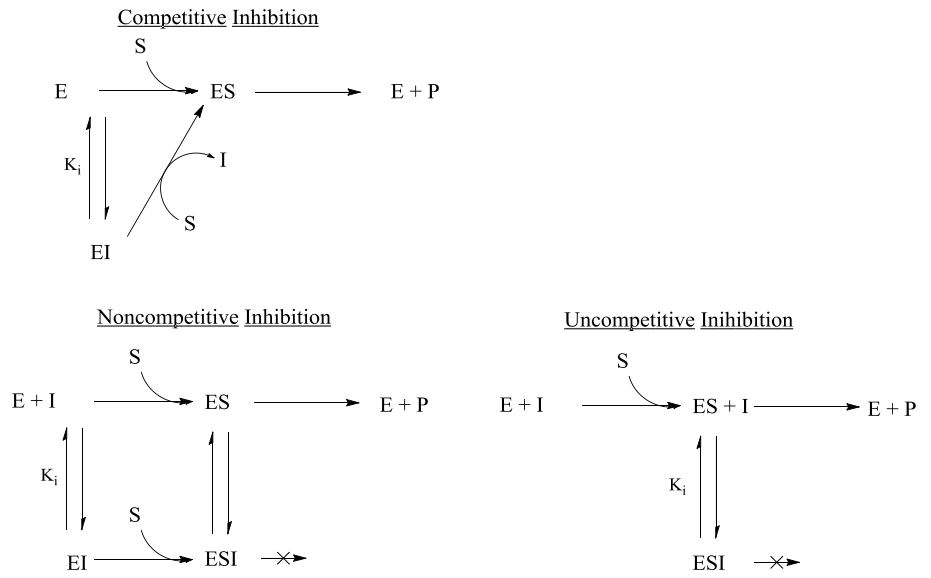

Scheme 7. Reaction pathways for competitive, noncompetitive, and uncompetitive inhibition.

In noncompetitive inhibition (See Figure 40), substrate can bind to the enzyme-inhibitor complex; however, the enzyme-inhibitor-substrate complex does not proceed to form product. The value of V_{max} is decrease to a new value, $V_{max,app}$, and the value of K_M is unchanged. $V_{max,app}$ can be determined from Equation 12.

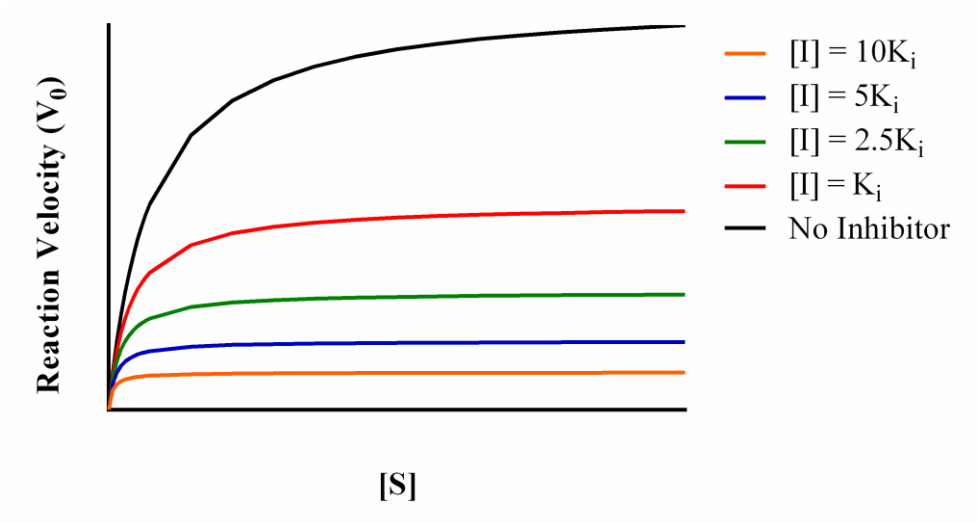

Figure 39. Data representative of uncompetitive inhibition.

$$V_{max,app} = \frac{V_{max}}{1+\frac{[I]}{K_i}} \qquad \text{(eq } \textit{12}\text{)}$$

Noncompetitive inhibition results in solutions that behave similarly to a dilute concentration of functional enzyme, thus the lowering of V_{max} is observed while K_M is unaltered.

The most facile method to ascertain the inhibitory mechanism is *via* double-reciprocal plots (See Figure 41). In competitive inhibition, the y-intercept remains unchanged; however, the slope is increased. In the presence of a competitive inhibitor, Equation 8 is replaced by Equation 13 (See Figure 41-B).

$$\frac{1}{V_o} = \frac{1}{V_{max}} + \frac{K_M}{V_{max}}\left(1 + \frac{[I]}{K_i}\right)\left(\frac{1}{[S]}\right) \quad (\textit{eq 13})$$

In uncompetitive inhibition, the inhibitor combines only with the enzyme-substrate complex. Therefore, Equation 10 is replaced with Equation 16 (See Figure 41-C).

$$\frac{1}{V_o} = \frac{K_M}{V_{max}[S]} + \frac{1}{V_{max}}\left(1 + \frac{[I]}{K_i}\right) \quad (\textit{eq 14})$$

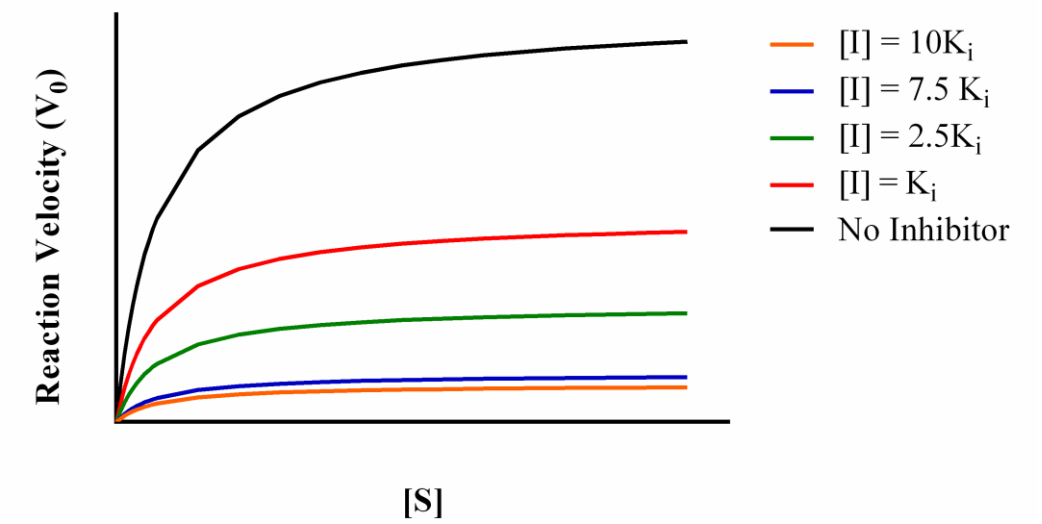

Figure 40. Data representative of noncompetitive inhibition.

In noncompetitive inhibition, the value of V_{max} is decreased to the new value $V_{max,app}$, and the y- intercept is increased. The new slope, which is equal to $K_M/V_{max,app}$, is increased by the same factor (See Figure 41-D).

From these plots, the inhibitory mechanism may be ascertained.

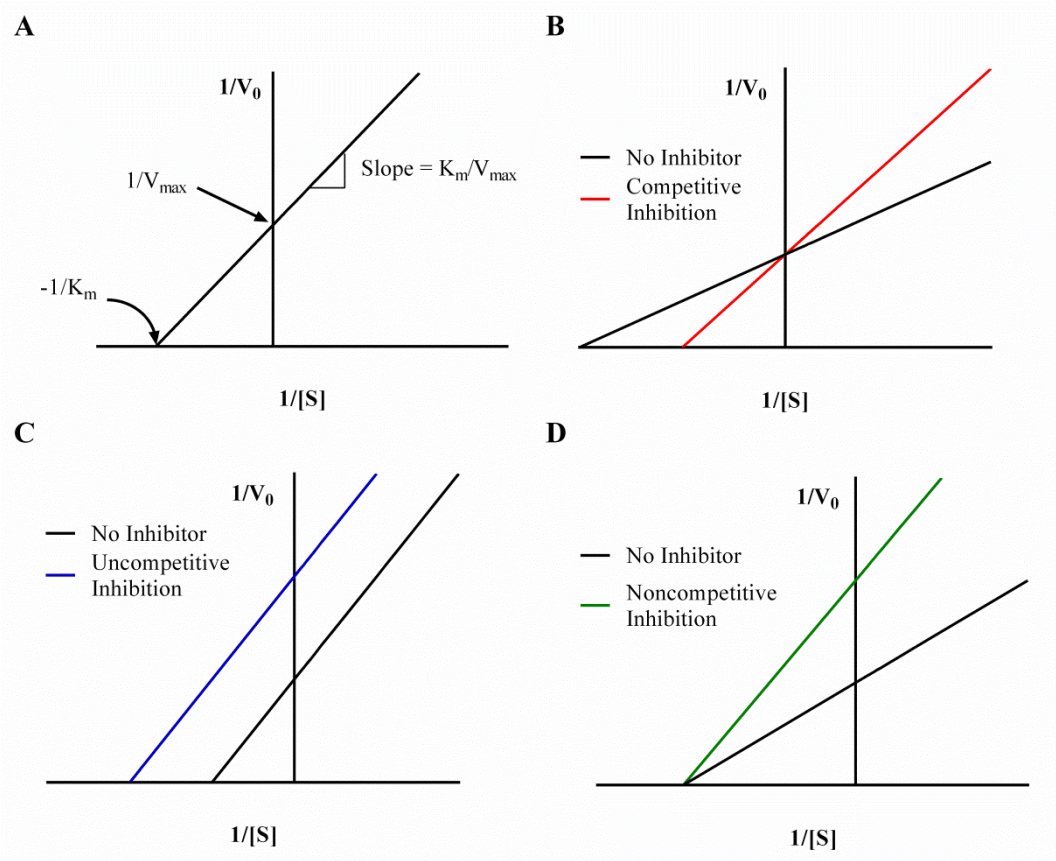

Figure 41. Representative double-reciprocal plots for Lineweaver-Burk (A), competitive inhibition (B), uncompetitive inhibition (C), and noncompetitive inhibition (D).

APPENDIX A

SUPPLEMENTARY TO SECTION I OF CHAPTER IV

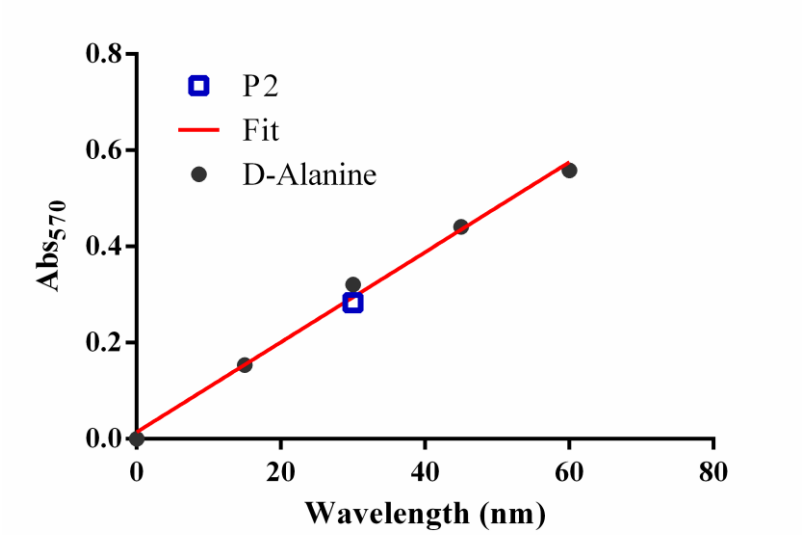

Figure A1 Absorbance of ninhydrin at 570 nm versus amine concentration for D-alanine (filled circles) and **P2** (open, blue square).

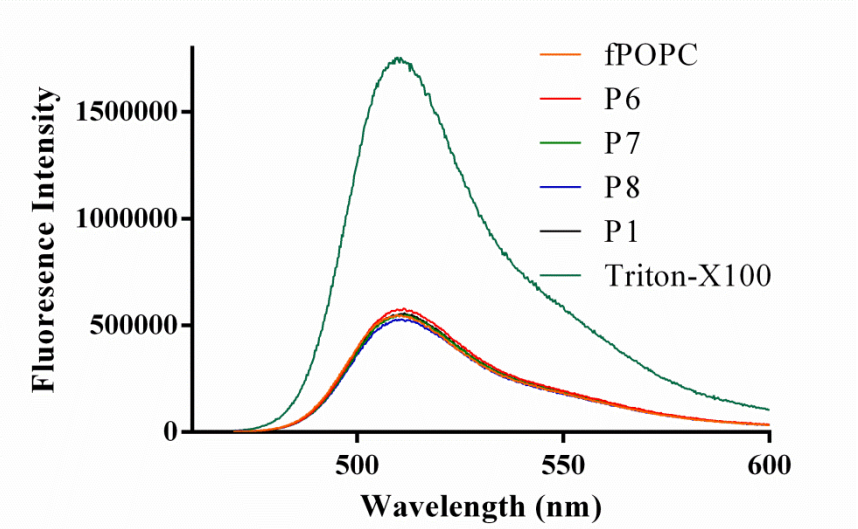

Figure A2. Fluorescence intensity of fPOPC at pH 7.4. fPOPC was incubated with **P1** and **P6**–**P8** copolymers. Triton-X100 was utilized as the positive control. No observable increase in fluorescein release was determined at pH 7.4 when incubated with **P6**–**P8** copolymers.

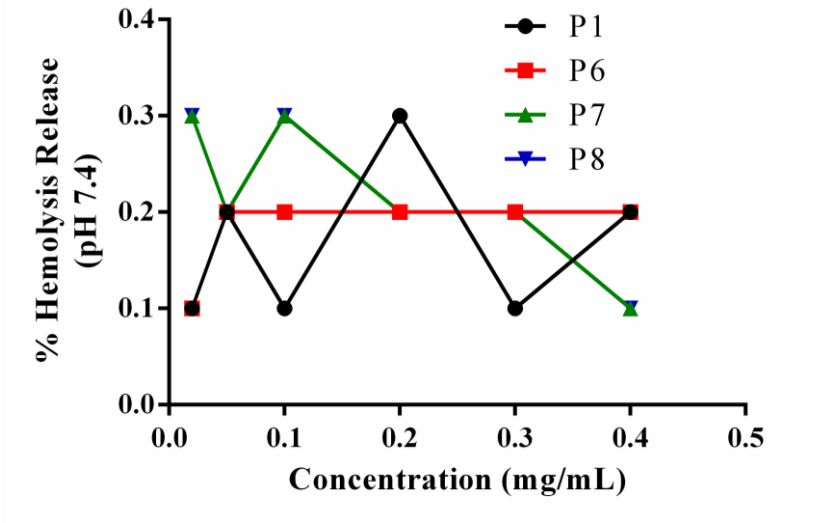

Figure A3. Percent hemolysis release as a function of concentration for **P1** and **P6**–**P8** copolymers. Triton-X100 was utilized as the positive control.

APPENDIX B

SUPPLEMENTARY TO SECTION II OF CHAPTER IV

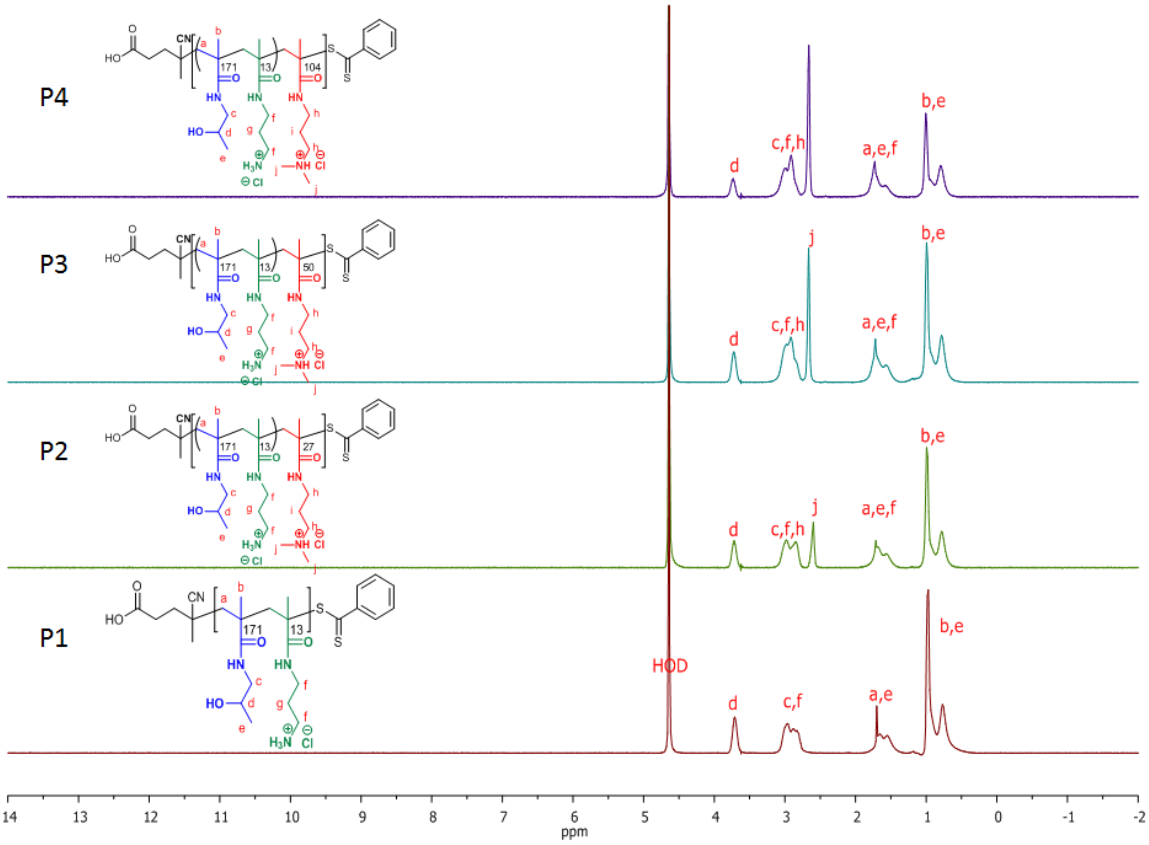

Figure B1. ^{1}H NMR of **P9**, **P10**, **P11**, and **P12** (the macroCTA and subsequent chain extensions with DMAPMA).

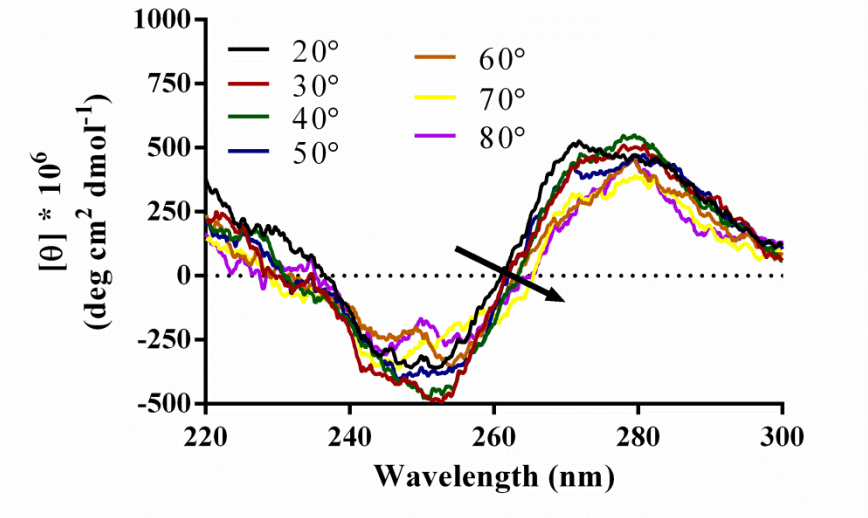

Figure B2. Circular dichroism melting spectra of GLuc DNA.

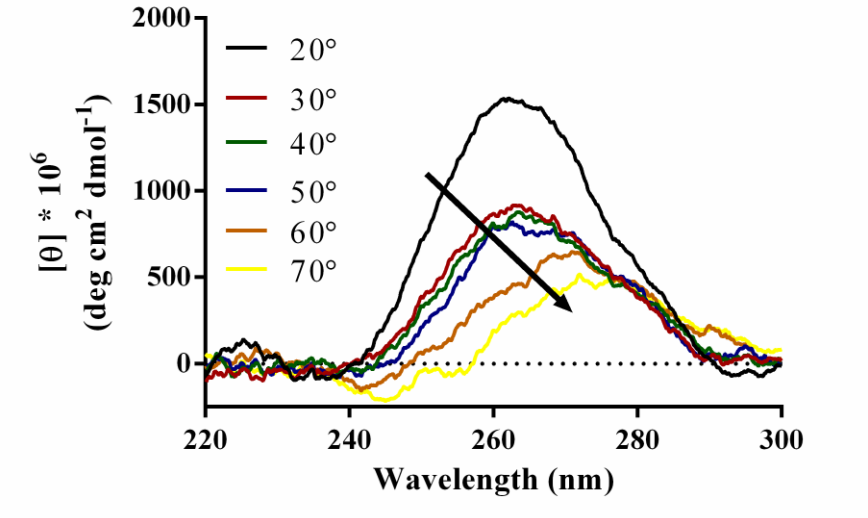

Figure B3. Circular dichroism melting spectra for siRNA.

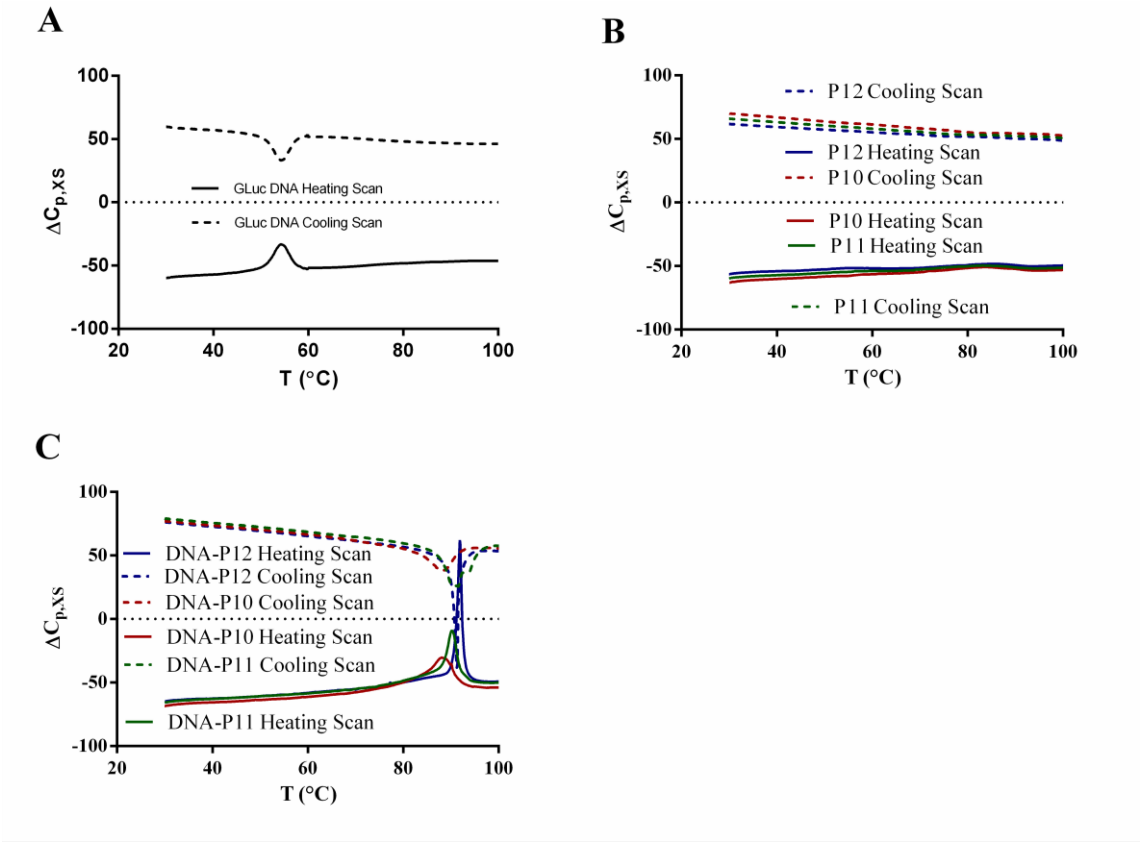

Figure B4. Heating and cooling solution DSC thermograms for (A) GLuc DNA, (B) hydrophilic-*block*-cationic copolymers (**P10**–**P12**), and (C) DNA-hydrophilic-*block*-cationic copolymer complexes. No hysteresis is evident between heating and cooling (i.e., these systems are reversible).

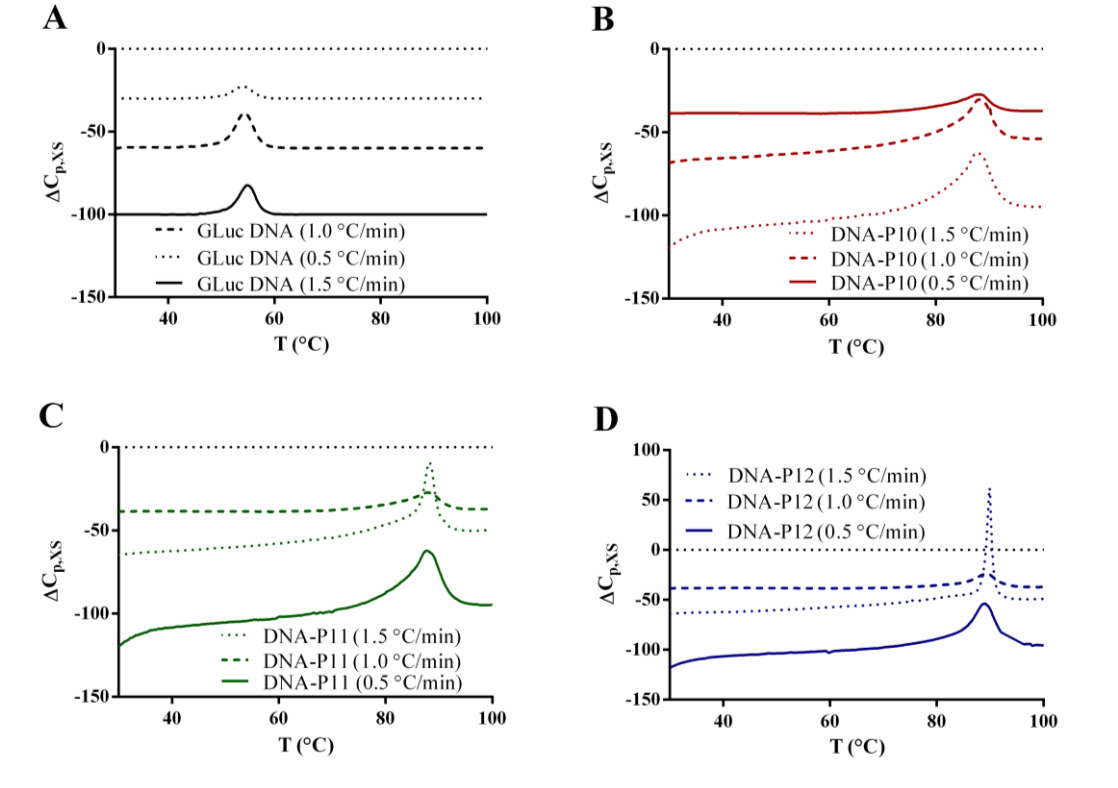

Figure B5. Solution DSC thermograms illustrating the scan rate dependence for (A) GLuc DNA, (B) DNA-**P10** complexes, (C) DNA-**P11** complexes, and (D) DNA-**P12** complexes. The melting temperature (T_m) remains constant with respect to scan rate (i.e., these systems are in equilibrium).

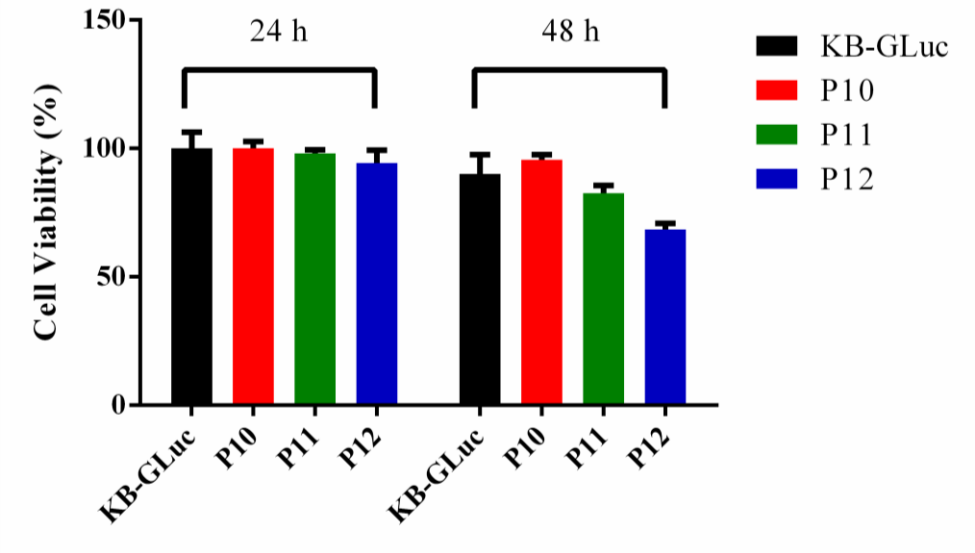

Figure B6. Cell viability assays of **P10**, **P11**, and **P12**.

Table B1

The melting temperature (T_m) calorimetric enthalpy (ΔH_{Cal}), van't Hoff enthalpy (ΔH_{VH}), entropy (ΔS) Gibb's free energy (ΔG) for GLuc DNA and GLuc DNA-hydrophilic-block-cationic copolymer complexes.

Sample	**ΔH_{Cal} (kcal/mol)**	**ΔH_{VH} (kcal/mol)**	**ΔS (kcal/mol *K)**	**ΔG (kcal/mol)**	**T_m (°C)**
Gluc DNA	240	240	106	204	54.4
DNA-**P10**	420	367	120	340	88.8
DNA-**P11**	483	686	140	413	90.2
DNA-**P12**	461	1900	143	393	91.8

APPENDIX C

SUPPLEMENTARY TO SECTION III OF CHAPTER IV

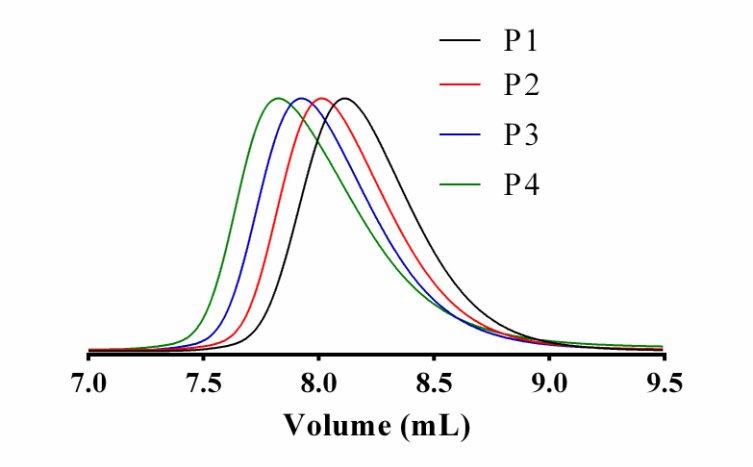

Figure C1. Light scattering traces of poly(HPMA$_{202}$-*stat*-APMA$_8$) macroCTA (**P1**), and subsequent chain extensions with DMAPMA (**P2**–**P4**).

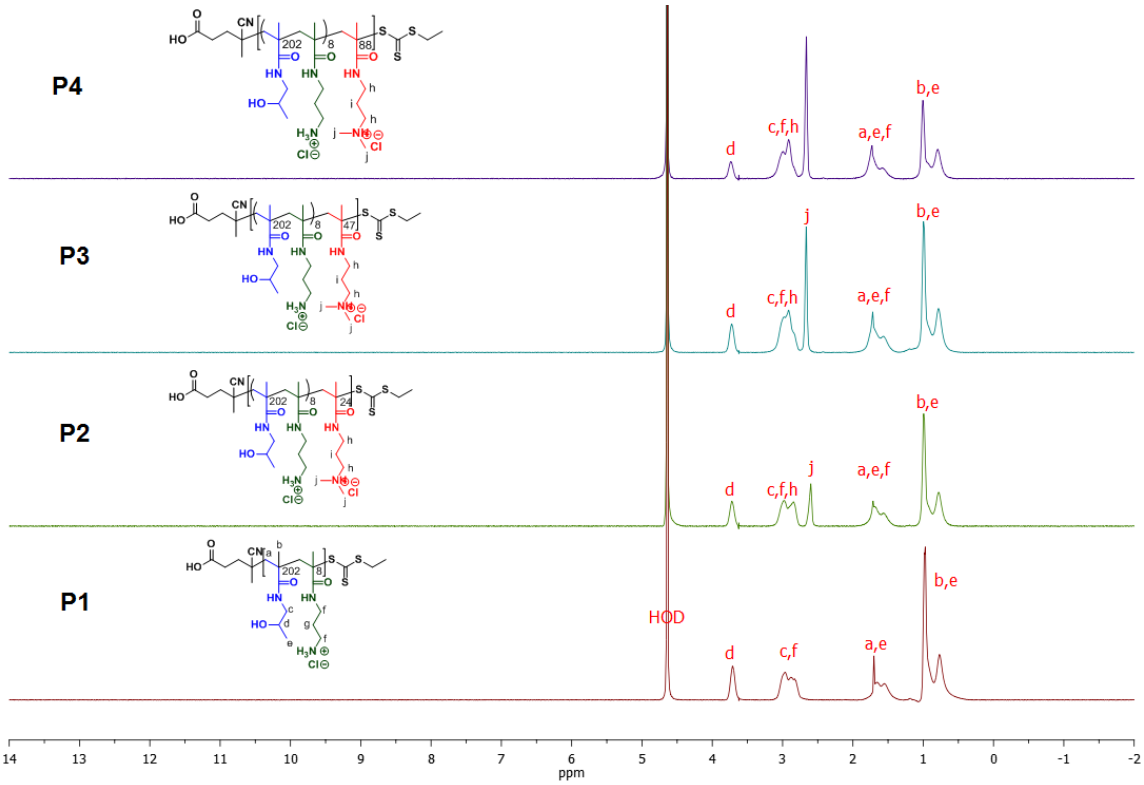

Figure C2. ^{1}H NMR of poly(HPMA$_{202}$-*stat*-APMA$_{8}$) macroCTA (**P1**) and subsequent chain extensions with DMAPMA (**P2**–**P4**).

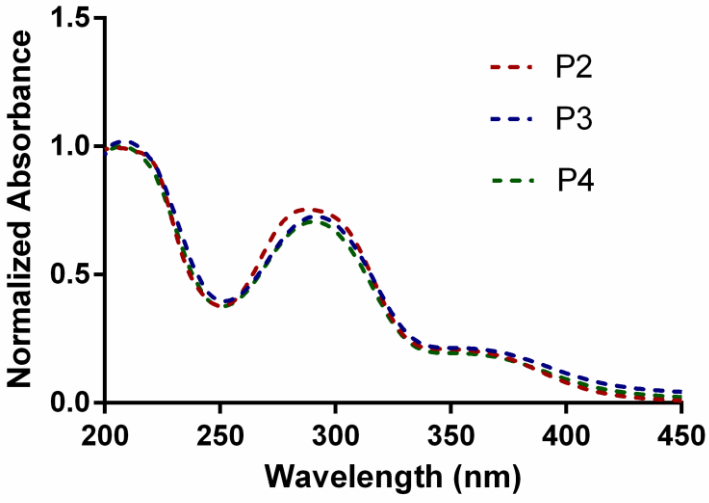

Figure C3. Uv/Vis spectroscopy of conjugated folic acid to **P2**, **P3**, and **P4**.

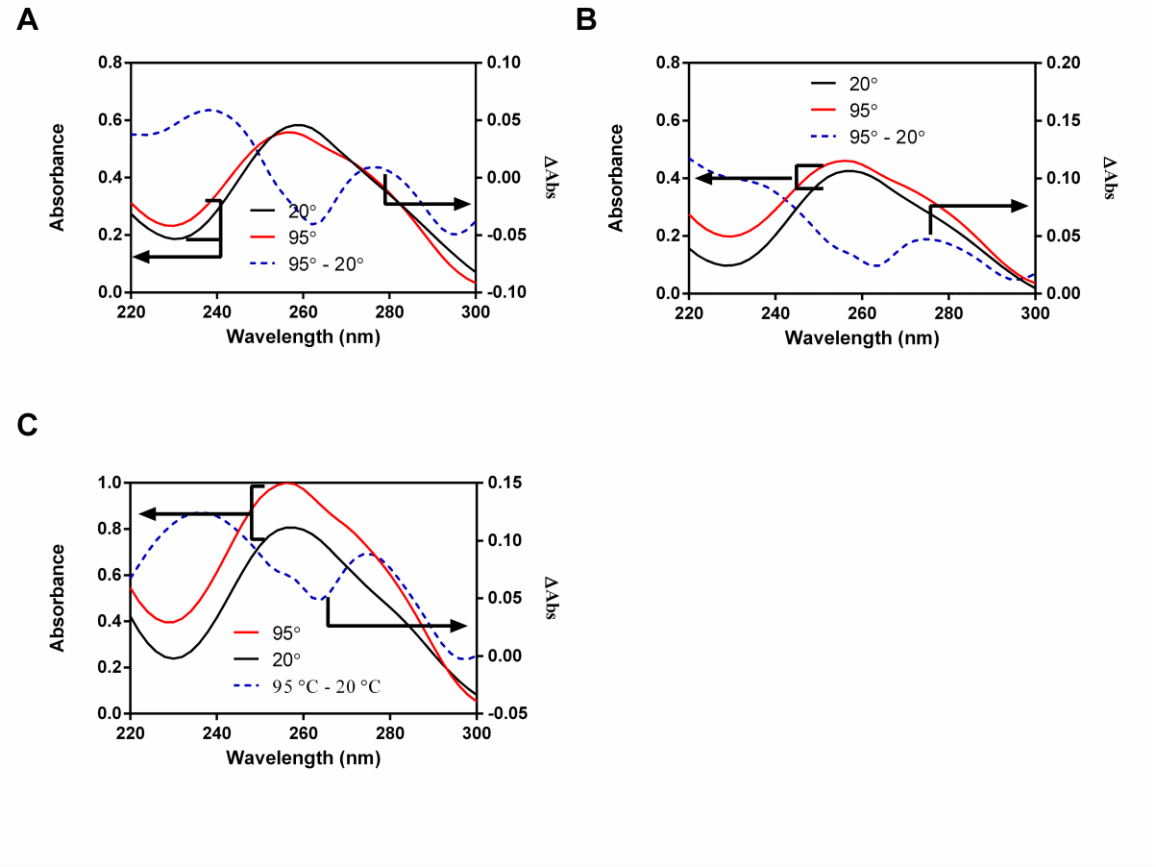

Figure C4.Heated (Red), cooled (Black), and difference (Blue, dashed) Uv/vis spectra of (A) 15APT, (B) 27S, and (C) AS1411 G-quadruplexes.

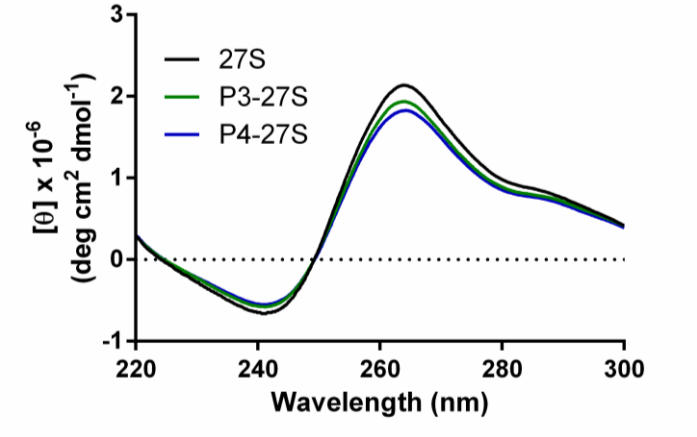

Figure C5. Circular dichroism spectra of 27S and hydrophilic-*block*-cationic copolymer/27S BICs.

Table C1

The maximum, minimum, and cross-over for AS1411 and hydrophilic-block-cationic copolymer/AS1411 BICs.

Sample	**λ_{Max} (nm)**	**λ_{Min} (nm)**	**$\lambda_{Cross\text{-}over}$ (nm)**
AS1411	261	238	252
P2-AS1411	261	239	255
P3-AS1411	261	238	253
P4-AS1411	261	239	255

Table C2

The maximum, minimum, and cross-over for 27S and hydrophilic-block-cationic copolymer/27S BICs.

Sample	**λ_{Max} (nm)**	**λ_{Min} (nm)**	**$\lambda_{Cross\text{-}over}$ (nm)**
27S	264	241	251
P2-27S	264	241	250
P3-27S	264	241	252
P4-27S	264	241	255

REFERENCES

(1) Fire, A.; Xu, S.; Montgomery, M. K.; Kostas, S. A.; Driver, S. E.; Mello, C. C. *Nature* **1998**, *391*, 806–811.

(2) Chiefari, J.; Chong, Y. K. (Bill); Ercole, F.; Krstina, J.; Jeffery, J.; Le, T. P. T.; Mayadunne, R. T. A.; Meijs, G. F.; Moad, C. L.; Moad, G.; Rizzardo, E.; Thang, S. H. *Macromolecules* **1998**, *31*, 5559–5562.

(3) Elbashir, S. M.; Harborth, J.; Lendeckel, W.; Yalcin, a; Weber, K.; Tuschl, T. *Nature* **2001**, *411*, 494–498.

(4) Mitsukami, Y.; Donovan, M. S.; Lowe, A. B.; Mccormick, C. L. *Macromolecules* **2001**, *34*, 2248–2256.

(5) McCormick, C. L.; Lowe, A. B. *Acc. Chem. Res.* **2004**, *37*, 312–325.

(6) Ringsdorf, H. *J. Polym. Sci. Polym. Symp.* **1975**, *51*, 135–153.

(7) Smith, A. E.; Xu, X.; McCormick, C. L. *Prog. Polym. Sci.* **2010**, *35*, 45–93.

(8) Gary, D. J.; Puri, N.; Won, Y.-Y. *J. Control. Release* **2007**, *121*, 64–73.

(9) Bader, H.; Ringsdorf, H.; Schmidt, B. *Die Angew. Makromol. Chemie* **1984**, *123*, 457–485.

(10) Davis, M. E.; Chen, Z. (Georgia); Shin, D. M. *Nat Rev Drug Discov* **2008**, *7*, 771–782.

(11) D'Emanuele, A.; Attwood, D. *Adv. Drug Deliv. Rev.* **2005**, *57*, 2147–2162.

(12) Heath, W. H.; Senyurt, A. F.; Layman, J.; Long, T. E. *Macromol. Chem. Phys.* **2007**, *208*, 1243–1249.

(13) Licciardi, M.; Tang, Y.; Billingham, N. C.; Armes, S. P.; Lewis, A. L. *Biomacromolecules* **2005**, *6*, 1085–1096.

(14) Merdan, T.; Kopeček, J.; Kissel, T. *Adv. Drug Deliv. Rev.* **2002**, *54*, 715–758.

(15) Napier, M. E.; DeSimone, J. M. *Polym. Rev.* **2007**, *47*, 321–327.

(16) Pack, D. W.; Hoffman, A. S.; Pun, S.; Stayton, P. S. *Nat. Rev. Drug Discov.* **2005**, *4*, 581–593.

(17) Park, T. G.; Jeong, J. H.; Kim, S. W. *Adv. Drug Deliv. Rev.* **2006**, *58*, 467–486.

(18) Svenson, S.; Tomalia, D. A. *Adv. Drug Deliv. Rev.* **2005**, *57*, 2106–2129.

(19) Wong, S. Y.; Pelet, J. M.; Putnam, D. *Prog. Polym. Sci.* **2007**, *32*, 799–837.

(20) York, A. W.; Kirkland, S. E.; McCormick, C. L. *Adv. Drug Deliv. Rev.* **2008**, *60*, 1018–1036.

(21) Xu, L.; Anchordoquy, T. *J. Pharm. Sci.* **2011**, *100*, 38–52.

(22) Gaynor, J. W.; Campbell, B. J.; Cosstick, R. *Chem. Soc. Rev.* **2010**, *39*, 4169–4184.

(23) Christie, R. J.; Nishiyama, N.; Kataoka, K. *Endocrinology* **2010**, *151*, 466–473.

(24) Grigsby, C. L.; Leong, K. W. *J. R. Soc. Interface* **2010**, *7* , S67–S82.

(25) Higuchi, Y.; Kawakami, S.; Hashida, M. *BioDrugs* **2010**, *24*, 195–205.

(26) Oh, Y.-K.; Park, T. G. *Adv. Drug Deliv. Rev.* **2009**, *61*, 850–862.

(27) Pichon, C.; Billiet, L.; Midoux, P. *Curr. Opin. Biotechnol.* **2010**, *21*, 640–645.

(28) Roth, C. M. *Biotechnol. Prog.* **2008**, *24*, 23–28.

(29) Wang, X.; Zhou, L.; Ma, Y.; Li, X.; Gu, H. *Nano Res.* **2009**, *2*, 365–372.

(30) Hawker, C. J.; Bosman, A. W.; Harth, E. *Chem. Rev.* **2001**, *101*, 3661–3688.

(31) Matyjaszewski, K.; Xia, J. *Chem. Rev.* **2001**, *101*, 2921–2990.

(32) Moad, G.; Rizzardo, E.; Thang, S. H. Living Radical Polymerization by the RAFT Process. *Australian Journal of Chemistry*, 2005, *58* , 379–410.

(33) Moad, G.; Rizzardo, E.; Thang, S. H. *Acc. Chem. Res.* **2008**, *41*, 1133–1142.

(34) Perrier, S.; Takolpuckdee, P. *J. Polym. Sci. Part A Polym. Chem.* **2005**, *43*, 5347–5393.

(35) Lowe, A. B.; McCormick, C. L. *Prog. Polym. Sci.* **2007**, *32*, 283–351.

(36) Lowe, A. B.; McCormick, C. L. In *Handbook of RAFT Polymerization*; Wiley-VCH Verlag GmbH & Co. KGaA, 2008; pp. 235–284.

(37) Alidedeoglu, A. L. P. H.; York, A. W.; Cormick, C. L. M. C.; Morgan, S. E. *J. Polym. Sci. Part A Polym. Chem.* **2009**, *47*, 5405–5415.

(38) Convertine, A. J.; Diab, C.; Prieve, M.; Paschal, A.; Hoffman, A. S.; Johnson, P. H.; Stayton, P. S. *Biomacromolecules* **2010**, 2904–2911.

(39) Convertine, A. J.; Benoit, D. S. W.; Duvall, C. L.; Hoffman, A. S.; Stayton, P. S. *J. Control. Release* **2009**, *133*, 221–229.

(40) Kirkland-York, S.; Zhang, Y.; Smith, A. E.; York, A. W.; Huang, F.; McCormick, C. L. *Biomacromolecules* **2010**, *11*, 1052–1059.

(41) Scales, C. W.; Huang, F.; Li, N.; Vasilieva, Y. A.; Ray, J.; Convertine, A. J.; McCormick, C. L. *Macromolecules* **2006**, *39*, 6871–6881.

(42) York, A. W.; Zhang, Y.; Holley, A. C.; Guo, Y.; Huang, F.; McCormick, C. L. *Biomacromolecules* **2009**, *10*, 936–943.

(43) Zhu, C.; Jung, S.; Luo, S.; Meng, F.; Zhu, X.; Park, T. G.; Zhong, Z. *Biomaterials* **2010**, *31*, 2408–2416.

(44) Valade, D.; Boyer, C.; Davis, T. P.; Bulmus, V. Synthesis of siRNA Polyplexes Adopting a Combination of RAFT Polymerization and Thiol-ene Chemistry. *Australian Journal of Chemistry*, 2009, *62* , 1344–1350.

(45) Convertine, A. J.; Lokitz, B. S.; Lowe, A. B.; Scales, C. W.; Myrick, L. J.; McCormick, C. L. *Macromol. Rapid Commun.* **2005**, *26*, 791–795.

(46) Donovan, M. S.; Lowe, A. B.; Sumerlin, B. S.; Mccormick, C. L. *Macromolecules* **2002**, *35*, 4123–4132.

(47) Donovan, M. S.; Sanford, T. A.; Lowe, A. B.; Sumerlin, B. S.; Mitsukami, Y.; McCormick, C. L. *Macromolecules* **2002**, *35*, 4570–4572.

(48) Lowe, A. B.; McCormick, C. L. *Aust. J. Chem.* **2002**, *55*, 367–379.

(49) Ulbrich, K.; Etrych, T.; Chytil, P.; Pechar, M.; Jelínková, M.; Rihova, B. *Int. J. Pharm.* **2004**, *277*, 63–72.

(50) Ulbrich, K.; Šubr, V. *Adv. Drug Deliv. Rev.* **2004**, *56*, 1023–1050.

(51) Tang, A.; Kopečková, P.; Kopeček, J. *Pharm. Res.* **2003**, *20*, 360–367.

(52) Scales, C. W.; Vasilieva, Y. A.; Convertine, A. J.; Lowe, A. B.; McCormick, C. L. *Biomacromolecules* **2005**, *6*, 1846–1850.

(53) Scales, C. W.; Convertine, A. J.; McCormick, C. L. *Biomacromolecules* **2006**, *7*, 1389–1392.

(54) Satchi-Fainaro, R.; Hailu, H.; Davies, J. W.; Summerford, C.; Duncan, R. *Bioconjug. Chem.* **2003**, *14*, 797–804.

(55) Putnam, D.; Kopeček, J. In *Biopolymers II SE - 2*; Peppas, N.; Langer, R., Eds.; Advances in Polymer Science; Springer Berlin Heidelberg, 1995; Vol. 122, pp. 55–123.

(56) Nori, A.; Kopeček, J. *Adv. Drug Deliv. Rev.* **2005**, *57*, 609–636.

(57) Nori, A.; Jensen, K. D.; Tijerina, M.; Kopečková, P.; Kopeček, J. *Bioconjug. Chem.* **2002**, *14*, 44–50.

(58) Kovář, M.; Kovář, L.; Šubr, V.; Etrych, T.; Ulbrich, K.; Mrkvan, T.; Loucká, J.; Říhová, B. *J. Control. Release* **2004**, *99*, 301–314.

(59) Kopeček, J. *Biomaterials* **1984**, *5*, 19–25.

(60) Jelínková, M.; Strohalm, J.; Etrych, T.; Ulbrich, K.; Říhová, B. *Pharm. Res.* **2003**, *20*, 1558–1564.

(61) Etrych, T.; Jelínková, M.; Říhová, B.; Ulbrich, K. *J. Control. Release* **2001**, *73*, 89–102.

(62) David, A.; Kopečková, P.; Minko, T.; Rubinstein, A.; Kopeček, J. *Eur. J. Cancer* **2004**, *40*, 148–157.

(63) Benoit, D. S. W.; Henry, S. M.; Shubin, A. D.; Hoffman, A. S.; Stayton, P. S. *Mol. Pharm.* **2010**, *7*, 442–455.

(64) Rzaev, Z. M. O.; Dinçer, S.; Pişkin, E. *Prog. Polym. Sci.* **2007**, *32*, 534–595.

(65) Heredia, K. L.; Bontempo, D.; Ly, T.; Byers, J. T.; Halstenberg, S.; Maynard, H. D. *J. Am. Chem. Soc.* **2005**, *127*, 16955–16960.

(66) Hong, C.-Y.; Pan, C.-Y. *Macromolecules* **2006**, *39*, 3517–3524.

(67) Joralemon, M. J.; Smith, N. L.; Holowka, D.; Baird, B.; Wooley, K. L. *Bioconjug. Chem.* **2005**, *16*, 1246–1256.

(68) Pan, D.; Turner, J. L.; Wooley, K. L. *Macromolecules* **2004**, *37*, 7109–7115.

(69) Vázquez-Dorbatt, V.; Maynard, H. D. *Biomacromolecules* **2006**, *7*, 2297–2302.

(70) York, A. W.; Huang, F.; McCormick, C. L. *Biomacromolecules* **2010**, *11*, 505–514.

(71) York, A. W.; Scales, C. W.; Huang, F.; McCormick, C. L. *Biomacromolecules* **2007**, *8*, 16–20.

(72) Convertine, A. J.; Ayres, N.; Scales, C. W.; Lowe, A. B.; McCormick, C. L. *Biomacromolecules* **2004**, *5*, 1177–1180.

(73) Convertine, A. J.; Lokitz, B. S.; Vasileva, Y.; Myrick, L. J.; Scales, C. W.; Lowe, A. B.; McCormick, C. L. *Macromolecules* **2006**, *39*, 1724–1730.

(74) Barner-Kowollik, C.; Du Prez, F. E.; Espeel, P.; Hawker, C. J.; Junkers, T.; Schlaad, H.; Van Camp, W. *Angew. Chemie Int. Ed.* **2011**, *50*, 60–62.

(75) Barner-Kowollik, C.; Inglis, A. J. *Macromol. Chem. Phys.* **2009**, *210*, 987–992.

(76) Golas, P. L.; Matyjaszewski, K. *Chem. Soc. Rev.* **2010**, *39*, 1338–1354.

(77) Hoyle, C. E.; Lowe, A. B.; Bowman, C. N. *Chem. Soc. Rev.* **2010**, *39*, 1355–1387.

(78) Iha, R. K.; Wooley, K. L.; Nyström, A. M.; Burke, D. J.; Kade, M. J.; Hawker, C. J. *Chem. Rev.* **2009**, *109*, 5620–5686.

(79) Kade, M. J.; Burke, D. J.; Hawker, C. J. *J. Polym. Sci. Part A Polym. Chem.* **2010**, *48*, 743–750.

(80) Lodge, T. P. *Macromolecules* **2009**, *42*, 3827–3829.

(81) Lowe, A. B.; Harvison, M. A. Thiol-Based “Click” Chemistries in Polymer Synthesis and Modification. *Australian Journal of Chemistry*, 2010, *63* , 1251–1266.

(82) Lowe, A. B.; Hoyle, C. E.; Bowman, C. N. *J. Mater. Chem.* **2010**, *20*, 4745–4750.

(83) Lutz, J.-F.; Börner, H. G. *Prog. Polym. Sci.* **2008**, *33*, 1–39.

(84) Lutz, J.-F.; Sumerlin, B. S. In *Click Chemistry for Biotechnology and Materials Science*; John Wiley & Sons, Ltd, 2009; pp. 69–88.

(85) Mansfeld, U.; Pietsch, C.; Hoogenboom, R.; Becer, C. R.; Schubert, U. S. *Polym. Chem.* **2010**, *1*, 1560–1598.

(86) Nandivada, H.; Jiang, X.; Lahann, J. *Adv. Mater.* **2007**, *19*, 2197–2208.

(87) Sinnwell, S.; Inglis, A. J.; Stenzel, M. H.; Barner-Kowollik, C. In *Click Chemistry for Biotechnology and Materials Science*; John Wiley & Sons, Ltd, 2009; pp. 89–117.

(88) Sumerlin, B. S.; Vogt, A. P. *Macromolecules* **2009**, *43*, 1–13.

(89) Dehn, S.; Chapman, R.; Jolliffe, K. A.; Perrier, S. *Polym. Rev.* **2011**, *51*, 214–234.

(90) De Smedt, S.; Demeester, J.; Hennink, W. *Pharm. Res.* **2000**, *17*, 113–126.

(91) Funhoff, A. M.; van Nostrum, C. F.; Koning, G. A.; Schuurmans-Nieuwenbroek, N. M. E.; Crommelin, D. J. A.; Hennink, W. E. *Biomacromolecules* **2003**, *5*, 32–39.

(92) Jones, R. A.; Poniris, M. H.; Wilson, M. R. *J. Control. Release* **2004**, *96*, 379–391.

(93) Reschel, T.; Koňák, Č.; Oupický, D.; Seymour, L. W.; Ulbrich, K. *J. Control. Release* **2002**, *81*, 201–217.

(94) Van de Wetering, P.; Cherng, J.-Y.; Talsma, H.; Crommelin, D. J. A.; Hennink, W. E. *J. Control. Release* **1998**, *53*, 145–153.

(95) Van de Wetering, P.; Cherng, J.-Y.; Talsma, H.; Hennink, W. E. *J. Control. Release* **1997**, *49*, 59–69.

(96) Verbaan, F. J.; Oussoren, C.; van Dam, I. M.; Takakura, Y.; Hashida, M.; Crommelin, D. J. A.; Hennink, W. E.; Storm, G. *Int. J. Pharm.* **2001**, *214*, 99–101.

(97) You, Y.-Z.; Manickam, D. S.; Zhou, Q.-H.; Oupický, D. *J. Control. Release* **2007**, *122*, 217–225.

(98) Eliyahu, H.; Barenholz, Y.; Domb, A. J. *Molecules* **2005**, *10*, 34–64.

(99) Bruckdorfer, T. *Eur. Biopharm. Rev.* **2008**, *96*, 100–104.

(100) Kataoka, K.; Itaka, K.; Nishiyama, N.; Yamasaki, Y.; Oishi, M.; Nagasaki, Y. *Nucleic Acids Symp. Ser.* **2005**, *49* , 17–18.

(101) Oishi, M.; Nagasaki, Y. In *Nanotechnology in Drug Delivery SE - 2*; de Villiers, M.; Aramwit, P.; Kwon, G., Eds.; Biotechnology: Pharmaceutical Aspects; Springer New York, 2009; Vol. X, pp. 35–67.

(102) Oupický, D.; Koňák, Č.; Ulbrich, K.; Wolfert, M. A.; Seymour, L. W. *J. Control. Release* **2000**, *65*, 149–171.

(103) Tan, J. F.; Hatton, T. A.; Tam, K. C.; Too, H. P. *Biomacromolecules* **2007**, *8*, 448–454.

(104) Hilgenbrink, A. R.; Low, P. S. *J. Pharm. Sci.* **2005**, *94*, 2135–2146.

(105) Lee, R. J.; Low, P. S. *J. Liposome Res.* **1997**, *7*, 455–466.

(106) Low, P. S.; Henne, W. A.; Doorneweerd, D. D. *Acc. Chem. Res.* **2007**, *41*, 120–129.

(107) Lu, Y.; Low, P. S. *Adv. Drug Deliv. Rev.* **2002**, *54*, 675–693.

(108) Lu, Y.; Sega, E.; Leamon, C. P.; Low, P. S. *Adv. Drug Deliv. Rev.* **2004**, *56*, 1161–1176.

(109) Cho, Y. W.; Kim, J.-D.; Park, K. *J. Pharm. Pharmacol.* **2003**, *55*, 721–734.

(110) De Bruin, K. G.; Fella, C.; Ogris, M.; Wagner, E.; Ruthardt, N.; Bräuchle, C. *J. Control. Release* **2008**, *130*, 175–182.

(111) Oliveira, S.; van Rooy, I.; Kranenburg, O.; Storm, G.; Schiffelers, R. M. *Int. J. Pharm.* **2007**, *331*, 211–214.

(112) Inglis, A. J.; Barner-Kowollik, C. *Macromol. Rapid Commun.* **2010**, *31*, 1247–1266.

(113) Malkoch, M.; Thibault, R. J.; Drockenmuller, E.; Messerschmidt, M.; Voit, B.; Russell, T. P.; Hawker, C. J. *J. Am. Chem. Soc.* **2005**, *127*, 14942–14949.

(114) Koo, S. P. S.; Stamenović, M. M.; Prasath, R. A.; Inglis, A. J.; Du Prez, F. E.; Barner-Kowollik, C.; Van Camp, W.; Junkers, T. *J. Polym. Sci. Part A Polym. Chem.* **2010**, *48*, 1699–1713.

(115) Lundy, B. B.; Convertine, A.; Miteva, M.; Stayton, P. S. *Bioconjug. Chem.* **2013**, *24*, 398–407.

(116) Sizovs, A.; Xue, L.; Tolstyka, Z. P.; Ingle, N. P.; Wu, Y.; Cortez, M.; Reineke, T. M. *J. Am. Chem. Soc.* **2013**, *135*, 15417–15424.

(117) Flores, J. D.; Xu, X.; Treat, N. J.; McCormick, C. L. *Macromolecules* **2009**, *42*, 4941–4945.

(118) Kellum, M. G.; Smith, A. E.; York, S. K.; McCormick, C. L. *Macromolecules* **2010**, *43*, 7033–7040.

(119) Li, Y.; Lokitz, B. S.; Armes, S. P.; McCormick, C. L. *Macromolecules* **2006**, *39*, 2726–2728.

(120) Lokitz, B. S.; Convertine, A. J.; Ezell, R. G.; Heidenreich, A.; Li, Y.; McCormick, C. L. *Macromolecules* **2006**, *39*, 8594–8602.

(121) Lokitz, B. S.; York, A. W.; Stempka, J. E.; Treat, N. D.; Li, Y.; Jarrett, W. L.; McCormick, C. L. *Macromolecules* **2007**, *40*, 6473–6480.

(122) Read, E. S.; Armes, S. P. *Chem. Commun.* **2007**, 3021–3035.

(123) Smith, A. E.; Xu, X.; Kirkland-York, S. E.; Savin, D. A.; McCormick, C. L. *Macromolecules* **2010**, *43*, 1210–1217.

(124) Wooley, K. L. *J. Polym. Sci. Part A Polym. Chem.* **2000**, *38*, 1397–1407.

(125) Harrisson, S.; Wooley, K. L. *Chem. Commun.* **2005**, 3259–3261.

(126) Joralemon, M. J.; O'Reilly, R. K.; Hawker, C. J.; Wooley, K. L. *J. Am. Chem. Soc.* **2005**, *127*, 16892–16899.

(127) Kujawa, P.; Watanabe, H.; Tanaka, F.; Winnik, F. M. *Eur. Phys. J. E* **2005**, *17*, 129–137.

(128) Li, Y.; Lokitz, B. S.; McCormick, C. L. *Macromolecules* **2005**, *39*, 81–89.

(129) Liu, B.; Perrier, S. *J. Polym. Sci. Part A Polym. Chem.* **2005**, *43*, 3643–3654.

(130) Lowe, A. B.; Wang, R.; Tiriveedhi, V.; Butko, P.; McCormick, C. L. *Macromol. Chem. Phys.* **2007**, *208*, 2339–2347.

(131) McCormick, C. L.; Kirkland, S. E.; York, A. W. *J. Macromol. Sci. Part C Polym. Rev.* **2006**, *46*, 421–443.

(132) McCormick, C. L.; Sumerlin, B. S.; Lokitz, B. S.; Stempka, J. E. *Soft Matter* **2008**, *4*, 1760.

(133) Mitsukami, Y.; Hashidzume, A.; Yusa, S.; Morishima, Y.; Lowe, A. B.; McCormick, C. L. *Polymer (Guildf).* **2006**, *47*, 4333–4340.

(134) Smith, A. E.; Xu, X.; Abell, T. U.; Kirkland, S. E.; Hensarling, R. M.; McCormick, C. L. *Macromolecules* **2009**, *42*, 2958–2964.

(135) Stenzel, M. H.; Barner-Kowollik, C.; Davis, T. P.; Dalton, H. M. *Macromol. Biosci.* **2004**, *4*, 445–453.

(136) Sumerlin, B. S.; Lowe, A. B.; Thomas, D. B.; Convertine, A. J.; Donovan, M. S.; McCormick, C. L. *J. Polym. Sci. Part A Polym. Chem.* **2004**, *42*, 1724–1734.

(137) Xu, X.; Smith, A. E.; Kirkland, S. E.; McCormick, C. L. *Macromolecules* **2008**, *41*, 8429–8435.

(138) Yusa, S.; Shimada, Y.; Mitsukami, Y.; Yamamoto, T.; Morishima, Y. *Macromolecules* **2004**, *37*, 7507–7513.

(139) Yusa, S.; Shimada, Y.; Mitsukami, Y.; Yamamoto, T.; Morishima, Y. *Macromolecules* **2003**, *36*, 4208–4215.

(140) Zhang, L.; Nguyen, T. L. U.; Bernard, J.; Davis, T. P.; Barner-Kowollik, C.; Stenzel, M. H. *Biomacromolecules* **2007**, *8*, 2890–2901.

(141) Nanoparticles, T. P.; Tran, N. T. D.; Truong, N. P.; Jia, Z.; Cooper, M. A.; Monteiro, M. J. 1–14.

(142) Truong, N. P.; Jia, Z.; Burgess, M.; Payne, L.; McMillan, N. a J.; Monteiro, M. J. *Biomacromolecules* **2011**, *12*, 3540–3548.

(143) Gu, W.; Jia, Z.; Truong, N. P.; Prasadam, I.; Xiao, Y.; Monteiro, M. J. *Biomacromolecules* **2013**, *14*, 3386–3389.

(144) Stayton, P. S.; Hoffman, A. S.; El-Sayed, M.; Kulkarni, S.; Shimoboji, T.; Murthy, N.; Bulmus, V.; Lackey, C. Intelligent Biohybrid Materials for Therapeutic and Imaging Agent Delivery. *Proceedings of the IEEE*, 2005, *93*, 726–736.

(145) Roy, I.; Mitra, S.; Maitra, A.; Mozumdar, S. *Int. J. Pharm.* **2003**, *250*, 25–33.

(146) Bardi, G.; Malvindi, M. A.; Gherardini, L.; Costa, M.; Pompa, P. P.; Cingolani, R.; Pizzorusso, T. *Biomaterials* **2010**, *31*, 6555–6566.

(147) Fuller, J. E.; Zugates, G. T.; Ferreira, L. S.; Ow, H. S.; Nguyen, N. N.; Wiesner, U. B.; Langer, R. S. *Biomaterials* **2008**, *29*, 1526–1532.

(148) Kar, M.; Vijayakumar, P. S.; Prasad, B. L. V; Gupta, S. Sen. *Langmuir* **2010**, *26*, 5772–5781.

(149) Gao, H.; Kong, Y.; Cui, D.; Ozkan, C. S. *Nano Lett.* **2003**, *3*, 471–473.

(150) Neves, V.; Heister, E.; Costa, S.; Tîlmaciu, C.; Borowiak-Palen, E.; Giusca, C. E.; Flahaut, E.; Soula, B.; Coley, H. M.; McFadden, J.; Silva, S. R. P. *Adv. Funct. Mater.* **2010**, *20*, 3272–3279.

(151) Nunes, A.; Amsharov, N.; Guo, C.; Van den Bossche, J.; Santhosh, P.; Karachalios, T. K.; Nitodas, S. F.; Burghard, M.; Kostarelos, K.; Al-Jamal, K. T. *Small* **2010**, *6*, 2281–2291.

(152) Pantarotto, D.; Singh, R.; McCarthy, D.; Erhardt, M.; Briand, J.-P.; Prato, M.; Kostarelos, K.; Bianco, A. *Angew. Chemie Int. Ed.* **2004**, *43*, 5242–5246.

(153) Sekhon, B. S.; Kamboj, S. R. Inorganic nanomedicine—Part 1. *Nanomedicine : nanotechnology, biology, and medicine*, 2010, *6*, 516–522.

(154) Sekhon, B. S.; Kamboj, S. R. Inorganic nanomedicine—Part 2. *Nanomedicine : nanotechnology, biology, and medicine*, 2010, *6*, 612–618.

(155) Berti, L.; Burley, G. A. *Nat Nano* **2008**, *3*, 81–87.

(156) Bilecka, I.; Niederberger, M. *Electrochim. Acta* **2010**, *55*, 7717–7725.

(157) Capek, I. In *Surfactant Science Series*; Starov, V. M., Ed.; CRC Press, 2010; pp. 779–861.

(158) Fadeel, B.; Garcia-Bennett, A. E. *Adv. Drug Deliv. Rev.* **2010**, *62*, 362–374.

(159) Minelli, C.; Lowe, S. B.; Stevens, M. M. *Small* **2010**, *6*, 2336–2357.

(160) Sonvico, F.; Dubernet, C.; Colombo, P.; Couvreur, P. *Curr. Pharm. Des.* **2005**, *11*, 2091–2105.

(161) Chen, J.; Yang, M.; Zhang, Q.; Cho, E. C.; Cobley, C. M.; Kim, C.; Glaus, C.; Wang, L. V; Welch, M. J.; Xia, Y. *Adv. Funct. Mater.* **2010**, *20*, 3684–3694.

(162) Janib, S. M.; Moses, A. S.; MacKay, J. A. *Adv. Drug Deliv. Rev.* **2010**, *62*, 1052–1063.

(163) MacKay, J. A.; Li, Z. *Adv. Drug Deliv. Rev.* **2010**, *62*, 1003–1004.

(164) McCarthy, J. R. *Adv. Drug Deliv. Rev.* **2010**, *62*, 1023–1030.

(165) Rai, P.; Mallidi, S.; Zheng, X.; Rahmanzadeh, R.; Mir, Y.; Elrington, S.; Khurshid, A.; Hasan, T. *Adv. Drug Deliv. Rev.* **2010**, *62*, 1094–1124.

(166) Xie, J.; Lee, S.; Chen, X. *Adv. Drug Deliv. Rev.* **2010**, *62*, 1064–1079.

(167) Lee, J.-H.; Jun, Y.; Yeon, S.-I.; Shin, J.-S.; Cheon, J. *Angew. Chemie Int. Ed.* **2006**, *45*, 8160–8162.

(168) Samanta, B.; Yan, H.; Fischer, N. O.; Shi, J.; Jerry, D. J.; Rotello, V. M. *J. Mater. Chem.* **2008**, *18*, 1204–1208.

(169) Boyer, C.; Priyanto, P.; Davis, T. P.; Pissuwan, D.; Bulmus, V.; Kavallaris, M.; Teoh, W. Y.; Amal, R.; Carroll, M.; Woodward, R.; St Pierre, T. *J. Mater. Chem.* **2010**, *20*, 255–265.

(170) Boyer, C.; Bulmus, V.; Priyanto, P.; Teoh, W. Y.; Amal, R.; Davis, T. P. *J. Mater. Chem.* **2009**, *19*, 111–123.

(171) Jun, Y.; Lee, J.-H.; Cheon, J. *Angew. Chemie Int. Ed.* **2008**, *47*, 5122–5135.

(172) Alexandridis, P. *Chem. Eng. Technol.* **2011**, *34*, 15–28.

(173) Kawamura, G.; Nogami, M. *J. Cryst. Growth* **2009**, *311*, 4462–4466.

(174) Moon, S. Y.; Sekino, T.; Kusunose, T.; Tanaka, S. *J. Cryst. Growth* **2009**, *311*, 651–656.

(175) Perrault, S. D.; Chan, W. C. W. *J. Am. Chem. Soc.* **2009**, *131*, 17042–17043.

(176) Sardar, R.; Funston, A. M.; Mulvaney, P.; Murray, R. W. *Langmuir* **2009**, *25*, 13840–13851.

(177) Alkilany, A.; Murphy, C. *J. Nanoparticle Res.* **2010**, *12*, 2313–2333.

(178) Krpetić, Z.; Porta, F.; Caneva, E.; Dal Santo, V.; Scarì, G. *Langmuir* **2010**, *26*, 14799–14805.

(179) Lin, J.; Zhang, H.; Chen, Z.; Zheng, Y. *ACS Nano* **2010**, *4*, 5421–5429.

(180) Massich, M. D.; Giljohann, D. A.; Schmucker, A. L.; Patel, P. C.; Mirkin, C. A. *ACS Nano* **2010**, *4*, 5641–5646.

(181) Patel, P. C.; Giljohann, D. A.; Daniel, W. L.; Zheng, D.; Prigodich, A. E.; Mirkin, C. A. *Bioconjug. Chem.* **2010**, *21*, 2250–2256.

(182) Shah, N. B.; Dong, J.; Bischof, J. C. *Mol. Pharm.* **2010**, *8*, 176–184.

(183) Cai, Q.-Y.; Kim, S. H.; Choi, K. S.; Kim, S. Y.; Byun, S. J.; Kim, K. W.; Park, S. H.; Juhng, S. K.; Yoon, K.-H. *Invest. Radiol.* **2007**, *42*.

(184) Hainfeld, J. F.; Slatkin, D. N.; Focella, T. M.; Smilowitz, H. M. *Br. J. Radiol.* **2006**, *79*, 248–253.

(185) Kim, J.-H.; Lee, T. R. *Chem. Mater.* **2004**, *16*, 3647–3651.

(186) Javier, D. J.; Nitin, N.; Levy, M.; Ellington, A.; Richards-Kortum, R. *Bioconjug. Chem.* **2008**, *19*, 1309–1312.

(187) Patra, C. R.; Bhattacharya, R.; Mukhopadhyay, D.; Mukherjee, P. *Adv. Drug Deliv. Rev.* **2010**, *62*, 346–361.

(188) Prabaharan, M.; Grailer, J. J.; Pilla, S.; Steeber, D. A.; Gong, S. *Biomaterials* **2009**, *30*, 6065–6075.

(189) Kim, D.; Park, S.; Lee, J. H.; Jeong, Y. Y.; Jon, S. *J. Am. Chem. Soc.* **2007**, *129*, 7661–7665.

(190) Li, Y.; Smith, A. E.; Lokitz, B. S.; McCormick, C. L. *Macromolecules* **2007**, *40*, 8524–8526.

(191) Smith, A. E.; Xu, X.; Savin, D. A.; McCormick, C. L. *Polym. Chem.* **2010**, *1*, 628.

(192) Boyer, C.; Bulmus, V.; Liu, J.; Davis, T. P.; Stenzel, M. H.; Barner-Kowollik, C. *J. Am. Chem. Soc.* **2007**, *129*, 7145–7154.

(193) Boyer, C.; Liu, J.; Wong, L.; Tippett, M.; Bulmus, V.; Davis, T. P. *J. Polym. Sci. Part A Polym. Chem.* **2008**, *46*, 7207–7224.

(194) Hansen, N. M. L.; Haddleton, D. M.; Hvilsted, S. *J. Polym. Sci. Part A Polym. Chem.* **2007**, *45*, 5770–5780.

(195) Henry, S. M.; Convertine, A. J.; Benoit, D. S. W.; Hoffman, A. S.; Stayton, P. S. *Bioconjug. Chem.* **2009**, *20*, 1122–1128.

(196) Heredia, K. L.; Nguyen, T. H.; Chang, C.-W.; Bulmus, V.; Davis, T. P.; Maynard, H. D. *Chem. Commun.* **2008**, 3245–3247.

(197) Kujawa, P.; Segui, F.; Shaban, S.; Diab, C.; Okada, Y.; Tanaka, F.; Winnik, F. M. *Macromolecules* **2005**, *39*, 341–348.

(198) Lai, J. T.; Filla, D.; Shea, R. *Macromolecules* **2002**, *35*, 6754–6756.

(199) Moad, G.; Chong, Y. K.; Postma, A.; Rizzardo, E.; Thang, S. H. *Polymer (Guildf).* **2005**, *46*, 8458–8468.

(200) Xu, J.; Boyer, C.; Bulmus, V.; Davis, T. P. *J. Polym. Sci. Part A Polym. Chem.* **2009**, *47*, 4302–4313.

(201) Liu, J.; Liu, H.; Jia, Z.; Bulmus, V.; Davis, T. P. *Chem. Commun.* **2008**, 6582–6584.

(202) Kim, S. H.; Jeong, J. H.; Lee, S. H.; Kim, S. W.; Park, T. G. *J. Control. Release* **2006**, *116*, 123–129.

(203) Oishi, M.; Nagasaki, Y.; Itaka, K.; Nishiyama, N.; Kataoka, K. *J. Am. Chem. Soc.* **2005**, *127*, 1624–1625.

(204) Rozema, D. B.; Lewis, D. L.; Wakefield, D. H.; Wong, S. C.; Klein, J. J.; Roesch, P. L.; Bertin, S. L.; Reppen, T. W.; Chu, Q.; Blokhin, A. V; Hagstrom, J. E.; Wolff, J. A. *Proc. Natl. Acad. Sci.* **2007**, *104* , 12982–12987.

(205) Chang, C.-W.; Bays, E.; Tao, L.; Alconcel, S. N. S.; Maynard, H. D. *Chem. Commun.* **2009**, 3580–3582.

(206) Mitsukami, Y.; Donovan, M. S.; Lowe, A. B.; McCormick, C. L. *Macromolecules* **2001**, *34*, 2248–2256.

(207) Kopeček, J.; Bažilová, H. *Eur. Polym. J.* **1973**, *9*, 7–14.

(208) Blout, E. R.; Idelson, M. *J. Am. Chem. Soc.* **1956**, *78*, 497–498.

(209) Perrier, S.; Takolpuckdee, P.; Mars, C. A. *Macromolecules* **2005**, *38*, 2033–2036.

(210) Gabriel, G. J.; Madkour, A. E.; Dabkowski, J. M.; Nelson, C. F.; Nüsslein, K.; Tew, G. N. *Biomacromolecules* **2008**, *9*, 2980–2983.

(211) Kelly, S. M.; Jess, T. J.; Price, N. C. *Biochim. Biophys. Acta* **2005**, *1751*, 119–139.

(212) Bishop, G. R.; Chaires, J. B. In *Current Protocols in Nucleic Acid Chemistry*; John Wiley & Sons, Inc., 2001.

(213) Philo, J. S. *Anal. Biochem.* **2006**, *354*, 238–246.

(214) Correia, J. J. In *Numerical Computer Methods, Part C*; Michael L. Johnson, L. B. B. T.-M. in E., Ed.; Academic Press, 2000; Vol. Volume 321, pp. 81–100.

(215) Gullotti, E.; Yeo, Y. *Mol. Pharm.* **2009**, *6*, 1041–1051.

(216) Alexis, F.; Pridgen, E.; Molnar, L. K.; Farokhzad, O. C. *Mol. Pharm.* **2008**, *5*, 505–515.

(217) Duncan, R.; Gaspar, R. *Mol. Pharm.* **2011**, *8*, 2101–2141.

(218) Miller, T.; Hill, A.; Uezguen, S.; Weigandt, M.; Goepferich, A. *Biomacromolecules* **2012**, *13*, 1707–1718.

(219) Jeong, J. H.; Mok, H.; Oh, Y.-K.; Park, T. G. *Bioconjug. Chem.* **2008**, *20*, 5–14.

(220) Merkel, O. M.; Zheng, M.; Debus, H.; Kissel, T. *Bioconjug. Chem.* **2011**, *23*, 3–20.

(221) Troiber, C.; Wagner, E. *Bioconjug. Chem.* **2011**, *22*, 1737–1752.

(222) Zelikin, A. N.; Putnam, D.; Shastri, P.; Langer, R.; Izumrudov, V. A. *Bioconjug. Chem.* **2002**, *13*, 548–553.

(223) Lee, C. C.; Yoshida, M.; Fréchet, J. M. J.; Dy, E. E.; Szoka, F. C. *Bioconjug. Chem.* **2005**, *16*, 535–541.

(224) Üzgün, S.; Akdemir, O.; Hasenpusch, G.; Maucksch, C.; Golas, M. M.; Sander, B.; Stark, H.; Imker, R.; Lutz, J.-F.; Rudolph, C. *Biomacromolecules* **2009**, *11*, 39–50.

(225) Christie, R. J.; Miyata, K.; Matsumoto, Y.; Nomoto, T.; Menasco, D.; Lai, T. C.; Pennisi, M.; Osada, K.; Fukushima, S.; Nishiyama, N.; Yamasaki, Y.; Kataoka, K. *Biomacromolecules* **2011**, *12*, 3174–3185.

(226) Smith, D.; Holley, A. C.; McCormick, C. L. *Polym. Chem.* **2011**, *2*, 1428–1441.

(227) Gaynor, J. W.; Campbell, B. J.; Cosstick, R. *Chem. Soc. Rev.* **2010**, *39*, 4169–4184.

(228) Griffiths, P. C.; Paul, a; Khayat, Z.; Wan, K.-W.; King, S. M.; Grillo, I.; Schweins, R.; Ferruti, P.; Franchini, J.; Duncan, R. *Biomacromolecules* **2004**, *5*, 1422–1427.

(229) Griffiths, P. C.; Khayat, Z.; Tse, S.; Heenan, R. K.; King, S. M.; Duncan, R. *Biomacromolecules* **2007**, *8*, 1004–1012.

(230) Wan, K.-W.; Malgesini, B.; Verpilio, I.; Ferruti, P.; Griffiths, P. C.; Paul, A.; Hann, A. C.; Duncan, R. *Biomacromolecules* **2004**, *5*, 1102–1109.

(231) Schaffert, D.; Troiber, C.; Wagner, E. *Bioconjug. Chem.* **2012**, *23*, 1157–1165.

(232) Miyata, K.; Oba, M.; Nakanishi, M.; Fukushima, S.; Yamasaki, Y.; Koyama, H.; Nishiyama, N.; Kataoka, K. *J. Am. Chem. Soc.* **2008**, *130*, 16287–16294.

(233) Miyata, K.; Christie, R. J.; Suma, T.; Takemoto, H.; Uchida, H.; Nishiyama, N.; Kataoka, K. In *Tailored Polymer Architectures for Pharmaceutical and Biomedical Applications*; ACS Symposium Series; American Chemical Society, 2013; Vol. 1135, pp. 11–189.

(234) Uchida, H.; Miyata, K.; Oba, M.; Ishii, T.; Suma, T.; Itaka, K.; Nishiyama, N.; Kataoka, K. *J. Am. Chem. Soc.* **2011**, *133*, 15524–15532.

(235) Duvall, C. L.; Convertine, A. J.; Benoit, D. S. W.; Hoffman, A. S.; Stayton, P. S. *Mol. Pharm.* **2009**, *7*, 468–476.

(236) Brogden, K. A. *Nat. Rev. Microbiol.* **2005**, *3*, 238–250.

(237) Meyer, M.; Philipp, A.; Oskuee, R.; Schmidt, C.; Wagner, E. *J. Am. Chem. Soc.* **2008**, *130*, 3272–3273.

(238) Dohmen, C.; Edinger, D.; Fröhlich, T.; Schreiner, L.; Lächelt, U.; Troiber, C.; Rädler, J.; Hadwiger, P.; Vornlocher, H.-P.; Wagner, E. *ACS Nano* **2012**, *6*, 5198–5208.

(239) Cheng, J.; Deming, T. J. In *Peptide-Based Materials*; Deming, T., Ed.; Springer Berlin Heidelberg, 2012; pp. 1–26.

(240) Deng, L.; Shi, K.; Zhang, Y.; Wang, H.; Zeng, J.; Guo, X.; Du, Z.; Zhang, B. *J. Colloid Interface Sci.* **2008**, *323*, 169–175.

(241) Zhang, X.; Li, J.; Li, W.; Zhang, A. *Biomacromolecules* **2007**, *8*, 3557–3567.

(242) Ray, J. G.; Johnson, A. J.; Savin, D. A. *J. Polym. Sci. Part B Polym. Phys.* **2013**, *51*, 508–523.

(243) Naik, S. S.; Ray, J. G.; Savin, D. A. *Langmuir* **2011**, *27*, 7231–7240.

(244) Treat, N. J.; Smith, D.; Teng, C.; Flores, J. D.; Abel, B. A.; York, A. W.; Huang, F.; McCormick, C. L. *ACS Macro Lett.* **2011**, *1*, 100–104.

(245) York, A. W.; Huang, F.; McCormick, C. L. *Biomacromolecules* **2010**, *11*, 505–514.

(246) Harvison, M. A.; Roth, P. J.; Davis, T. P.; Lowe, A. B. *Aust. J. Chem.* **2011**, *64*, 992.

(247) Willcock, H.; O'Reilly, R. K. *Polym. Chem.* **2010**, *1*, 149.

(248) York, A. W.; Scales, C. W.; Huang, F.; McCormick, C. L. *Biomacromolecules* **2007**, *8*, 16–20.

(249) Ballard, D. G. H.; Bamford, C. H. *J. Chem. Soc.* **1956**, 381–387.

(250) Pickel, D. L.; Politakos, N.; Avgeropoulos, A.; Messman, J. M. *Macromolecules* **2009**, *42*, 7781–7788.

(251) Szwarc, M. In *Fortschritte der Hochpolymeren-Forschung SE - 1*; Advances in Polymer Science; Springer Berlin Heidelberg, 1965; Vol. 4/1, pp. 1–65.

(252) Vayaboury, W.; Giani, O.; Cottet, H.; Deratani, A.; Schué, F. *Macromol. Rapid Commun.* **2004**, *25*, 1221–1224.

(253) Ray, J. G.; Naik, S. S.; Hoff, E. A.; Johnson, A. J.; Ly, J. T.; Easterling, C. P.; Patton, D. L.; Savin, D. A. *Macromol. Rapid Commun.* **2012**, *33*, 819–826.

(254) Sreerama, N.; Woody, R. W. In *Numerical Computer Methods, Part D*; Enzymology, L. B. and M. L. J. B. T.-M. in, Ed.; Academic Press, 2004; Vol. Volume 383, pp. 318–351.

(255) Kypr, J.; Kejnovská, I.; Bednářová, K.; Vorlíčková, M. In *Comprehensive Chiroptical Spectroscopy*; John Wiley & Sons, Inc., 2012; pp. 575–586.

(256) Gottarelli, G.; Lena, S.; Masiero, S.; Pieraccini, S.; Spada, G. P.; Mater, A.; Universita, S. *Chirality* **2008**, *20*, 471–485.

(257) Hristova, K.; Selsted, M. E.; White, S. H. *J. Biol. Chem.* **1997**, *272*, 24224–24233.

(258) Ladokhin, A. S.; Selsted, M. E.; White, S. H. *Biophys. J.* **1997**, *72*, 1762–1766.

(259) Matsuzaki, K.; Yoneyama, S.; Miyajima, K. *Biophys. J.* **1997**, *73*, 831–838.

(260) Zhao, H.; Mattila, J.-P.; Holopainen, J. M.; Kinnunen, P. K. J. *Biophys. J.* **2001**, *81*, 2979–2991.

(261) Elbashir, S. M.; Harborth, J.; Lendeckel, W.; Yalcin, A.; Weber, K.; Tuschl, T. *Nature* **2001**, *411*, 494–498.

(262) Pack, D. W.; Hoffman, A. S.; Pun, S.; Stayton, P. S. *Nat Rev Drug Discov* **2005**, *4*, 581–593.

(263) Dorsett, Y.; Tuschl, T. *Nat Rev Drug Discov* **2004**, *3*, 318–329.

(264) Smith, D.; Holley, A. C.; McCormick, C. L. *Polym. Chem.* **2011**, *2*, 1428–1441.

(265) Braasch, D. A.; Jensen, S.; Liu, Y.; Kaur, K.; Arar, K.; White, M. A.; Corey, D. R. *Biochemistry* **2003**, *42*, 7967–7975.

(266) Gebhart, C. L.; Kabanov, A. V. *J. Control. Release* **2001**, *73*, 401–416.

(267) Kabanov, A. V; Kabanov, V. A. *Adv. Drug Deliv. Rev.* **1998**, *30*, 49–60.

(268) Moad, G.; Rizzardo, E.; Thang, S. H. *Polymer (Guildf).* **2008**, *49*, 1079–1131.

(269) Matyjaszewski, K. *Macromolecules* **2012**, *45*, 4015–4039.

(270) Smith, D.; Pentzer, E. B.; Nguyen, S. T. *Polym. Rev.* **2007**, *47*, 419–459.

(271) Gebhart, C. L.; Sriadibhatla, S.; Vinogradov, S.; Lemieux, P.; Alakhov, V.; Kabanov, A. V. *Bioconjug. Chem.* **2002**, *13*, 937–944.

(272) Tribet, C. In *Physical Chemistry of Polyelectrolytes*; Radeva, T., Ed.; Marcel Dekker, 2001; pp. 687–742.

(273) Dautzenberg, H. In *Physical Chemistry of Polyelectrolytes*; Radeva, T., Ed.; Marcel Dekker, 2001; pp. 743–792.

(274) Azegami, S.; Tsuboi, A.; Izumi, T.; Hirata, M.; Dubin, P. L.; Wang, B.; Kokufuta, E. *Langmuir* **1999**, *15*, 940–947.

(275) Kokufuta, E.; Nishimura, H. *Polym. Bull.* **1991**, *26*, 277–282.

(276) Hallberg, R. K.; Dubin, P. L. *J. Phys. Chem. B* **1998**, *102*, 8629–8633.

(277) Teramoto, A.; Watanabe, M.; Iizuka, E.; Abe, K. *J. Macromol. Sci. Part A* **1994**, *31*, 53–64.

(278) Xia, J.; Dubin, P. L.; Morishima, Y.; Sato, T.; Muhoberac, B. B. *Biopolymers* **1995**, *35*, 411–418.

(279) Railsback, J. G.; Singh, A.; Pearce, R. C.; McKnight, T. E.; Collazo, R.; Sitar, Z.; Yingling, Y. G.; Melechko, A. V. *Adv. Mater.* **2012**, *24*, 4261–4265.

(280) Li, Y.; Bronich, T. K.; Chelushkin, P. S.; Kabanov, A. V. *Macromolecules* **2008**, *41*, 5863–5868.

(281) Bakeev, K. N.; Izumrudov, V. A.; Kuchanov, S. I.; Zezin, A. B.; Kabanov, V. A. *Macromolecules* **1992**, *25*, 4249–4254.

(282) Ahn, C.-H.; Chae, S. Y.; Bae, Y. H.; Kim, S. W. *J. Control. Release* **2002**, *80*, 273–282.

(283) Duvall, C. L.; Convertine, A. J.; Benoit, D. S. W.; Hoffman, A. S.; Stayton, P. S. *Mol. Pharm.* **2009**, *7*, 468–476.

(284) Floch, V.; Loisel, S.; Guenin, E.; Hervé, A. C.; Clement, J. C.; Yaouanc, J. J.; des Abbayes H; Férec, C. *J. Med. Chem.* **2000**, *43*, 4617–4628.

(285) Guénin, E.; Hervé, A.-C.; Floch, V.; Loisel, S.; Yaouanc, J.-J.; Clément, J.-C.; Férec, C.; des Abbayes, H. *Angew. Chemie Int. Ed.* **2000**, *39*, 629–631.

(286) Picquet, E.; Le Ny, K.; Delépine, P.; Montier, T.; Yaouanc, J.-J.; Cartier, D.; des Abbayes, H.; Férec, C.; Clément, J.-C. *Bioconjug. Chem.* **2005**, *16*, 1051–1053.

(287) Ornelas-Megiatto, C.; Wich, P. R.; Fréchet, J. M. J. *J. Am. Chem. Soc.* **2012**, *134*, 1902–1905.

(288) Hemp, S. T.; Allen, M. H.; Green, M. D.; Long, T. E. *Biomacromolecules* **2011**, *13*, 231–238.

(289) Prevette, L. E.; Kodger, T. E.; Reineke, T. M.; Lynch, M. L. *Langmuir* **2007**, *23*, 9773–9784.

(290) Prevette, L. E.; Lynch, M. L.; Kizjakina, K.; Reineke, T. M. *Langmuir* **2008**, *24*, 8090–8101.

(291) Flores, J. D.; Shin, J.; Hoyle, C. E.; McCormick, C. L. *Polym. Chem.* **2010**, *1*, 213.

(292) Flores, J. D.; Treat, N. J.; York, A. W.; McCormick, C. L. *Polym. Chem.* **2011**, *2*, 1976–1985.

(293) Holley, A. C.; Ray, J. G.; Wan, W.; Savin, D. A.; McCormick, C. L. *Biomacromolecules* **2013**, *14*, 3793–3799.

(294) Kelly, S. M.; Jess, T. J.; Price, N. C. *Biochim. Biophys. Acta* **2005**, *1751*, 119–139.

(295) Kypr, J.; Kejnovská, I.; Renčiuk, D.; Vorlíčková, M. *Nucleic Acids Res.* **2009**, *37* , 1713–1725.

(296) Sturtevant, J. M. *Annu. Rev. Phys. Chem.* **1987**, *38*, 463–488.

(297) Izumrudov, V. A.; Kargov, S. I.; Zhiryakova, M. V; Zezin, A. B.; Kabanov, V. A. *Biopolymers* **1995**, *35*, 523–531.

(298) Gleave, M. E.; Monia, B. P. *Nat Rev Cancer* **2005**, *5*, 468–479.

(299) Duca, M.; Vekhoff, P.; Oussedik, K.; Halby, L.; Arimondo, P. B. *Nucleic Acids Res.* **2008**, *36* , 5123–5138.

(300) Doluca, O.; Withers, J. M.; Filichev, V. V. *Chem. Rev.* **2013**, *113*, 3044–3083.

(301) Xu, X.; Hamhouyia, F.; Thomas, S. D.; Burke, T. J.; Girvan, A. C.; McGregor, W. G.; Trent, J. O.; Miller, D. M.; Bates, P. J. *J. Biol. Chem.* **2001**, *276* , 43221–43230.

(302) Reyes-Reyes, E. M.; Teng, Y.; Bates, P. J. *Cancer Res.* **2010**, *70*, 8617–8629.

(303) Bates, P. J.; Laber, D. A.; Miller, D. M.; Thomas, S. D.; Trent, J. O. *Exp. Mol. Pathol.* **2009**, *86*, 151–164.

(304) Ginisty, H.; Sicard, H.; Roger, B.; Bouvet, P. *J. Cell Sci.* **1999**, *112* , 761–772.

(305) Mongelard, F.; Bouvet, P. *Trends Cell Biol.* **2007**, *17*, 80–86.

(306) Wu, J.; Song, C.; Jiang, C.; Shen, X.; Qiao, Q.; Hu, Y. *Mol. Pharm.* **2013**, *10*, 3555–3563.

(307) Ai, J.; Xu, Y.; Lou, B.; Li, D.; Wang, E. *Talanta* **2014**, *118*, 54–60.